

**NATIONAL BUREAU OF STANDARDS REPORT**

9905

**PRELIMINARY REPORT  
ON THE THERMODYNAMIC PROPERTIES OF  
SELECTED LIGHT-ELEMENT AND  
SOME RELATED COMPOUNDS**

(The previous semiannual reports in this series have the NBS Report Nos. 6297, 6484, 6645, 6928, 7093, 7192, 7437, 7587, 7796, 8033, 8186, 8504, 8628, 8919, 9028, 9389, 9500, 9601, and 9803.)



**U.S. DEPARTMENT OF COMMERCE  
NATIONAL BUREAU OF STANDARDS**

## NATIONAL BUREAU OF STANDARDS

The National Bureau of Standards<sup>1</sup> was established by an act of Congress March 3, 1901. Today, in addition to serving as the Nation's central measurement laboratory, the Bureau is a principal focal point in the Federal Government for assuring maximum application of the physical and engineering sciences to the advancement of technology in industry and commerce. To this end the Bureau conducts research and provides central national services in three broad program areas and provides central national services in a fourth. These are: (1) basic measurements and standards, (2) materials measurements and standards, (3) technological measurements and standards, and (4) transfer of technology.

The Bureau comprises the Institute for Basic Standards, the Institute for Materials Research, the Institute for Applied Technology, and the Center for Radiation Research.

**THE INSTITUTE FOR BASIC STANDARDS** provides the central basis within the United States of a complete and consistent system of physical measurement, coordinates that system with the measurement systems of other nations, and furnishes essential services leading to accurate and uniform physical measurements throughout the Nation's scientific community, industry, and commerce. The Institute consists of an Office of Standard Reference Data and a group of divisions organized by the following areas of science and engineering:

Applied Mathematics—Electricity—Metrology—Mechanics—Heat—Atomic Physics—Cryogenics<sup>2</sup>—Radio Physics<sup>2</sup>—Radio Engineering<sup>2</sup>—Astrophysics<sup>2</sup>—Time and Frequency.<sup>2</sup>

**THE INSTITUTE FOR MATERIALS RESEARCH** conducts materials research leading to methods, standards of measurement, and data needed by industry, commerce, educational institutions, and government. The Institute also provides advisory and research services to other government agencies. The Institute consists of an Office of Standard Reference Materials and a group of divisions organized by the following areas of materials research:

Analytical Chemistry—Polymers—Metallurgy—Inorganic Materials—Physical Chemistry.

**THE INSTITUTE FOR APPLIED TECHNOLOGY** provides for the creation of appropriate opportunities for the use and application of technology within the Federal Government and within the civilian sector of American industry. The primary functions of the Institute may be broadly classified as programs relating to technological measurements and standards and techniques for the transfer of technology. The Institute consists of a Clearinghouse for Scientific and Technical Information,<sup>3</sup> a Center for Computer Sciences and Technology, and a group of technical divisions and offices organized by the following fields of technology:

Building Research—Electronic Instrumentation—Technical Analysis—Product Evaluation—Invention and Innovation—Weights and Measures—Engineering Standards—Vehicle Systems Research.

**THE CENTER FOR RADIATION RESEARCH** engages in research, measurement, and application of radiation to the solution of Bureau mission problems and the problems of other agencies and institutions. The Center for Radiation Research consists of the following divisions:

Reactor Radiation—Linac Radiation—Applied Radiation—Nuclear Radiation.

<sup>1</sup> Headquarters and Laboratories at Gaithersburg, Maryland, unless otherwise noted; mailing address Washington, D. C. 20234.

<sup>2</sup> Located at Boulder, Colorado 80302.

<sup>3</sup> Located at 5285 Port Royal Road, Springfield, Virginia 22151.

# NATIONAL BUREAU OF STANDARDS REPORT

## NBS PROJECT

221-0404  
221-0405  
221-0426  
222-0423  
313-0430  
316-0426  
316-0513

## NBS REPORT

1 July 1968

9905

### PRELIMINARY REPORT ON THE THERMODYNAMIC PROPERTIES OF SELECTED LIGHT-ELEMENT AND SOME RELATED COMPOUNDS

(The previous semiannual reports in this series have the NBS Report Nos. 6297, 6484, 6645, 6928, 7093, 7192, 7437, 7587, 7796, 8033, 8186, 8504, 8628, 8919, 9028, 9389, 9500, 9601, and 9803.)

Technical Summary Report  
on the Thermodynamic Properties  
of Light-Element Compounds

Reference: U. S. Air Force, Office of Scientific Research,  
Order No. ISSA 67-6

#### IMPORTANT NOTICE

NATIONAL BUREAU OF STANDARDS  
for use within the Government. Before  
being used, the Report must be  
examined and approved by the  
Director of the National Institute of  
Standards and Technology (NIST).  
The Report has been specifically prepared

Approved for public release by the  
Director of the National Institute of  
Standards and Technology (NIST)  
on October 9, 2015

accounting documents intended  
to be subjected to additional evaluation  
and testing of this Report, either in  
the Office of the Director, National  
Institute of Standards and Technology,  
or in the Government agency for which  
the Report was prepared.



U.S. DEPARTMENT OF COMMERCE  
NATIONAL BUREAU OF STANDARDS



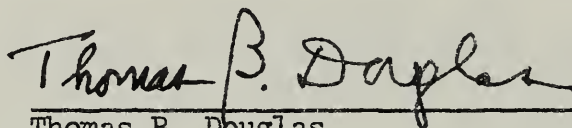


## ABSTRACT

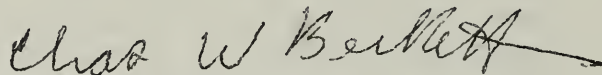
Thermodynamic and related properties of substances important in current high-temperature research and development activities are being investigated under contract with the U. S. Air Force Office of Scientific Research (USAF Order No. ISSA 67-6) and the Advanced Research Projects Agency (ARPA Order No. 20). This research program is a direct contribution to the Interagency Chemical Rocket Propulsion Group (Working Group on Thermochemistry) and, simultaneously, to other organizations oriented toward acquiring the basic information needed to solve not only the technical problems in propulsion but also those associated with ballistics, reentry, and high-strength high-temperature materials. For given substances this needed basic information comprises an ensemble of closely related properties being determined by an extensive array of techniques. Some of these techniques, by relating thermodynamic properties to molecular or crystal structure, make it possible to tabulate these properties over far wider ranges of temperature and pressure than those actually employed in the basic investigations.

This report presents in detail the methods, results, and interpretation of six recent NBS experimental investigations of thermodynamic and related properties. Measurements of the heats of reaction with hydrogen of chlorine trifluoride and its two free elements gave on preliminary calculation  $\Delta H_{303}^{\circ}(\text{ClF}_3) = -38.61 \text{ kcal/mol}$ , which agrees with two published values and disproves a formerly credited value that is 10 kcal/mol less exothermic. Precise measurements of the heat capacity of sintered beryllium oxide gave generally lower heat capacities (by up to 30% at 55 K) and an appreciably lower entropy ( $S_{298.15}^{\circ} = 3.291 \pm 0.004 \text{ cal/K mol}$ ) than

previously accepted. A new millisecond apparatus for measuring simultaneously the heat capacity, electrical resistivity, and hemispherical total emittance of electrical conductors is described (respective estimated errors: 1.5%, 0.6%, and 3% at 2500 K; less at 1800 K). Preliminary results are given for molybdenum (1800-2800 K). The reaction between beryllium metal and aluminum oxide was studied mass-spectrometrically (1511-1743 K). The resulting second-law and third-law heats of four reactions involving the gas species Be, Al, O,  $\text{Al}_2\text{O}$ , and  $\text{AlO}$  are compared. From a continuation of the spectroscopic investigation of the alkali-hydroxide molecules, the high-temperature microwave spectra of RbOH and the matrix-isolation infrared spectra of RbOH and NaOH (plus the deuterioxides in all cases) were observed, and are analyzed to give bond lengths, frequency fundamentals, nuclear quadrupole coupling constants, and vibration-rotation interaction constants. The essentially linear shapes and unusual bending potentials of these molecules are very similar to those found earlier for CsOH, and suggest a similar behavior of all the alkali hydroxides.



Thomas B. Douglas  
Project Leader



Charles W. Beckett  
Assistant Division Chief for Thermodynamics  
Heat Division, Institute for Basic Standards

# TABLE OF CONTENTS

	<u>Page</u>
Abstract . . . . .	i
Chap. 1. <u>FLUORINE FLAME CALORIMETRY III. THE HEAT</u> <u>OF FORMATION OF CHLORINE TRIFLUORIDE</u> . . . .	
(by R. C. King and G. T. Armstrong) . . . . .	1
1. Introduction . . . . .	1
2. Experimental Apparatus and Procedures . . . .	2
2.1 The Reaction Vessel and Flow System . .	2
Fig. 1. Assembly of Reaction Vessel . . . . .	3
Fig. 2. Combustion Chamber and Primary Solution Vessel . .	4
Fig. 3. The Oxidizer Flow Line . .	5
2.2 Water Removal from the Reaction Vessel .	6
2.3 Experimental Procedures . . . . .	6
Table 1. Water Changes in Reaction Vessel . . . .	7
2.4 The Samples . . . . .	8
Table 2. Analyses of Oxidizer Gases . . . . .	10
3. Calibration of the Calorimeter . . . . .	11
Table 3. Calibration of the Calorimeter. The O <sub>2</sub> -H <sub>2</sub> Reaction . . . .	12
4. The Completeness of the Reactions . . . . .	13
Table 4. The Completeness of the ClF <sub>3</sub> -H <sub>2</sub> -H <sub>2</sub> O Reaction . . . .	14
5. Reaction Heat Measurements . . . . .	15
Table 5. The Completeness of the Cl <sub>2</sub> -H <sub>2</sub> -H <sub>2</sub> O and Cl <sub>2</sub> -H <sub>2</sub> -HF <sub>aq</sub> Reactions . .	17
Table 6. The ClF <sub>3</sub> -H <sub>2</sub> -H <sub>2</sub> O Reaction: Typical Reaction Quantities . . . . .	18
Table 7. The ClF <sub>3</sub> -H <sub>2</sub> -H <sub>2</sub> O Reaction: Typical Heat Measurements . .	19
Table 8. The Heat of the ClF <sub>3</sub> -H <sub>2</sub> -H <sub>2</sub> O Reaction (303 °K) . . . . .	20

# TABLE OF CONTENTS (Continued)

	<u>Page</u>
Table 9. The $\text{Cl}_2\text{-H}_2\text{-H}_2\text{O}$ and $\text{Cl}_2\text{-H}_2\text{-HF}_{\text{aq}}$ Typical Reaction Quantities . . .	21
Table 10. The $\text{Cl}_2\text{-H}_2\text{-H}_2\text{O}$ and $\text{Cl}_2\text{-H}_2\text{-HF}_{\text{aq}}$ Reactions: Typical Heat Measurements .	22
Table 11. The Heats of the $\text{Cl}_2\text{-H}_2\text{-H}_2\text{O}$ and $\text{Cl}_2\text{-H}_2\text{-HF}_{\text{aq}}$ Reactions (303 °K) . . . . .	23
Table 12. The $\text{F}_2\text{-H}_2\text{-HCl}_{\text{aq}}$ Reaction: Typical Heat Measurements .	24
Table 13. The Heat of the $\text{F}_2\text{-H}_2\text{-HCl}_{\text{aq}}$ Reaction (303.6 °K) . . . . .	25
Table 14. Preliminary Calculation of the Heat of Formation of Chlorine Trifluoride . . . . .	26
References . . . . .	27
 Chap. 2. <u>HEAT CAPACITY AND THERMODYNAMIC PROPERTIES OF BERYLLIUM OXIDE, <math>\text{BeO}</math>, FROM 15 TO 370 K</u> (by George T. Furukawa and Martin L. Reilly) . . . . .	
Abstract . . . . .	28
I. Introduction . . . . .	28
II. Sample . . . . .	30
III. Apparatus and Method . . . . .	31
IV. Results . . . . .	33
Table 1. Spectrochemical Analysis of the Sintered Beryllium Oxide ( $\text{BeO}$ ) Pellet . . . . .	37
Table 2. Thermodynamic Functions for Beryllium Oxide ( $\text{BeO}$ ), Solid Phase . . . . .	38
Table 3. Comparison of Enthalpy Values of Table 2 with the Experimental Relative Enthalpy Data of Victor and Douglas . . . . .	39
References . . . . .	40
Fig. 1. Percentage Deviation of the Empty Sample Vessel Heat Capacities . . . . .	43



## TABLE OF CONTENTS (Continued)

	<u>Page</u>
Fig. 2. Percentage Deviation of the Beryllium Oxide Sample Heat Capacities . . .	44
Fig. 3. Percentage Deviation of the Beryllium Oxide Sample Heat Capacities . . .	45
Fig. 4. Observed Values of $C/T^3$ vs. T. . . . .	46
Fig. 5. A Comparison of Results Published by Other Investigators with Those Obtained in this Research . .	47
Chap. 3. <u>DYNAMIC MEASUREMENT OF HEAT CAPACITY,</u> <u>ELECTRICAL RESISTIVITY AND HEMISPHERICAL</u> <u>TOTAL EMITTANCE OF MOLYBDENUM IN THE</u> <u>RANGE 1800-2800 K</u>	
(by A. Cezairliyan, M. S. Morse, H. A. Berman, G. M. Foley, and C. W. Beckett) . . . . .	48
Abstract . . . . .	48
I. Introduction . . . . .	49
II. Description of the Method . . . . .	51
a. Heating Period . . . . .	52
b. Cooling Period . . . . .	53
c. Relations for Properties . . . . .	53
III. Description of the System . . . . .	54
a. Specimen and Test Cell . . . . .	54
Fig. 1. Functional Diagram of Millisecond Thermodynamic Measurements System . . . . .	55
b. Rest of Main Circuit . . . . .	56
c. High-Speed Pyrometer . . . . .	56
d. High-Speed Digital Data Acquisition System . . . . .	57
Fig. 2. Functional Diagram of High-Speed Digital Data Acquisition System . . . . .	59
IV. Experimental Results . . . . .	60
Fig. 3. Heat Capacity of Molybdenum as a Function of Temperature . . . . .	61
Fig. 4. Electrical Resistivity of Molybdenum as a Function of Temperature . . . . .	62

# TABLE OF CONTENTS (Continued)

	<u>Page</u>
Fig. 5. Hemispherical Total Emittance of Molyb- denum as a Function of Temperature . . . . .	63
V. Discussion . . . . .	64
Table 1. Estimated Errors . . . . .	65
Acknowledgment . . . . .	66
References . . . . .	67
Chap. 4. <u>MASS SPECTROMETRIC STUDY OF THE BERYLLIUM-</u> <u>ALUMINA REACTION</u> (by J. Efimenko) . . . . .	
Introduction . . . . .	69
Experimental . . . . .	69
Results . . . . .	69
Discussion . . . . .	70
Table 1. Data: Ion Intensities . . . . .	72
Table 2. Auxiliary Data . . . . .	73
Table 3. Reaction Enthalpies . . . . .	74
Table 4. Partial Pressures . . . . .	75
Fig. 1. A van't Hoff plot for the reaction $\text{Be(g)} + \text{Al}_2\text{O}_3\text{(s)}$ $= \text{BeO(s)} + 2\text{Al(g)} + 2\text{O(g)}$ . . . . .	76
Fig. 2. A van't Hoff plot for the reaction $2\text{Al(g)} + \text{O(g)} = \text{Al}_2\text{O(g)}$ . . . . .	77
Fig. 3. A van't Hoff plot for the reaction $\text{Be(g)} + \text{Al}_2\text{O(g)}$ $= \text{BeO(s)} + 2\text{Al(g)}$ . . . . .	78
Fig. 4. A van't Hoff plot for the reaction $\text{Be(g)} + \text{Al}_2\text{O}_3\text{(s)}$ $= \text{BeO(s)} + 2\text{AlO(g)}$ . . . . .	79
Chap. 5. <u>STRUCTURE OF THE ALKALI HYDROXIDES. III.</u> <u>MICROWAVE SPECTRA OF RbOH AND RbOD</u> (by Chi Matsumura and David R. Lide, Jr.) . . . . .	
Abstract . . . . .	80
Introduction . . . . .	81
Experimental . . . . .	81
Analysis of Spectrum . . . . .	83

# TABLE OF CONTENTS (Continued)

	<u>Page</u>
Nuclear Quadrupole Coupling . . . . .	84
Vibration-Rotation Interactions . . . . .	85
Structure . . . . .	86
Acknowledgments . . . . .	86
References . . . . .	87
Table I. Observed frequencies in Rb <sup>85</sup> OH and Rb <sup>85</sup> OD . . . . .	88
Table II. Observed frequencies in Rb <sup>87</sup> OH and Rb <sup>87</sup> OD . . . . .	92
Table III. Effective rotational constants and nuclear coupling constants for various vibration- al states of RbOH and RbOD . . . . .	94
Table IV. <i>l</i> -doubling constants . . . . .	95
Table V. Variation of rotation- al constants with $\nu_1$ . . . . .	96
Table VI. Fit of $B_{0v}^{20}_{30}$ to power series . . . . .	97
Table VII. Structural parameters of rubidium hydroxide . . . . .	98

## Chap. 6. STRUCTURE OF THE ALKALI HYDROXIDES. IV. THE INFRARED SPECTRA OF MATRIX ISOLATED RbOH, RbOD AND NaOH, NaOD

(by N. Acquista and Stanley Abramowitz) . . . . .	99
Abstract . . . . .	99
Introduction . . . . .	100
Experimental . . . . .	100
Experimental Results . . . . .	102
Table 1. Observed Bands for Monomeric Alkali Metal Hydroxides . . . . .	105
References . . . . .	106
Fig. 1. The spectra of matrix isolated RbOH in argon . . . . .	107

# TABLE OF CONTENTS (Continued)

	<u>Page</u>
Fig. 2. The spectra of matrix isolated NaOH in argon . . .	108
Fig. 3. The spectrum of matrix isolated NaOH in argon . . .	109
Fig. 4. The spectrum of matrix isolated NaOH (and that of NaOD) in argon . . .	110
Fig. 5. The spectrum of matrix isolated NaOD in argon . . .	111



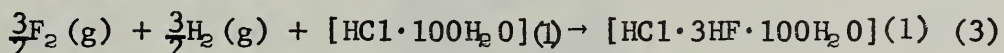
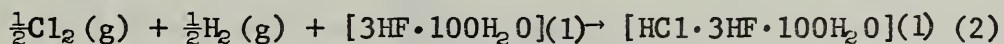
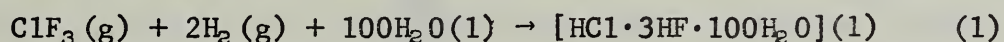
FLUORINE FLAME CALORIMETRY III.  
THE HEAT OF FORMATION OF CHLORINE TRIFLUORIDE

R. C. King and G. T. Armstrong

## 1. INTRODUCTION

A study of the heat of formation of chlorine trifluoride has been conducted using flame calorimetry. Chlorine trifluoride is an extremely reactive compound, which reacts spontaneously with many substances leading to multiple reaction products. For this reason there are few reactions which are suitable for a well-defined study of its heat of formation.

For this study the chlorine trifluoride was reacted with hydrogen, using an experimental approach and procedures similar to those used in an earlier study on the heat of formation of oxygen difluoride [1]. The product acids were dissolved in water to form an aqueous solution inside the calorimeter. The heats of the auxiliary reactions of chlorine and fluorine with hydrogen to form the aqueous solutions of the mixed acids were also measured. The equations for the reactions studied are:



Retaining the product acids inside of the calorimeter in a known thermodynamic state has several advantages which have already been discussed [1]. It is believed that the systematic errors in the heats of reactions (2) and (3) are similar to those in reaction (1), and that most of the systematic errors will cancel in the calculation of the heat of formation of chlorine trifluoride, leading to a more accurate value. The agreement between the heats of reactions (2) and (3) and the heats of formation of the aqueous solutions of the respective acids can be used as an indication of the overall validity of the procedures used in this study.

This report presents a brief description of the experiments and some preliminary results on the heats of the reactions and the calculated heat of formation of chlorine trifluoride.

## 2. Experimental Apparatus and Procedures

### 2.1 The Reaction Vessel and Flow System

The overall design of the reaction vessel is illustrated in figure 1. It is similar to the one used and described earlier [1]. The main modification is the use of a secondary solution vessel of larger volume (more like the primary solution vessel).

The mixture of hydrogen chloride and hydrogen fluoride formed in the chlorine trifluoride-hydrogen reaction was observed to be extremely corrosive. To lessen loss of the acid by corrosion, a removable platinum liner (0.002 in. thick) was placed in the combustion chamber (A). (See figure 2) For the chlorine-hydrogen reactions, a platinum liner was placed on the underside of the lid to the combustion chamber. Platinum in this position was found to be very unsuitable for the chlorine-trifluoride experiments. In these experiments the liner on the lid would vaporize, leading a soot-like deposit on the walls of the combustion chamber. A spectrochemical analysis of this deposit revealed it to be platinum.

The undersides of the Monel lids (J) to the solution chambers were coated with Teflon. For an experiment each solution vessel contains 100 cm<sup>3</sup> of water. Additional details of the reaction vessel and the procedures for using it have already been described [1].

The overall design of the flow system is similar to that used earlier. The major modification was introduced in the oxidizer flow line. Previously, a Pyrex float-type flowmeter was used to indicate the rate of flow of the oxidizer. Because of the extreme reactivity of chlorine trifluoride, a mass flowmeter was inserted in the oxidizer flow line to be used in addition to the float-type flowmeter. This modification is shown in figure 3. For the chlorine-trifluoride-hydrogen reactions, the Pyrex flowmeter was replaced with a stand-in Monel tube. However, the Pyrex flowmeter was used satisfactorily for the O<sub>2</sub>-H<sub>2</sub>, Cl<sub>2</sub>-H<sub>2</sub>, and F<sub>2</sub>-H<sub>2</sub> reactions and was found very useful for monitoring the O<sub>2</sub>-H<sub>2</sub> and Cl<sub>2</sub>-H<sub>2</sub> flames.



Figure 1. Assembly of Reaction Vessel



# COMBUSTION CHAMBER AND SOLUTION VESSEL

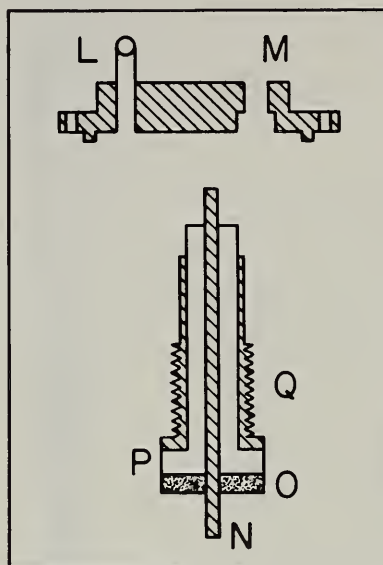
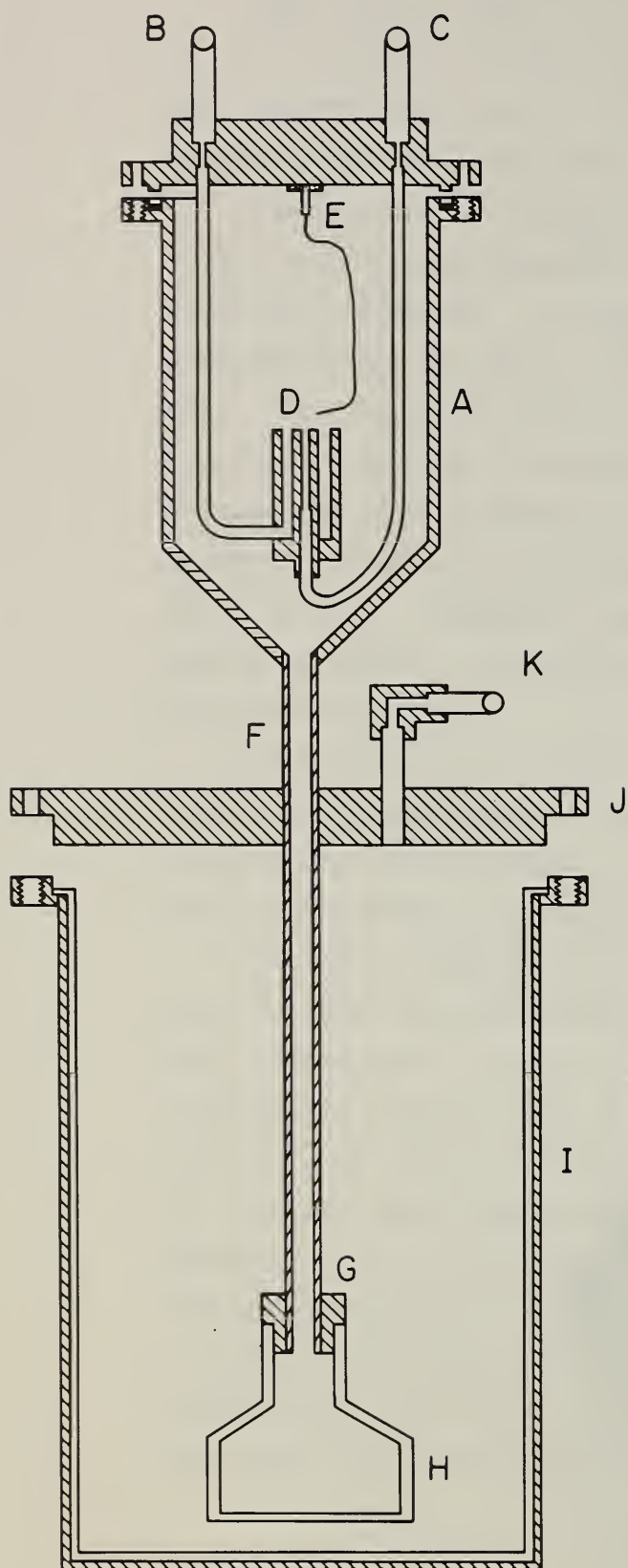


Figure 2. Combustion Chamber and Primary Solution Vessel. A, Combustion chamber; B, Hydrogen inlet; C, Oxidizer inlet; D, Flame position; E, Spark electrode; F, Platinum tubing; G, Teflon adapter; H, Polyethylene gas disperser; I, Primary solution chamber; J, Lid for solution vessel; K, To secondary solution vessel.



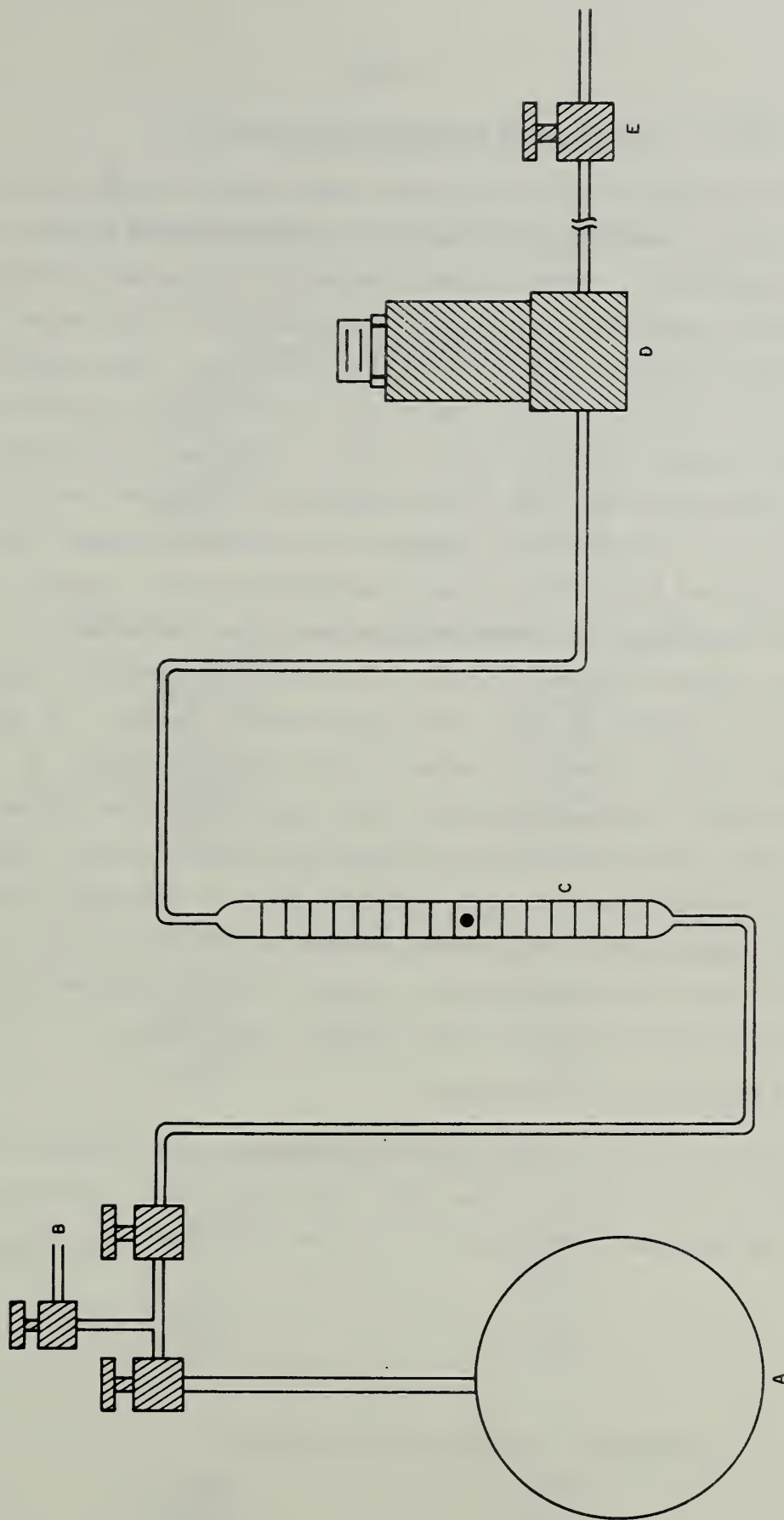


Figure 3. The Oxidizer Flow Line -  
A, Sample Container; B, Helium source;  
C, Pyrex flowmeter; D, Mass flowmeter;  
transducer; E, Valve directly preceding  
reaction vessel.

## 2.2 Water Removal from the Reaction Vessel

The water changes in the reaction vessel were checked by weighing the saturators and absorber (magnesium perchlorate) before and after each experiment. These water changes are compared in Table 1. It is generally observed that there is consistency in the water changes in the reaction vessel for a given reaction. The addition of water by the hydrogen which enters into reaction can account for the increase in water for the  $O_2-H_2$ ,  $ClF_3-H_2-H_2O$ , and  $Cl_2-H_2-H_2O$  reactions. The reactions for these experiments extended over periods ranging from 15 to 20 minutes, whereas the reaction periods for the  $Cl_2-H_2-H_{aq}$  and  $F_2-H_2-HCl_{aq}$  reactions were shorter, ranging from eight to twelve minutes. Therefore, in the latter experiments less hydrogen was reacted and as a result, less water was added, yielding an overall net removal of water from the reaction vessel. It is assumed that the net change in water in the reaction vessel is averaged over the entire experiment, which lasts for about 65 minutes. We assume also that the heat effect associated with the net change in water in the reaction vessel is a constant part of the drift of the calorimeter temperature. Therefore, no correction is applied to the temperature rise of the calorimeter, except for the condensation of water carried in by the part of the hydrogen that reacts.

## 2.3 Experimental Procedures

The procedures for conducting an experiment, the ignition system, and methods for calculations have been described [1]. For each reaction, the oxidizer was reacted in excess hydrogen -  $n_{H_2}/n_{oxidizer} = 2$ .

Table 1

## Water Changes in Reaction Vessel

Expt. No.	Water Removed g	Water Carried in g	Increase g
Oxygen-Hydrogen Reaction			
1	0.7634	0.8615	0.0981
2	0.8477	0.8574	0.0097
3	1.0371	1.0635	-0.0264
4	1.0463	0.9446	-0.1017
5	0.7795	0.8828	0.1033
6	0.7060	0.7508	+0.0448

## Chlorine Trifluoride-Hydrogen-Water Reaction

1	0.5458	0.5975	+0.0517
2	0.5959	0.5781	0.0178
3	0.7055	0.7589	-0.0534
4	0.5679	0.6636	0.0957
5	0.6038	0.6484	+0.0446
6	0.7337	0.7408	0.0071
7	0.6448	0.7184	0.0186

## Chlorine-Hydrogen-Water-Reaction

1	0.3229	0.6809	+0.3580
2	0.3016	0.5931	0.2915
3	0.5554	0.8235	0.2681
4	0.8892	1.4887	0.5995

Chlorine-Hydrogen-HF<sub>aq</sub> -Reaction

1	0.8163	0.7222	-0.0941
2	0.9960	0.8689	-0.1271
3	-	0.8010	-
4	0.7147	0.7313	+0.0166
5	0.6777	0.6136	-0.0641
6	0.8135	0.7377	-0.0758

Fluorine-Hydrogen-HCl<sub>aq</sub> - Reaction

1	0.7667	0.7328	-0.0429
2	0.8284	0.7703	-0.0581
3	0.9450	0.8921	-0.0529
4	1.0401	0.8510	-0.1891

## 2.4 The Samples

### a. Hydrogen

A commercial grade of high-purity hydrogen was used directly from the cylinder. The analysis of the sample has already been presented [1].

### b. The Oxidizer Gases

Each sample of the oxidizer gases was obtained commercially. The high-purity oxygen was obtained in a 200 cu.ft. cylinder and was transferred to a weighable spherical bulb for the calibration experiments. The pressure in the sample bulb was 17 atm. The analysis of the sample has already been presented [1].

Chlorine Trifluoride. A large sample (80 g) of the chlorine trifluoride was transferred to a 250 cm<sup>3</sup> weighable bulb for the reactions. The sampling procedure consisted of evacuating and conditioning the bulb and then filling with chlorine trifluoride by condensation with dry ice. The chlorine trifluoride was passed over activated NaF to remove the HF in the sample.

The chlorine trifluoride sample was contained as a liquid under its vapor pressure of about 0.4 atm gauge at room temperature. So that the gas and liquid phases of the sample would have similar concentrations of the impurities, a smaller container would have been more desirable. In preliminary experiments, a smaller cylindrical container was used and found to be less satisfactory because of difficulties in controlling the flame. Therefore, the 250 cm<sup>3</sup> bulbs were used and were immersed in a beaker of water (30°C) to maintain the pressure of chlorine trifluoride.



After removal of the hydrogen fluoride, the remaining impurities are more volatile than the chlorine trifluoride. It is possible that the sample becomes purer in chlorine trifluoride as a series of experiments is completed. To check this point, duplicate analyses were performed on the sample at different times. The results showed the sample to contain 0.47 and 0.45 mole % impurities.

No one method is available which can provide a complete and accurate analysis of the chlorine trifluoride sample. For this study, a combination of the mercury absorption, mass spectrometric and infrared methods are being used. The limitation of the mercury absorption method is that other reactive fluorides are absorbed with the chlorine trifluoride. The Cl-O-F compounds are possible impurities in the chlorine trifluoride sample. These gases would be absorbed by the mercury, causing an error in the overall mole percent of the  $\text{ClF}_3$ , and the absorption of these gases may liberate oxygen, causing an error in the analysis for free oxygen in the sample. Because of the unavailability of a better method for a complete analysis of the gas, mercury absorption was used and the residual gas was analyzed by mass spectrometry. The general procedures for these methods have been described [1]. An improvement in the mercury absorption introduced for these analyses was first to condition the mercury and container and then re-evacuate prior to filling to the final pressure of one atm. The results of the analyses are given in Table 2. Additional analyses on the chlorine trifluoride sample using other methods including infrared analysis are planned.

Chlorine. The chlorine was a commercial research grade sample and no attempt was made to purify it. The chlorine was determined by mercury absorption and the impurities were measured by mass spectrometry. In the mercury-absorption, it was necessary to heat the

Table 2  
Analyses of Oxidizer Gases

Constituent	Sample		
	$\text{ClF}_3$ (gas phase)	$\text{Cl}_2$	$\text{F}_2$
	Weight Percent		
$\text{ClF}_3$	99.82	-	-
$\text{Cl}_2$	-	99.93	-
$\text{F}_2$	-	-	99.85
$\text{O}_2$	.15	.02	.11
$\text{N}_2$	.01	.05	.004
Ar	*	*	*
$\text{CO}_2$	.01	*	.012
$\text{CF}_4$	*	-	.02
$\text{C}_3\text{F}_8$	*	-	*
$\text{C}_2\text{F}_6$	*	-	*
$\text{C}_4\text{F}_8$	*	-	*
$\text{SO}_2\text{F}_2$	-	-	*
$\text{SiF}_4$	-	-	*

- Not detected

\* Detected

sampling bulb to achieve complete absorption of the chlorine. The Pyrex bulb was filled to one atm and then agitated and heated gradually with hot water. The analysis of the chlorine sample is given in Table 2.

Fluorine. The analysis of the fluorine sample given in Table 2 was obtained earlier by the mercury absorption and mass spectrometric methods [2]. The fluorine was transferred to the sample bulbs using a manifold described earlier [1].

It is noted that the major impurities in the oxidizer gases are oxygen and nitrogen. It is shown later that a correction is applied to the heat measurement data for the heat of reaction of the impurity oxygen with hydrogen.

### 3. Calibration of the Calorimeter

A preliminary calibration of the calorimeter is obtained from the known heat of the oxygen-hydrogen reaction. The selected value for the heat of this reaction is based on the work of Rossini [4]. The procedures and corrections for using this reaction for calibrations are outlined by Rossini.

Table 3 shows the heat measurement data and the corrections applied for a typical experiment on the oxygen-hydrogen reaction.  $m_s$  is the mass of the oxygen sample. The mass of oxygen reacted is based on the analysis which shows the sample to be 99.987 weight percent oxygen.  $\Delta t$  (corr),  $\Delta t_c$  and  $t_{ave}$  are respectively, the corrected temperature rise, the correction to the temperature rise and the average temperature of the calorimeter.  $t(ave)$  is the temperature of the reaction. The heat corrections applied are  $q(ign)$ , the ignition energy,  $q(vap)$ , the heat effect of the condensation of the water in the reacting hydrogen, and  $q(temp)$ , the heat of tempering the reacting gases from the room temperature to  $t_{ave}$ . These corrections were applied to  $q(O_2)$ , the heat of the reacting oxygen, to

Table 3

## Calibration of the Calorimeter.

The  $O_2-H_2$  Reaction.

## Experiment 6

$m_s$ , g	2.7795
$\Delta t(\text{corr})$ , $^{\circ}\text{C}$	2.26511
$\Delta t_c$ , $^{\circ}\text{C}$	0.05849
$t(\text{ave})$ , $^{\circ}\text{C}$	30.43
$q(O_2)$ , J	-49,619
$q(\text{ign})$ , J	-28
$q(\text{vap})$ , J	-215
$q(\text{temp})$ , J	38
$q(\text{obs})$ , J	-49,824
$E$ , $\text{J}(^{\circ}\text{C})^{-1}$	21995.8
$\Delta e$ , $\text{J}(^{\circ}\text{C})^{-1}$	-6.5
$E(\text{calorim})$ , $\text{J}(^{\circ}\text{C})^{-1}$	21989.3

---

$E(\text{calorim})$ Average for 6 expts., $\text{J}(^{\circ}\text{C})^{-1}$	21983.9
Standard deviation of the mean, $\text{J}(^{\circ}\text{C})^{-1}$	4.5

---



obtain the observed heat,  $q(\text{obs})$ .  $\Delta e$  is a correction to the energy equivalent for one-half of the water formed in the reaction. The average value for six experiments is given. In an earlier study, the heat of the  $\text{O}_2\text{-H}_2$  reaction based on electrical calibrations was determined in our apparatus. The close agreement between Rossini's value and our value suggests that our procedures are valid. The standard deviation of the mean shown in Table 3 is larger (0.02%) than expected. Additional calculations of the data may reveal the reason for this standard deviation of the mean.

#### 4. The Completeness of the Reactions

For the oxygen-hydrogen reaction, the amount of reaction is based on the weight of oxygen introduced into the reaction vessel. Earlier comparisons between the amount of oxygen reacted and the amount of water formed showed that the oxygen was completely reacted.

The completeness of the  $\text{ClF}_3\text{-H}_2\text{-H}_2\text{O}$  reaction was determined by analyses of the product solutions. Each solution was analyzed for  $\text{H}^+$ , and for two typical experiments analyses were performed for  $\text{Cl}^-$  and  $\text{F}^-$ . These results are given in Table 4.  $n_{\text{H}^+}(\text{obs})/n_{\text{H}^+}(\text{calc})$  for these experiment resembles the results for the  $\text{F}_2\text{-H}_2\text{-H}_2\text{O}$  reactions [1]. The generally low values can be explained by the extremely reactive nature of the product acid mixture  $[\text{HCl}\cdot 3\text{HF}]$  the lowest value for experiment 1 suggests that more conditioning of the combustion chamber took place in that experiment. No explanation is offered for the erratic but favorable value for experiment 6.

A comparison between the  $n_{\text{Cl}^-}$  and  $n_{\text{F}^-}$  shows a value of 0.3337, which agrees fairly closely with the theoretical ratio of 0.3333. This suggests that very little, if any of the  $\text{ClF}_3$  sample is other Cl-F compounds. The presence of these would change the value for  $n_{\text{Cl}^-}/n_{\text{F}^-}$ .

Table 4

The Completeness of the  $\text{ClF}_3\text{-H}_2\text{-H}_2\text{O}$  Reaction

Experiment No.	$m_s$ g	$n(\text{HF}+\text{HCl}), \text{obs}$ moles	$\frac{n_{\text{H}^+}(\text{obs})}{n_{\text{H}^+}(\text{calc})}$
1	5.3218	0.22313	0.9710
2	5.5074	.23262	.9782
3	5.3577	.22461	.9757
4	5.1142	.21545	.9756
5	4.4999	.19024	.9790
* 6	5.2142	.22349	.9926
7	4.9769	.21035	.9787

---


$$*n_{\text{Cl}^-} = 0.05579 \text{ mole}$$

$$n_{\text{F}^-} = 0.16716 \text{ mole}$$

$$\frac{n_{\text{Cl}^-}}{n_{\text{F}^-}} = 0.3337$$

All of the analyses for the  $\text{ClF}_3$  experiments were performed in the Analytical Chemistry Division at the National Bureau of Standards. The  $\text{H}^+$  and  $\text{Cl}^-$  were determined by the conductometric method and the  $\text{F}^-$  was measured by potentiometric titration with  $\text{La}(\text{NO}_3)_3$ .

The data for the  $\text{Cl}_2\text{-H}_2\text{-H}_2\text{O}$  and  $\text{Cl}_2\text{-H}_2\text{-HF}_{\text{aq}}$  reactions are given in Table 5. The reactions are generally more complete than the  $\text{ClF}_3\text{-H}_2\text{-H}_2\text{O}$  reactions. The  $n_{\text{Cl}^-}/n_{\text{H}^+}$  is larger than the stoichiometric, suggesting that the amount of acid not recovered is consumed by corrosion.

## 5. Reaction Heat Measurements

$\text{ClF}_3\text{-H}_2\text{-H}_2\text{O}$ . Typical reaction quantities for this system are given in Table 6.  $n_{\text{ClF}_3}$  (reacted) is based on  $n_{\text{H}^+}(\text{obs})$ , and  $\Delta n_{\text{ClF}_3}(\text{corros})$  is based on  $n_{\text{H}^+}(\text{calc-obs})$ . The other notations have the same meaning given earlier [1].

The typical heat measurements and the corrections to the heat data are given in Table 7. With the exception of  $\Delta e$ ,  $q(\text{corros})$  and  $q'_{\text{ClF}_3}$ , the symbols have the same meaning as for the oxygen-hydrogen experiments.  $\Delta e$  is a correction to the energy equivalent for one-half the product formed.  $q(\text{corros})$  corrects for the corrosion by  $\text{ClF}_3$ .  $q_{\text{ClF}_3}$  is the total heat without  $q(\text{corros})$  and  $q'_{\text{ClF}_3}$  includes  $q(\text{corros})$ . In calculating  $q(\text{corros})$ , it is assumed that the  $\text{ClF}_3$  reacts with nickel to give  $\text{NiCl}_2$  and  $\text{NiF}_2$ .

The heat of the  $\text{ClF}_3\text{-H}_2\text{-H}_2\text{O}$  reaction is given in Table 8. Similar to the earlier work the heat of reactions were calculated in three different ways [1]. Referring to Table 7,  $\Delta H(1)$  is  $q_{\text{ClF}_3}/n_{\text{H}^+}(\text{calc})$ ;  $\Delta H(2)$  is  $q_{\text{ClF}_3}/n_{\text{H}^+}(\text{obs})$ , and  $\Delta H(3)$  is  $q'_{\text{ClF}_3}/n_{\text{H}^+}(\text{obs})$ . We assume that  $\Delta H(3)$  is the most valid treatment of the data because it is based on the heat effect, corrected for corrosion, which the reaction showed evidence of, and also because  $n_{\text{H}^+}(\text{obs})$  is the actual amount of acid present in the solution. The  $\Delta H(2)$  and  $\Delta H(1)$  values for experiment six suggest that the good recovery of the acid as shown in Table 4



may be high. This is suggested also because the standard deviation of the mean for  $\Delta H(1)$  where the amount of reaction is based on  $n_{H^+}(\text{calc})$  is lower than that for  $\Delta H(3)$  based on  $n_{H^+}(\text{obs})$ . A check on the analyses for experiment six may explain the discrepancy. In the meantime, the average value for  $\Delta H(3)$  is used in the calculation of the heat of formation of chlorine trifluoride.

Calculations similar to those given for the  $\text{ClF}_3\text{-H}_2\text{-H}_2\text{O}$  reaction were made for the  $\text{Cl}_2\text{-H}_2\text{-H}_2\text{O}$  and  $\text{Cl}_2\text{-H}_2\text{-HF}_{\text{aq}}$  solutions and the results are given in Tables 9-11. The notations have been explained for the  $\text{ClF}_3\text{-H}_2\text{-H}_2\text{O}$  experiment. Table 10 shows typical calculations for  $\Delta H(1)$ ,  $\Delta H(2)$ , and  $\Delta H(3)$ .  $q(\text{corros})$  is based on the heat of the reaction of chlorine with nickel.

Table 11 gives the values of  $\Delta H(1)$ ,  $\Delta H(2)$  and  $\Delta H(3)$ . The uncertainty figures are the standard deviation of the mean and do not represent the overall uncertainty in the heats of reaction. We assume here also that  $\Delta H(3)$  is the most accurate treatment of the data. We observe that the average values for the heat of formation  $[\text{HCl}\cdot\text{H}_2\text{O}]$  and  $[\text{HCl}\cdot\text{HF}_{\text{aq}}]$  differ by  $0.22 \text{ kcal mol}^{-1}$ , but become identical when the standard deviation of the mean is applied to each. The preliminary value for  $\Delta H_f[\text{HCl}\cdot 50\text{H}_2\text{O}]$  of  $-39.71 \text{ kcal mol}^{-1}$  can be compared with the "selected" value of  $-39.521 \text{ kcal mol}^{-1}$  [1].

Preliminary data for the  $\text{F}_2\text{-H}_2\text{-HCl}_{\text{aq}}$  reaction are given in Tables 12 and 13. These results are based on the amount of fluorine reacted. The notations used are the same as described for the earlier reactions.

In Table 14, the preliminary value for the heat of formation of chlorine trifluoride is calculated. This value can be compared with the current selected values of  $-38. [3]$  and  $-38.869 \pm 1.0 [5] \text{ kcal mol}^{-1}$ .



Table 5

The Completeness of the  
 $\text{Cl}_2\text{-H}_2\text{-H}_2\text{O}$  and  $\text{Cl}_2\text{-H}_2\text{-HF}_{\text{aq}}$  Reactions

Experiment No.	$m_s$  g	$n_{\text{HCl}}(\text{obs})$  moles	$\frac{n_{\text{HCl}}(\text{obs})}{n_{\text{HCl}}(\text{calc})}$
<hr/>			
$\text{Cl}_2\text{-H}_2\text{-H}_2\text{O}$			
1	9.6607	0.26976	0.9907
2	6.7661	.19053	.9990
*3	6.6417	.18702	.9990
4	7.6865	.21625	.9982
<hr/>			
$\text{Cl}_2\text{-H}_2\text{-HF}_{\text{aq}}$			
1	2.1408	0.06019	0.9975
2	2.5748	.07250	.9989
3	4.4517	.12526	.9982
4	4.5999	.12793	-
5	2.2925	.06416	.9923
<hr/>			

$$*n_{\text{Cl}}(\text{obs}) = 0.18715 \text{ mole}$$

$$\frac{n_{\text{Cl}}(\text{obs})}{n_{\text{H}^+}} = 1.0007$$

Table 6

The  $\text{ClF}_3\text{-H}_2\text{-H}_2\text{O}$  Reaction  
Typical Reaction Quantities

Expt. No.	6
$n_{\text{H}^+}(\text{calc}), \text{ moles}$	0.22516
$n_{\text{H}^+}(\text{obs}), \text{ moles}$	.22349
$n_{\text{ClF}_3}(\text{reacted}), \text{ moles}$	.055873
$\Delta n_{\text{ClF}_3}(\text{corros}), \text{ moles}$	.00042
$n_{\text{H}_2\text{O}}, \text{ moles}$	5.55
$n_{\text{H}_2\text{O}}/n_{\text{HF}}$	84
$n_{\text{H}_2\text{O}}/n_{\text{HCl}}$	33

Table 7

The  $\text{ClF}_3\text{-H}_2\text{-H}_2\text{O}$  Reaction  
Typical Heat Measurements

Expt. No.	6
$m_s$ , g	5.2142
$\Delta t_{\text{(corr)}}$ , °C	2.48202
$\Delta t_c$ , °C	.05437
$t(\text{ave})$ , °C	30.69
$\Delta e$ , $\text{J}(\text{°C})^{-1}$	6.5
$E(\text{calorim})$ , $\text{J}(\text{°C})^{-1}$	21990.4
$q(\text{obs})$ , J	54581

---

Corrections to the heat measurements

---

$q(\text{ign})$ , J	-33
$q(\text{O}_2)$ , J	-131
$q(\text{vap})$ , J	-144
$q(\text{temp})$ , J	36
$q(\text{corros})$ , J	-421
$q_{\text{ClF}_3}$ , J	-54303
$q_{\text{ClF}_3}$ , J	-53882

Table 8

The Heat of the  $\text{ClF}_3\text{-H}_2\text{-H}_2\text{O}$  Reaction. 303°K  
 $\text{ClF}_3(\text{g}) + 2\text{H}_2(\text{g}) + 100\text{H}_2\text{O}(\text{l}) \rightarrow [\text{HCl} \cdot 3\text{HF} \cdot 100\text{H}_2\text{O}](\text{l})$

Expt. No.	$-\Delta\text{H}(1)$	$-\Delta\text{H}(2)$	$-\Delta\text{H}(3)$
	$\text{kJ}(\text{mol ClF}_3)^{-1}$		
2	963.51	985.06	962.64
3	962.74	987.09	961.74
4	962.57	986.70	961.58
5	964.61	985.30	963.81
6	964.70	981.95	964.42
7	963.65	984.54	962.80
Av.	963.63	985.11	962.83
s.d.m.	.37	.75	.45



Table 9

The  $\text{Cl}_2\text{-H}_2\text{-H}_2\text{O}$  and  $\text{Cl}_2\text{-H}_2\text{-HFaq}$ .  
Typical Reaction Quantities

	$\text{Cl}_2\text{-H}_2\text{-H}_2\text{O}$	$\text{Cl}_2\text{-H}_2\text{-HFaq}$
Experiment No.	4	1
$n_{\text{HCl}}$ (calc), mole	0.21625	0.06034
$n_{\text{HCl}}$ (obs), mole	0.21636	0.06019
$n_{\text{HF}}$ , mole	-	.16665
$n_{\text{H}_2\text{O}}$ , mole	5.55	5.45
$n_{\text{HCl}}$ (obs)- $n_{\text{HCl}}$ (calc)	.00028	.00015
$\Delta n_{\text{Cl}_2}$ (corros)	.00014	.00008
$n_{\text{H}_2\text{O}}/n_{\text{HCl}}$	25.7	90.3
$n_{\text{H}_2\text{O}}/n_{\text{HF}}$	-	32.7
$n_{\text{HCl}} \cdot n_{\text{HF}}$	-	0.36

Table 10

The  $\text{Cl}_2\text{-H}_2\text{-H}_2\text{O}$  and  $\text{Cl}_2\text{-H}_2\text{-HFaq}$  Reactions  
Typical Heat Measurements

Expt. No.	$\text{Cl}_2\text{-H}_2\text{-H}_2\text{O}$ 4	$\text{Cl}_2\text{-H}_2\text{-HFaq}$ 6
$m_s$ , g	7.6865	1.5869
$\Delta t(\text{corr})$ , $^{\circ}\text{C}$	1.63739	.33382
$\Delta t_c$ , $^{\circ}\text{C}$	.04724	.02717
$t(\text{ave})$ , $^{\circ}\text{C}$	30.92	30.33
$\Delta e$ , $\text{J}(^{\circ}\text{C})^{-1}$	6.3	-7.1
$E(\text{calorim})$ , $\text{J}(^{\circ}\text{C})^{-1}$	21998.9	21985.5
$q(\text{obs})$ , J	36020	7339
Corrections to the heat measurements		
$q(\text{ign})$ , J	-28	-15
$q(\text{O}_2)$ , J	-23	-6
$q(\text{vap})$ , J	-132	-27
$q(\text{temp})$ , J	40	9
$q(\text{corros})$ , J	-3	-
$q_{\text{Cl}_2}$ , J	-35861	-7297
$q_{\text{Cl}_2}/n(\text{calc})$ , $\text{kJ}(\text{mol soln})^{-1}$	-166.21	-165.08
$q'_{\text{Cl}_2}/n(\text{obs})$ , $\text{kJ}(\text{mol soln})^{-1}$	-166.51	-164.60
$q'_{\text{Cl}_2}/n(\text{obs})$ , $\text{kJ}(\text{mol soln})^{-1}$	-165.83	-163.72

Table 11

The Heats of the  $\text{Cl}_2\text{-H}_2\text{-H}_2\text{O}$  and  $\text{Cl}_2\text{-H}_2\text{-HFaq}$  Reactions. 303°K

Experiment No.	$-\Delta\text{H}(1)$ kJ	$-\Delta\text{H}(2)$ kJ	$-\Delta\text{H}(3)$ kJ	$n_{\text{HF}}$
$\frac{1}{2}\text{Cl}_2(\text{g}) + \frac{1}{2}\text{H}_2(\text{g}) + 50\text{H}_2\text{O}(\text{l}) \rightarrow [\text{HCl} \cdot 50\text{H}_2\text{O}](\text{l})$				
1	165.64	167.19	165.70	
2	166.50	166.65	165.63	
3	167.13	167.29	166.30	
4	167.30	167.60	166.42	
Av. kJ(mol soln) <sup>-1</sup>	$166.43 \pm 0.39$	$167.18 \pm 0.20$	$166.14 \pm 0.3$	
kcal(mol soln) <sup>-1</sup>	$39.78 \pm .09$	$39.96 \pm .05$	$39.71 \pm .07$	
$\frac{1}{2}\text{Cl}_2(\text{g}) + \frac{1}{2}\text{H}_2(\text{g}) + [\text{nHF} \cdot 50\text{H}_2\text{O}](\text{l}) \rightarrow [\text{HCl} \cdot \text{nHF} \cdot 50\text{H}_2\text{O}](\text{l})$				
1	165.83	167.16	165.06	2.76
2	165.01	165.95	164.28	2.29
3	166.74	167.03	166.32	1.33
4	165.79	168.03	167.25	1.30
5	164.85	166.90	165.02	2.60
6	164.53	164.05	163.17	3.74
Av. kJ(mol soln) <sup>-1</sup>	$165.46 \pm 0.33$	$166.52 \pm 0.56$	$165.18 \pm 0.59$	
kcal(mol soln) <sup>-1</sup>	$39.54 \pm .08$	$39.80 \pm .13$	$39.48 \pm .14$	

Table 12

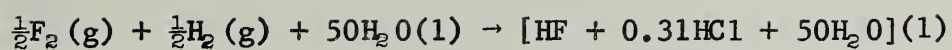
The  $F_2-H_2-HCl_{aq}$  Reaction  
Typical Heat Measurements.

Expt. No.	3
$m_s$ , g	3.3330
$\Delta t(\text{corr})$ , $^{\circ}\text{C}$	2.55912
$\Delta t_c$ , $^{\circ}\text{C}$	0.05977
$t(\text{ave})$ , $^{\circ}\text{C}$	30.51
$\Delta e$ , $\text{J}(^{\circ}\text{C})^{-1}$	-3.4
$E(\text{calorim})$ , $\text{J}(^{\circ}\text{C})^{-1}$	21980.5
$q(\text{obs})$ , J	56251
<hr/> Corrections to the heat measurements <hr/>	
$q(\text{ign})$ , J	-51
$q(O_2)$ , J	-86
$q(\text{vap})$ , J	-112
$q(\text{temp})$ , J	28
$q_{F_2}$ , J	56030
$n_{HF}(\text{calc})$ , moles	0.17518
$\Delta H_{F_2}$ , $\text{kJ}(\text{mol HF soln})^{-1}$	-319.84



Table 13

The Heat of the  $\text{F}_2\text{-H}_2\text{-HCl}_{\text{aq}}$  Reaction. 303.6°K



Expt. No.	$n_{\text{HF}}$ mole	$n_{\text{HCl}}$ mole	$n_{\text{H}_2\text{O}}/n_{\text{HF}}$	$-\Delta H_{\text{R}}$ $\text{kJ}(\text{mol HF soln})^{-1}$
1	0.11626	0.0549	48	320.50
2	0.17518	0.0549	32	319.84
3	0.13190	0.0549	42	318.84
Average				319.72

Table 14

Preliminary Calculation of the  
Heat of Formation of Chlorine Trifluoride.

		$\Delta H_R(303^\circ \text{K})$ kJ
(1)	$\text{ClF}_3(\text{g}) + 2\text{H}_2(\text{g}) + 100\text{H}_2\text{O}(\text{l}) \rightarrow [3\text{HF} \cdot \text{HCl} \cdot 100\text{H}_2\text{O}](\text{l})$	-962.83
(2)	$\frac{1}{2}\text{Cl}_2(\text{g}) + \frac{1}{2}\text{H}_2(\text{g}) + [3\text{HF} \cdot 100\text{H}_2\text{O}](\text{l}) \rightarrow [3\text{HF} \cdot \text{HCl} \cdot 100\text{H}_2\text{O}](\text{l})$	-165.18
(3)	$\frac{3}{2}\text{F}_2(\text{g}) + \frac{3}{2}\text{H}_2(\text{g}) + [\text{HCl} \cdot 100\text{H}_2\text{O}](\text{l}) \rightarrow [3\text{HF} \cdot \text{HCl} \cdot 100\text{H}_2\text{O}](\text{l})$	-959.19
(4)	$\frac{1}{2}\text{Cl}_2(\text{g}) + \frac{3}{2}\text{F}_2(\text{g}) \rightarrow \text{ClF}_3(\text{g})$	$\left\{ \begin{array}{l} -161.54 \\ -38.61 \text{ kcal} \end{array} \right.$

## References

1. R. C. King and G. T. Armstrong, J. Res. NBS 72A, 113 (1968).
2. E. S. Domalski and G. T. Armstrong, J. Res. NBS 71A, 195-202 (1967).
3. D. D. Wagman, W. H. Evans, I. Halow, V. B. Parker, S. M. Bailey, and R. H. Schumm, Selected Values of Chemical Thermodynamic Properties, Part 1. Tables for the First Twenty-Three Elements in the Standard Order of Arrangement, NBS Technical Note 270-1 (U. S. Government Printing Office, Washington, D. C. 20402, 1965).
4. F. D. Rossini, J. Res. NBS 6, 1 (1931) R. P. 259; see also Chapter 4 Experimental Thermochemistry, ed. F. D. Rossini (Interscience Publishers, Inc., New York, N. Y., 1956).
5. JANAF Thermochemical Tables, PB 168370, Dow Chemical Co., Midland, Michigan (Clearinghouse for Federal Scientific and Technical information, Springfield, Va., August 1966).

The heat capacity of very fine powders is expected to be higher than that of large crystals, the relative effect of particle size becoming larger with decrease in temperature. The values of heat capacity of MgO powder of average cube size of  $2 \times 10^{-8}$  m (200Å) reported by Giaque and Archibald [7] are considerably higher than those of large fused MgO crystals reported by Barron, Berg, and Morrison [2] (130% at 20 K, 17% at 50 K, 7% at 100 K, 3.5% at 150 K, 2.6% at 200 K, and 1.3% at 250 K). Kelley [15] reported heat-capacity measurements on BeO powder of unspecified crystallite size. The measurements reported by Aslanian and Weil [1] and by Gmelin [8] were on samples from the same source prepared by hot sintering under pressure (sintering temperature unspecified). Aslanian and Weil [1] reported that the three measurements (between 2 and 4 K) made on the sample (as received, annealed at 800 C, and annealed at 1200 C) were the same within the experimental accuracy.

Commercially available beryllium oxide powder is usually prepared by thermal decomposition of the hydroxide, the hydroxide being obtained by precipitation from the halide, sulfate, or acetate solution by increasing the pH. The crystallite size of the powder is dependent largely upon the decomposition temperature. Duval and Duval [3] interpreted their thermal gravimetric analysis work to indicate that the decomposition of  $\text{Be}(\text{OH})_2$  to BeO and  $\text{H}_2\text{O}$  starts around 150 C and complete decomposition occurs only on heating to 951 C. Funston, Kirkpatrick, and Turner [4] reported a flat in the thermogram of the decomposition process at about 850 C. The crystallite size of the BeO powder obtained by decomposing  $\text{Be}(\text{OH})_2$  (precipitated from beryllium basic acetate  $(\text{Be}_4\text{O}(\text{OCOCH}_3)_6)$  at 850 to 1000 C was reported by Funston et al [4] to be around  $2$  to  $5 \times 10^{-8}$  m (200 to 500 Å). Calcination at higher temperatures yield larger crystallites [4].



The sample investigated by Kelley [15] was assumed to be a very fine powder, considering the probable method of preparation and the expected particle size discussed above. For the heat-capacity measurements presented in this report the BeO sample was sintered at 1700 to 1800°C for about 24 hours in order to obtain large crystallites. The results of the measurements obtained on the sample of average crystallite size of  $3 \times 10^{-5}$  m were found to be considerably lower than those reported by Kelley [15]. The values were so extremely different that repeat measurements on a sample of even larger crystallite were considered to be desirable. A BeO sample prepared by arc fusion and of fairly uniform crystallite size of about  $6 \times 10^{-5}$  m was subsequently obtained. Since the measurements on the second sample are being delayed because of pressing work on other substances and since the measurements on the second sample will probably show relatively small differences, if any, the results of the measurements on the first sample are being given in this report. (The crystallite sizes of the two samples are not widely different.)

## II. Sample

In order to obtain a BeO sample of large crystallite size, commercially available high-purity BeO powder was pelletized by F. P. Knudsen of the Inorganic Materials Division of the Bureau into short cylinders of about 3/8" diameter and 1/8" long. The pellets were then fired in a gas furnace at about 1700 to 1800°C for 24 hours. Some erosion and, consequently, reduction in the size of the pellets occurred through vaporization of BeO in presence of water vapor at the furnace temperatures [10, 13, 25].

Spectrochemical analysis of the sintered sample by B. F. Scribner of the Spectrochemical Analysis Section of the Bureau showed the impurities given in Table 1.

A petrographic (microscopic) examination of the BeO sample was made by A. Van Valkenburg of the Crystallography Section of the Bureau. The crystallites were found to have an average length of about  $3 \times 10^{-5}$  m with the smallest ones about  $1 \times 10^{-6}$  m. The crystals were clear with some voids.

Since the BeO pellets were slightly too large, they were split into halves along their axes and introduced into the calorimeter sample vessel through its 1/4" opening [5]. The vessel containing the sample was alternately pumped to a high vacuum and purged several times with dry helium gas and finally sealed with  $1.316 \times 10^4$  N/m<sup>2</sup> (98.7 mm Hg) pressure of helium gas. The mass of sample investigated was 77.354 g.

### III. Apparatus and Method

The heat-capacity measurements on the BeO sample were carried out in an adiabatic calorimeter very similar in principle and design to that described previously [21]. The sample vessel was suspended within the adiabatic shield system by means of a nylon string instead of the filling tube shown in the above reference. Details of the calorimeter design and its operation will be described in a subsequent publication.

Briefly, the calorimeter sample vessel, constructed principally of copper, was a short cylinder with spherical sections for its ends. A re-entrant well, located at the axis with its opening at the bottom of the vessel, contained a heater-platinum resistance thermometer assembly. In order to attain rapid temperature equilibrium, copper vanes were arranged radially from the central well to the outer wall of the vessel. A thin coating of pure tin applied to the entire inner surfaces held the vanes in good thermal contact with the vessel and provided a chemically inert surface. The space between the vanes was no greater than 8 mm. A specially designed gold-gasket, screw-cap closure was attached at the top of the vessel. The outer surface of

the vessel was gold plated and polished. A thin gold-plated copper shell enclosed the sample vessel to provide a more reproducible surface temperature for adiabatic control. The shell was in good thermal contact with the sample vessel around a ring located on the upper cylindrical portion of the vessel.

The adiabatic shield was constructed entirely of copper. It was a cylindrical shell with conical ends. Heater wires were wound on the outer surface. The inner surface was gold plated and polished to minimize the heat transfer by radiation.

Constantan versus Chromel-P differential thermocouples were attached to the adiabatic shield and to the outer thin shell of the sample vessel for temperature control. During the heat-capacity measurements the shield temperature was maintained as close as possible to that of the thin shell of the sample vessel by means of the thermocouples and the shield heaters.

The electrical power to the calorimeter heater was measured by means of a Wenner potentiometer in conjunction with a saturated standard cell, volt box, and standard resistors. The standard cell and the standard resistors were calibrated at the National Bureau of Standards in terms of the United States standards of emf and ohm. A constant-current power supply stable to about 2ppm was used to furnish electrical power to the calorimeter heater. The duration of each heating interval was determined by means of a high-precision interval timer operated on the 60-Hz frequency standard provided by the National Bureau of Standards. The 60-Hz frequency standard is based on a 100-kHz quartz oscillator which is stable to 1 part in  $10^{10}$  over a 24-hour period. The 100-kHz oscillator is maintained in terms of the 60-kHz broadcast from WWVB. An electronic counter containing a 1-MHz quartz oscillator was used simultaneously in the measurement of the heating interval. The estimated uncertainty, including the asymmetry in the on-off switch operation to the calorimeter heater, in the determination of the heating interval is not greater than



$\pm 0.01$  sec for any heating period, none of which was less than 2 min in these experiments.

Temperatures were determined by means of a platinum-resistance thermometer installed in the re-entrant well of the calorimeter vessel. At the time of these measurements the resistance of the thermometer was measured with a high-precision manually operated Mueller bridge capable of measurements up to 422.11110 ohms to the nearest 0.00001 ohm. (At present an automatic Mueller bridge is being used.) The thermometer (laboratory designation: L-18) was calibrated above 90 K in accordance with the 1948 International Practical Temperature Scale [22]. The temperatures in kelvin were obtained by adding 273.15 to the temperatures in degrees Celsius ( $^{\circ}\text{C}$ ). Below 90 K, the thermometer was calibrated on the NBS-1955 provisional scale which is numerically 0.01 K lower than the former NBS-1939 provisional scale [12].

#### IV. Results

Two series of heat-capacity measurements were carried out, one on the calorimeter vessel with the sample (gross) and the other on the empty vessel (tare). The measured energy increments ( $\Delta Q$ ) and the corresponding thermometer resistances ( $R$ ) before and after heating [Chapter 2, NBS Report No. 9500, issued 1 January 1967] were analyzed on the high-speed digital computer to obtain  $dQ/dR$  of the sample (net) as a function of the thermometer resistance [6]. After adjusting for the heat capacity of the helium exchange gas and for the small difference in the mass of the vessel for the tare and gross measurements, the values of heat capacity ( $dQ/dT$ ) of the sample were then calculated at equally spaced integral temperatures from the  $R$  versus  $T$  calibration and  $dR/dT$  for the thermometer using the relation:

$$dQ/dT = (dQ/dR)(dR/dT) . \quad (1)$$

Briefly, the procedure was to obtain the polynomial equation of the form

$$dQ/dR = \sum_{n=0}^N a_n ((\ln R)/R)^n \quad (2)$$



to represent the experimental data on the empty calorimeter vessel (tare). The polynomial equation for the empty vessel was then evaluated to obtain values of  $\Delta Q$  (tare) corresponding to the thermometer resistance intervals observed for the gross measurements in order to obtain the energy increments for sample only, i.e.,

$$\Delta Q(\text{sample}) = \Delta Q(\text{gross}) - \Delta Q(\text{tare}). \quad (3)$$

The best polynomial equation giving  $dQ/dR$  for sample only was next obtained and  $dQ/dT$  calculated according to eq. (1) above. For the sample an equation of the form

$$dQ/dR = \sum a_n R^n \quad (4)$$

was found to fit the data adequately.

Figure 1 shows the percentage deviation of the experimental data on the empty vessel from the polynomial equation fitted to the data by the method of least squares. A fifteenth degree polynomial equation (eq. (2),  $n = 0$  to  $n = 15$ ) was found to fit the data from 15 to 370 K well within  $\pm 0.04$  percent. The slight trend shown in the figure suggests that a better equation could be obtained, but the maximum deviations are small enough to be negligible for the present study. The first and second derivatives of the equation were found also to have the properties expected of a "heat-capacity curve".

Figures 2 and 3 show the deviation of the sample data (net) from the final smooth values based upon the polynomial equation (eq. (4),  $n$  ranging from -1 to +8) fitted to the data in the range 15 to 370 K combined with the extrapolation of the data to 0 K as shown in Figure 4. The values of  $dQ/dT$  obtained from the polynomial were adjusted slightly below 40 K to be consistent with the extrapolated values to 0 K. Figure 4 shows the  $C/T^3$  versus  $T$  plot of the final values of heat capacity extrapolated to 0 K. The values of heat capacity on MgO reported by Barron, Berg, and Morrison [2] were used as a guide in the extrapolation. The observed values of heat capacity on BeO are shown for comparison with the extrapolation. The Debye characteristic temperature  $\theta$  at 0 K corresponds to 1269 K (0 K intercept =  $(2 \times 12 \pi^4/5)(1/\theta^3)$ ).

Considering the precision of the measurements and the possible systematic errors, the estimated uncertainty in the smoothed values of heat capacities is 0.1 percent above 100 K. Below 100 K the net heat capacity becomes a progressively smaller fraction of the gross heat capacity with decrease in temperature. At the lowest temperature of the measurements (15.6 K) the heat capacity of the sample constituted only 2.3 percent of the gross, hence the uncertainty in the values at 15 K may be as high as 5 to 10 percent.

The thermodynamic properties were calculated by tabular numerical integration using the values of heat capacity obtained from 0 to 370 K with the usual thermodynamic relations:

$$H_T - H_{0\text{ K}}^{\circ} = \int_0^T C dT, \quad (5)$$

$$S_T = \int_0^T (C/T) dT, \quad (6)$$

and

$$G_T - H_{0\text{ K}}^{\circ} = (H_T - H_{0\text{ K}}^{\circ}) - TS_T.$$

The values are given in Table 2.

The values of heat capacity reported by previous investigators are compared with the present measurements in Figure 5. The values reported by Kelley [15] and those by Gmelin [8] are for most of the temperature range of the measurements unusually higher than the values found in the present study. The deviations of the values reported by Kelley [15] were found to increase with decrease in temperature. At 55 K the deviation is +45 percent and from about 200 to 290 K the deviations do not exceed 1 percent. The values reported by Gmelin [8] are on the average about 20 percent higher between 15 and 75 K. The extrapolated values (below 15 K) obtained for this report are higher than the experimental values reported by Gmelin [8]. The Debye characteristic temperature reported by Gmelin is 1400  $\pm$  10 K as

compared to 1269 K taken for this study. The values reported by Günther [11] are about 30 percent lower.

The enthalpy difference between 273.15 and 373.15 K obtained from the heat-capacity measurements (Table 2) was compared with the experimental relative enthalpy values reported by Victor and Douglas [23]. Victor and Douglas reported measurements on two samples. Sample 1 consisting of crystallites of  $2.5 \times 10^{-5}$  m on an edge was similar to the sample used in the present study. Sample 2 was needle-like,  $1 \times 10^{-5}$  m in length and  $1 \times 10^{-6}$  m in cross section. The comparison is summarized in Table 3. The results of the present study are between the values reported by Victor and Douglas for the two samples. The agreement is within a few tenths of a percent of either sample.

The unusually large deviation in the values of heat capacity at the lower temperatures with fairly close agreement at the higher temperatures can be ascribed to the particle size effects [2,16,17]. The increasing positive deviation with decrease in temperature of the values reported by Kelley [15] suggests that his sample was probably very finely divided. The heat treatment of the samples investigated by Gmelin [8] suggests that his samples and the sample used in the present study were similar. The wide deviations in the results shown in Figure 5 are probably due to experimental differences. Finely divided samples are subject to contamination by adsorbed impurities. Unless special precautions are taken to remove the adsorbed impurities, significant variations in the experimental heat capacities would be expected from the impurities present, any change in the surface properties, or compound formation at the surface.

The new values of heat capacity are now being combined with other high temperature relative enthalpy data up to 2500 K. A combined table of thermodynamic properties will be presented in the forth-coming semi-annual report. The measurements on the second sample of BeO are being considered for the near future.

Table 1

Spectrochemical Analysis of the  
Sintered Beryllium Oxide (BeO) Pellet

<u>Element</u>	<u>Parts per Million</u>
Al	40
Ca	200
Fe	10
Mg	<15
Mn	<10
Si	25

The limit of detection for Ti was 20 ppm and for  
P was 200 ppm



TABLE 2

## THERMODYNAMIC FUNCTIONS FOR BERYLLIUM OXIDE (BE O )

## SOLID PHASE

1 MOL = 0.0250116 KG

CAL = 4.1840 J

$$K = 273.15 + ^\circ C$$

T	$-(G_T^0 - H_C^0)/T$	$(H_T^0 - H_C^0)/T$	$(S_T^0 - S_C^0)$	$(H_T^0 - H_C^0)$	$C_P^0$	$-(G_T^0 - H_C^0)$
K	$\frac{\text{CAL}}{\text{K} \cdot \text{MOL}}$	$\frac{\text{CAL}}{\text{K} \cdot \text{MOL}}$	$\frac{\text{CAL}}{\text{K} \cdot \text{MOL}}$	$\frac{\text{CAL}}{\text{MOL}}$	$\frac{\text{CAL}}{\text{K} \cdot \text{MOL}}$	$\frac{\text{CAL}}{\text{MOL}}$
.00	.000	.000	.000	.000	.000	.000
5.00	.000	.000	.000	.000	.000	.000
10.00	.000	.000	.000	.001	.000	.000
15.00	.000	.000	.001	.006	.002	.002
20.00	.000	.001	.001	.018	.004	.006
25.00	.001	.002	.002	.045	.007	.015
30.00	.001	.003	.004	.094	.013	.031
35.00	.002	.005	.007	.176	.020	.058
40.00	.002	.008	.010	.304	.031	.099
45.00	.004	.011	.015	.495	.046	.160
50.00	.005	.015	.020	.770	.065	.247
55.00	.007	.021	.028	1.153	.089	.366
60.00	.009	.028	.037	1.674	.120	.526
65.00	.011	.036	.048	2.367	.158	.736
70.00	.014	.047	.061	3.264	.202	1.007
75.00	.018	.059	.077	4.402	.254	1.350
80.00	.022	.073	.095	5.820	.314	1.778
85.00	.027	.089	.116	7.560	.383	2.305
90.00	.033	.107	.140	9.661	.458	2.944
95.00	.039	.128	.167	12.155	.540	3.710
100.00	.046	.151	.197	15.077	.630	4.619
105.00	.054	.176	.230	18.463	.726	5.685
110.00	.063	.203	.266	22.349	.829	6.924
115.00	.073	.233	.305	26.769	.939	8.351
120.00	.083	.265	.348	31.753	1.055	9.983
125.00	.095	.299	.393	37.331	1.177	11.834
130.00	.107	.335	.442	43.532	1.304	13.921
135.00	.120	.373	.494	50.380	1.436	16.259
140.00	.135	.414	.548	57.899	1.572	18.862
145.00	.150	.456	.606	66.108	1.712	21.747
150.00	.166	.500	.666	75.027	1.856	24.926
155.00	.183	.546	.730	84.671	2.002	28.415
160.00	.201	.594	.795	95.053	2.151	32.227
165.00	.220	.644	.864	106.19	2.302	36.374
170.00	.240	.695	.935	118.08	2.455	40.871
175.00	.261	.747	1.008	130.73	2.609	45.728
180.00	.283	.801	1.084	144.16	2.763	50.958
185.00	.306	.856	1.162	158.37	2.918	56.572
190.00	.329	.912	1.242	173.35	3.074	62.580
195.00	.354	.970	1.324	189.10	3.229	68.992
200.00	.379	1.028	1.407	205.63	3.384	75.819
205.00	.405	1.088	1.493	222.94	3.538	83.068
210.00	.432	1.148	1.580	241.01	3.691	90.748
215.00	.460	1.209	1.668	259.84	3.843	98.868
220.00	.488	1.270	1.759	279.44	3.994	107.44
225.00	.518	1.332	1.850	299.78	4.143	116.46
230.00	.548	1.395	1.943	320.86	4.291	125.94
235.00	.578	1.458	2.036	342.68	4.437	135.88
240.00	.610	1.522	2.131	365.23	4.581	146.30
245.00	.642	1.586	2.227	388.50	4.724	157.20
250.00	.674	1.650	2.324	412.47	4.865	168.58
255.00	.708	1.714	2.422	437.14	5.003	180.44
260.00	.742	1.779	2.520	462.50	5.140	192.80
265.00	.776	1.844	2.620	488.54	5.274	205.65
270.00	.811	1.908	2.719	515.24	5.407	218.99
273.15	.833	1.949	2.783	532.40	5.489	227.66
275.00	.847	1.973	2.820	542.60	5.537	232.84
280.00	.883	2.038	2.921	570.61	5.665	247.19
285.00	.919	2.103	3.022	599.25	5.791	262.05
290.00	.957	2.167	3.124	628.51	5.914	277.42
295.00	.994	2.232	3.226	658.38	6.035	293.29
298.15	1.018	2.272	3.291	677.51	6.110	303.55
300.00	1.032	2.296	3.328	688.86	6.154	309.68
305.00	1.071	2.360	3.431	719.92	6.270	326.57
310.00	1.110	2.424	3.534	751.55	6.384	343.99
315.00	1.149	2.488	3.637	783.75	6.495	361.91
320.00	1.189	2.552	3.740	816.50	6.605	380.36
325.00	1.229	2.615	3.843	849.79	6.711	399.32
330.00	1.269	2.678	3.947	883.61	6.816	418.79
335.00	1.310	2.740	4.050	917.95	6.918	438.78
340.00	1.351	2.802	4.153	952.79	7.018	459.29
345.00	1.392	2.864	4.256	988.13	7.116	480.32
350.00	1.434	2.926	4.359	1024.0	7.213	501.86
355.00	1.476	2.987	4.462	1060.3	7.308	523.91
360.00	1.518	3.047	4.565	1097.0	7.401	546.48
365.00	1.560	3.108	4.668	1134.3	7.494	569.56
370.00	1.603	3.167	4.771	1172.0	7.586	593.16
373.15	1.630	3.205	4.835	1195.9	7.645	608.36

 $H_0^C$  AND  $S_0^C$  APPLY TO THE REFERENCE STATE OF THE SOLID AT ZERO DEK K.

Table 3

Comparison of Enthalpy Values of Table 2 with the  
Experimental Relative Enthalpy Data of Victor and Douglas

$$1 \text{ cal} = 4.1840 \text{ J}$$

Temperature Intervals K	Victor and Douglas [23]		This Work J/mol
	Sample 1 J/mol	Sample 2 J/mol	
273.15-323.15	1270.3	1278.6	1276.1
	1271.5	1278.2	
	1270.9	1278.4	
	(average)	(average)	
273.15-373.15	2765.2	2784.5	2775.9
	2776.5	2785.7	
		2789.1	
	2770.9 (average)	2786.4 (average)	

## References

- [1] J. Aslanian and L. Weil, Contribution of Specific Heat Measurements below 4°K to the Observation of Helium Diffusion after Annealing in Irradiated Beryllium Oxide, *Cryogenics* 3, 36-39 (1963).
- [2] T. H. K. Barron, W. T. Berg, and J. A. Morrison, On the heat capacity of crystalline magnesium oxide, *Proc. Roy. Soc. (London)* 250A, 70-83 (1959).
- [3] T. Duval and C. Duval, Sur la Thermogravimétrie des Précipités Analytiques. VI. Dosage du Glucinium (Béryllium), *Anal. Chim. Acta.* 2, 53-56 (1948).
- [4] E. S. Funston, W. J. Kirkpatrick, and P. P. Turner, Preparation of High Purity BeO Powder, *J. Nuclear Mat.* 11, 310-319 (1964).
- [5] G. T. Furukawa, M. L. Reilly, and J. H. Piccirelli, Calorimetric Properties of Some Alkali Pentaborate Hydrates from 15 to 370°K, *J. Res. NBS* 68A (Phys. and Chem.) No. 4, 381-389 (1964).
- [6] G. T. Furukawa and M. L. Reilly, Application of Precise Heat-Capacity Data to the Analysis of the Temperature Intervals of the NBS (1955) and the International Practical Temperature Scales in the Region of 90°K, *J. Res. NBS (Phys. and Chem.)* 69A, 5-12 (1965).
- [7] W. F. Giauque and R. C. Archibald, The Entropy of Water from the Third Law of Thermodynamics. The Dissociation Pressure and Calorimetric Heat of the Reaction  $\text{Mg(OH)}_2 = \text{MgO} + \text{H}_2\text{O}$ . The Heat Capacities of  $\text{Mg(OH)}_2$  and MgO from 20 to 300°K, *J. Am. Chem. Soc.* 59, 561-569 (1937).
- [8] E. Gmelin, Mesures de la chaleur spécifique de l'oxyde de béryllium et de l'oxyde de calcium a basses températures, *Compt. rend.* 262C, 1452-1455 (1966).
- [9] M. A. Greenbaum, J. Weiher, and M. Farber, The Thermodynamic and Physical Properties of Beryllium Compounds. VIII. Heat of Fusion and High-Temperature Heat Capacity of Beryllium Oxide, *J. Phys. Chem.* 69, 4035-4037 (1965).
- [10] L. I. Grossweiner and R. L. Seifert, The Reaction of Beryllium Oxide with Water Vapor, *J. Am. Chem. Soc.* 74, 2701-2704 (1952).
- [11] P. Günther, Untersuchungen über die spezifische Wärme bei tiefen Temperaturen, *Ann. Physik* 51, 828-846 (1916).



- [12] H. J. Hoge and F. G. Brickwedde, Establishment of a Temperature Scale for the Calibration of Thermometers between 14° and 83°K, J. Res. NBS 22, 351-373 (1939) RP1188.
- [13] C. A. Hutchison, Jr. and J. G. Malm, The Volatilization of Beryllium Oxide in the Presence of Water, J. Am. Chem. Soc. 71, 1338-1339 (1949).
- [14] V. V. Kandyba, P. B. Kantor, R. M. Krasovitskaya, and E. N. Fomichev, Determination of Enthalpy and Heat Capacity of Beryllium Oxide in the Temperature Range 1200-2820°K, Doklady. Akad. Nauk. S.S.S.R. 131, 566-567 (1960).
- [15] K. K. Kelley, The Specific Heats at Low Temperatures of Beryllium Oxide and Beryllium Orthosilicate (Phenacite), J. Am. Chem. Soc. 61, 1217-1218 (1939).
- [16] W. H. Lien, Heat-Capacity Studies at Liquid Helium Temperatures and Below. Part I: The Alkali Metals, Part II: Small Particles of Magnesium Oxide, U. S. At. Energy Comm. UCRL-9880, 72pp. (1962).
- [17] W. H. Lien and N. E. Phillips, Heat Capacity of Small Particles of MgO between 1.5° and 4°K, J. Chem. Phys. 29, 1415-1416 (1958).
- [18] A. Magnus and H. Danz, Die spezifische Wärme von Wolfram, Bor, Borstickstoff und Berylliumoxyd, Ann. Physik (4) 81, 407-424 (1926).
- [19] L. F. Nilson and O. Pettersson, Ueber Molekularwärme und Molekularvolumina der seltenen Erden und deren Sulfate, Ber. chem. Gesell. 13, 1459-1465 (1880).
- [20] E. N. Rodigina and K. Z. Gomel'skii, Enthalpy of Beryllium and Lithium Oxides at High Temperatures, Zhur. Fiz. Khim. 35, 1828-1831 (1961).
- [21] R. B. Scott, C. H. Meyers, R. D. Rands, Jr., F. G. Brickwedde, and N. Bekkedahl, Thermodynamic Properties of 1,3-Butadiene in the Solid, Liquid, and Vapor States, J. Res. Natl. Bur. Std. 35, 39-85 (1945).
- [22] H. F. Stimson, International Practical Temperature Scale of 1948. Text Revision of 1960. J. Res. NBS (Phys. and Chem.) 65A, No. 3, 139-145 (1961).
- [23] A. C. Victor and T. B. Douglas, Thermodynamic Properties of Magnesium Oxide and Beryllium Oxide from 298 to 1200°K, J. Res. NBS (Phys. and Chem.) 67A, No. 4, 325-329 (1963).



- [24] B. E. Walker, Jr., C. T. Ewing, and R. R. Miller, Specific Heat of Some High Temperature Materials, J. Chem. Eng. Data 7, 595-597 (1962).
- [25] W. A. Young, The Reactions of Water Vapor with Beryllia-Alumina Compounds, J. Phys. Chem. 64, 1003-1006 (1960).

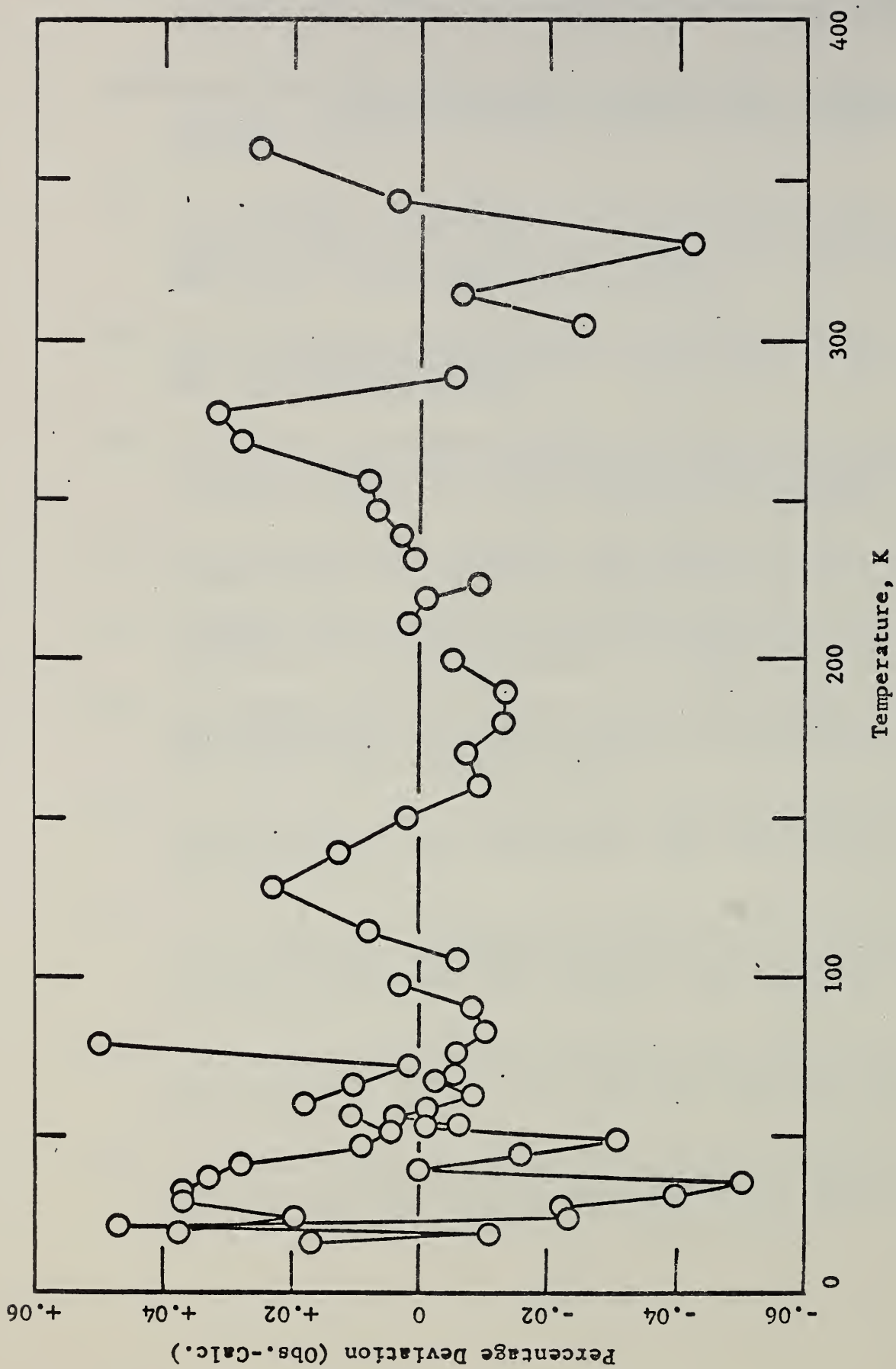


Fig. 1. Percentage Deviation of the Empty Sample Vessel Heat Capacities.

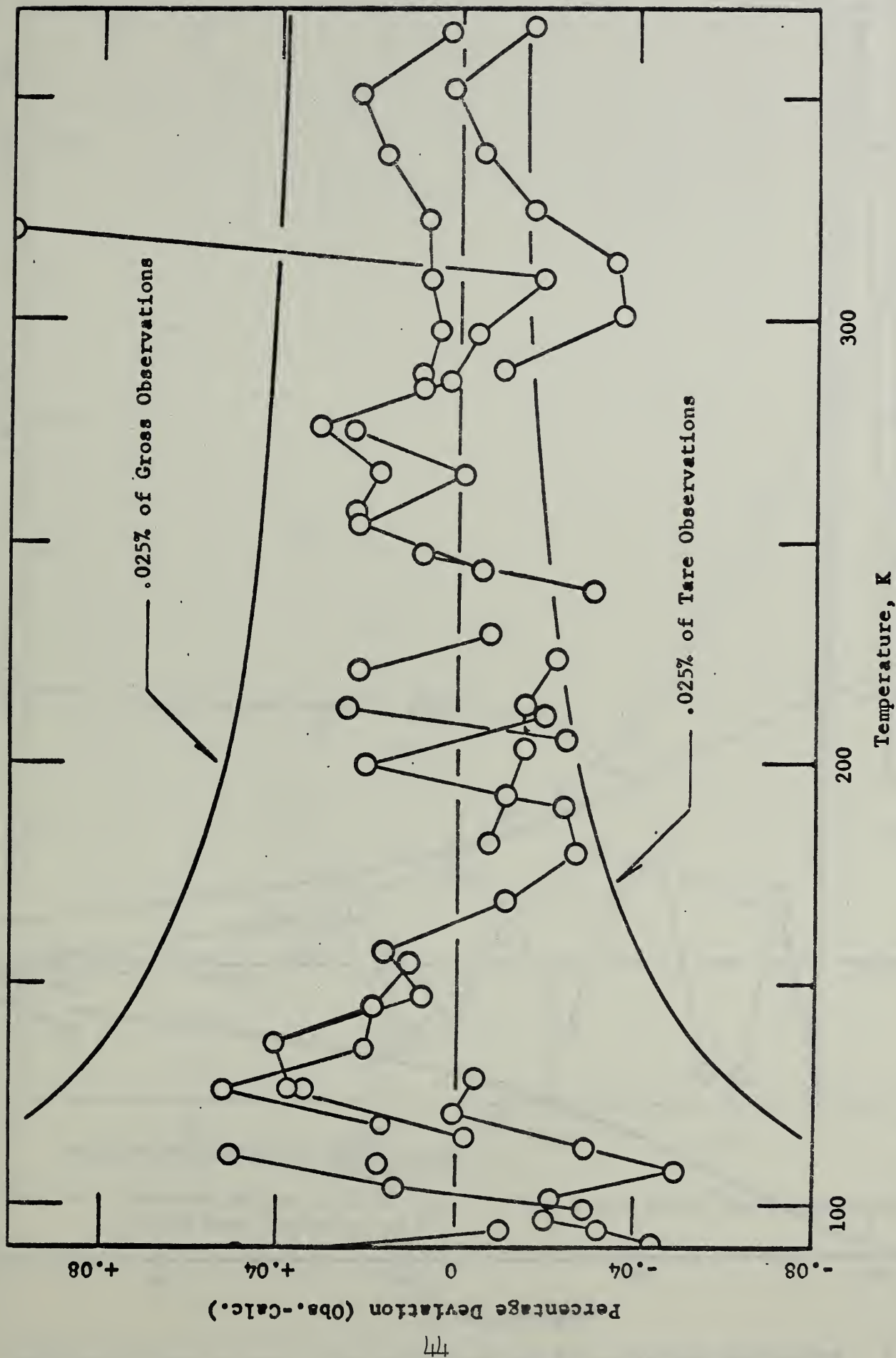


Fig. 2. Percentage Deviation of the Beryllium Oxide Sample Heat Capacities.

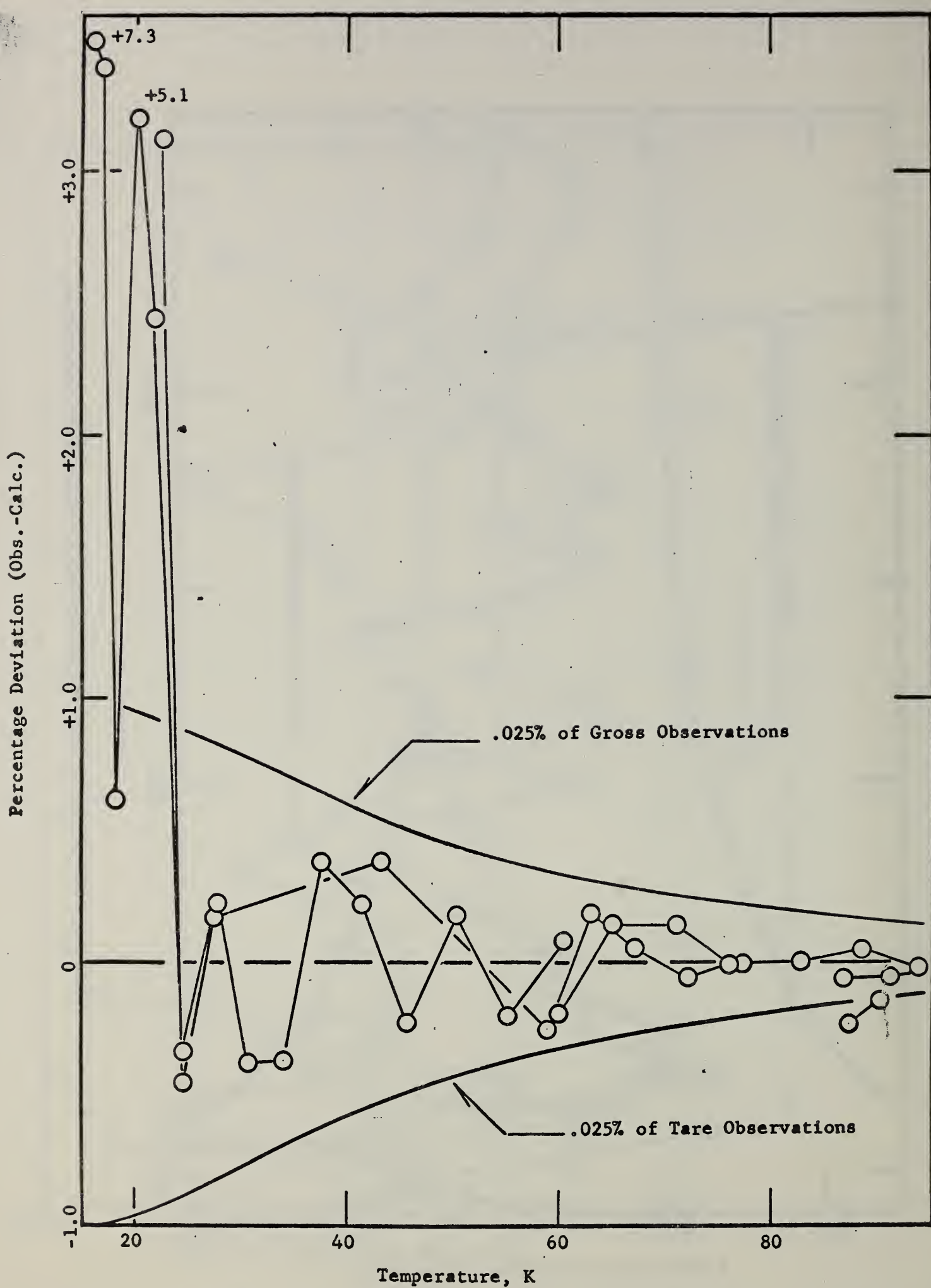


Fig. 3. Percentage Deviation of the Beryllium Oxide Sample Heat Capacities.

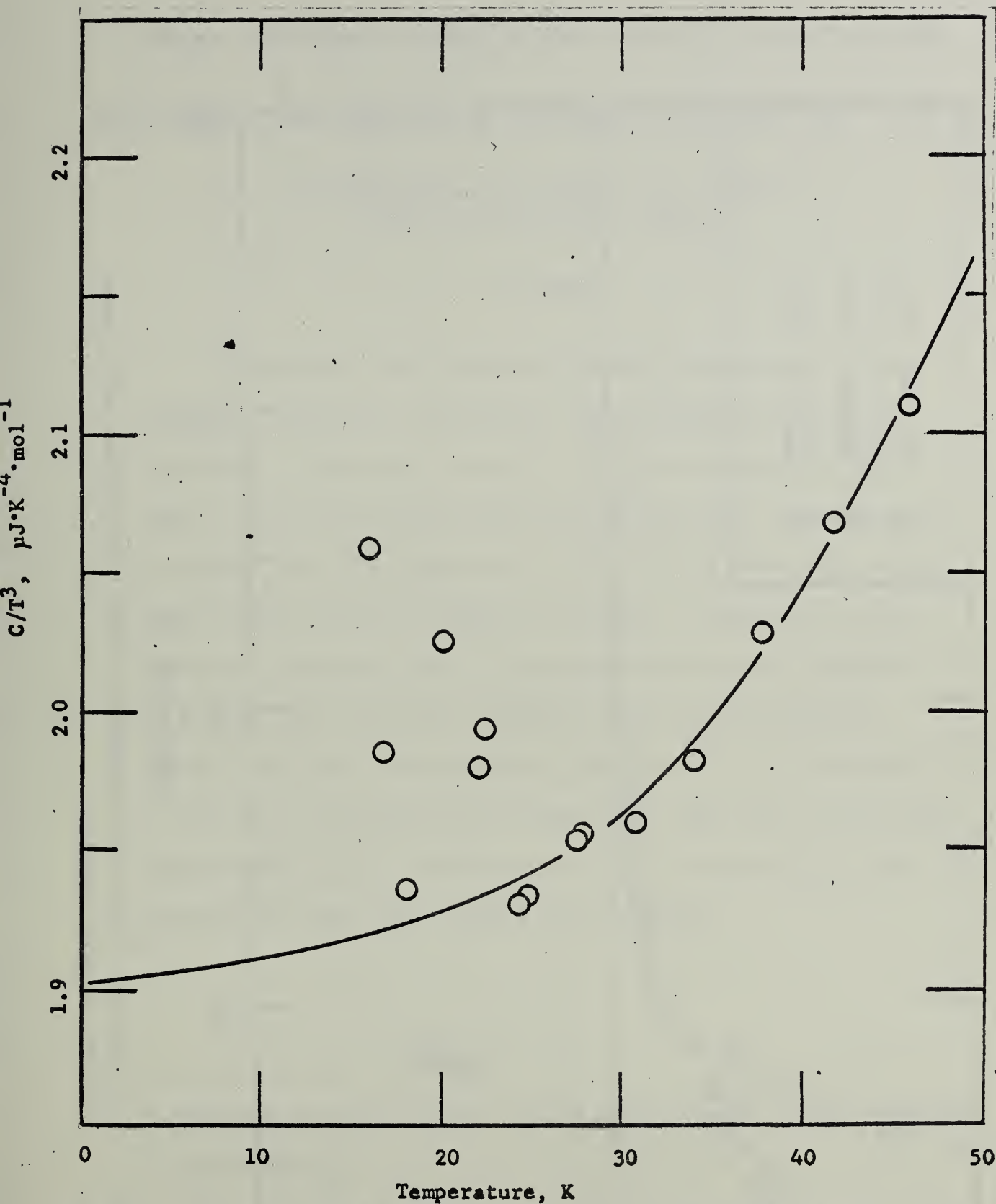


Fig. 4. Observed Values of  $C/T^3$  vs.  $T$ . The Curve Shows the Extrapolation of the Heat Capacity to 0 K.



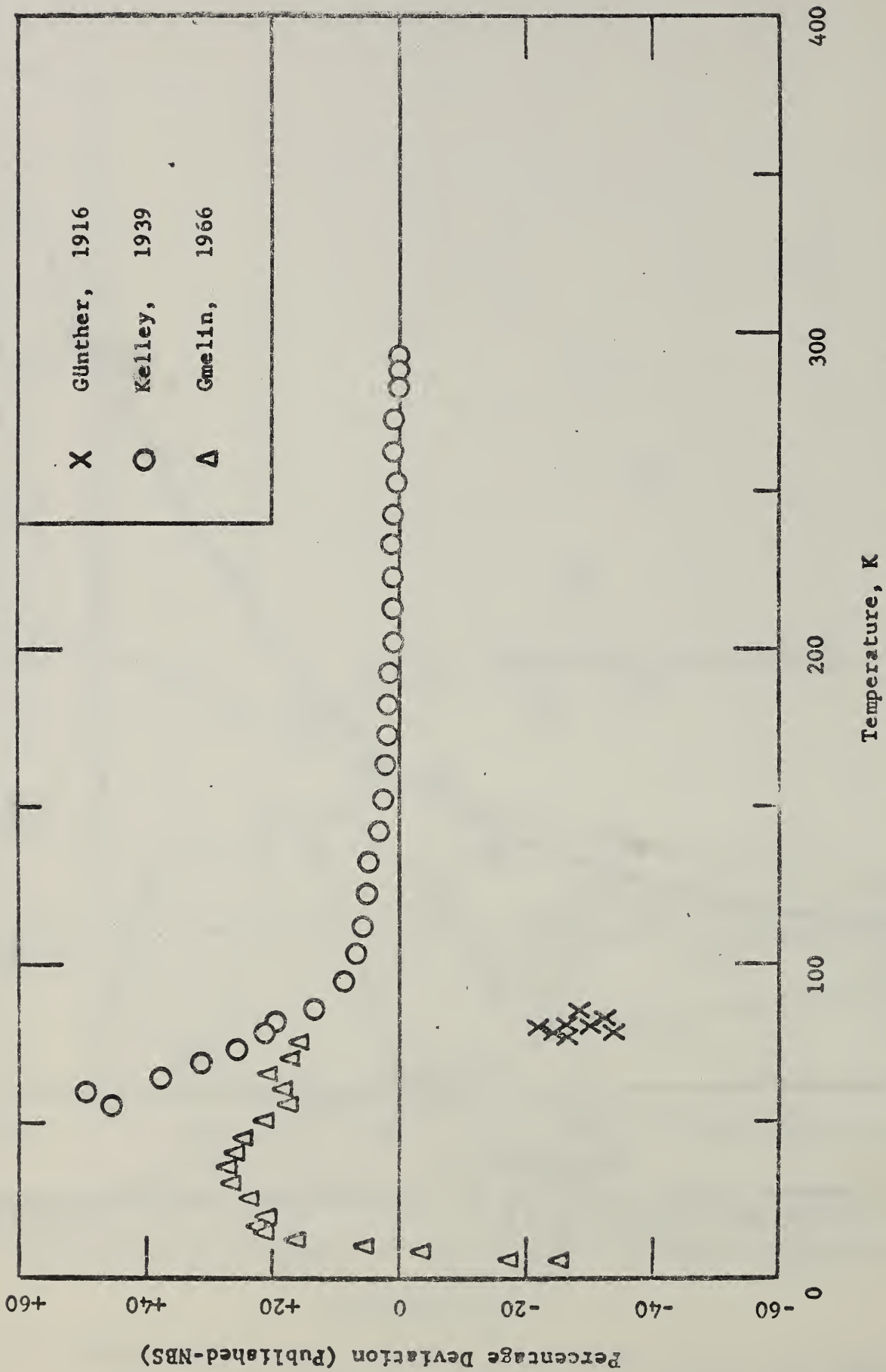


Fig. 5. A Comparison of Results Published by Other Investigators with Those Obtained in this Research.

DYNAMIC MEASUREMENT OF HEAT CAPACITY, ELECTRICAL RESISTIVITY AND  
HEMISPHERICAL TOTAL EMITTANCE OF MOLYBDENUM IN THE RANGE 1800 - 2800 K

A. Cezairliyan, M.S. Morse, H.A. Berman,  
G.M. Foley\*, and C.W. Beckett

ABSTRACT

A system for the simultaneous dynamic measurement of heat capacity, electrical resistivity, and hemispherical total emittance of electrical conductors at high temperatures (above 1800 K) with millisecond resolution is described. The specimen is heated from room temperature to its melting point by a single heavy current pulse of subsecond duration. Temperature of the specimen is measured with a high-speed photoelectric pyrometer of 0.4 ms time resolution. Dynamic recording of variables: current, voltage, and temperature, required for the determination of the above properties, is achieved by a high-speed digital data acquisition system. Preliminary results on molybdenum in the temperature range 1800 - 2800 K are presented.

---

\* Leeds and Northrup Company, North Wales, Pennsylvania, also Guest Worker at NBS.

## I. Introduction

In view of the growing interest and urgency in understanding the behavior of matter at temperatures above the limit of accurate steady-state experiments, it has become necessary to develop dynamic methods for the measurement of properties of substances. They show great promise at high temperatures since the duration of a dynamic experiment may be so short that the role of various phenomena, such as heat transfer, chemical reactions, evaporation, diffusion, etc. which set the upper limit in steady-state experiments, becomes negligible. In recent years, considerable progress has been made in high-speed thermodynamic measurement methods and related instrumentation techniques. A general review of these methods is in preparation [5].

Over the past fifty years several investigators [3, 4, 6, 9, 11-16, 19-22] have developed dynamic techniques for the measurement of specific heat of electrical conductors. They differ considerably from each other depending on the pulse power source and the method of measurement of specific variables. In general, either heavy batteries or capacitors were used as the pulse power source. In all cases, power imparted to the specimen was obtained from pulse current and voltage measurements. The temperature of the heating specimen was measured either by thermocouples or was determined from dynamic electrical resistivity measurements. The first method has several limitations and cannot be used for very high speed work. The second

one requires a separate steady-state determination of the electrical resistivity of the specimen as a function of temperature. In almost all of the recent investigations oscilloscopic techniques were employed for the dynamic recording of variables.

As a step toward establishing accurate high-speed thermodynamic measurement methods, investigations have been and continue to be undertaken in the High-Speed Thermodynamics Laboratory at the National Bureau of Standards. The first phase of this program is concentrated on the development of a dynamic technique for the accurate measurement of heat capacity of solid electrical conductors at high temperatures. The preliminary version of a high-speed (millisecond resolution) method for the measurement of heat capacity has been described [6]. The present study is an extension of this earlier work with several major changes in the physical system, measurement techniques, and calculation methods. They are summarized in the following paragraph.

Instead of the continuous detection of the radiation from the specimen by means of a photomultiplier tube, a millisecond resolution photoelectric pyrometry technique was employed for the dynamic temperature measurements. This eliminates most of the uncertainties that result from the instability of the radiation detector. A high-speed, multichannel, digital data acquisition system has replaced the oscilloscopes, improving the recording accuracy by approximately two orders of magnitude. Also, several changes were made in the test cell,



specimen, and voltage probes. Another major improvement in the results is due to a change in the formulation of the calculations. Instead of assuming a constant value for the emittance, obtained from the literature, in the present work the hemispherical total emittance of the specimen was measured under dynamic conditions and this value was used in the calculations for the thermal radiation correction.

In order to check the operation of the system, dynamic experiments of millisecond resolution were conducted and heat capacity, electrical resistivity, and hemispherical total emittance of molybdenum were measured in the temperature range 1800 - 2800 K. Results reported in this chapter are of preliminary nature in the sense that they are based on only a small portion of the data taken, and that simplified relations are used in computing the pertinent properties.

## II. Description of the Method

The dynamic method employed in this study for the measurement of specified properties is based upon rapid joulean heating of the specimen by a single pulse of direct current and measuring the pertinent variables with millisecond resolution. Heat capacity and electrical resistivity are calculated from data obtained during the heating period. In order to apply a correction for the radiation loss, hemispherical total emittance is calculated from the data of the initial cooling period. In the following paragraphs the formulation

of the relationships between various variables is presented.

#### a. Heating Period

The energy balance for the specimen during the heating period can be expressed as

$$\text{Energy Imparted} = \text{Energy Stored} + \text{Energy Losses}$$

In high temperature dynamic experiments of millisecond resolution the major source of power loss is that due to thermal radiation. Using the proper quantities, the above relation for unit time becomes

$$ei = c_p n(dT/dt)_h + \epsilon \sigma A_s (T^4 - T_e^4) \quad (1)$$

Where

$e$  = potential difference across the effective specimen (V)

$i$  = current through the specimen (A)

$c_p$  = heat capacity (J gm-at<sup>-1</sup> K<sup>-1</sup>)

$n$  = weight of the effective specimen (gm-at)

$\epsilon$  = hemispherical total emittance

$\sigma$  = Stephan-Boltzmann constant ( $5.6697 \times 10^{-8}$  W m<sup>-2</sup> K<sup>-4</sup>)

$A_s$  = effective surface area (m<sup>2</sup>)

$T$  = temperature (K)

$T_e$  = room temperature (K)

$(dT/dt)_h$  = heating rate (K s<sup>-1</sup>)

Solving Eq. (1) for  $c_p$  one obtains

$$c_p = \frac{ei - \epsilon \sigma A_s (T^4 - T_e^4)}{n(dT/dt)_h} \quad (2)$$

### b. Cooling Period

The energy balance for the specimen during the initial cooling period can be written as

$$\text{Energy Loss} = \text{Energy Radiated}$$

which for unit time can be expressed as

$$-c_p n(dT/dt)_c = \epsilon \sigma A_s (T^4 - T_e^4) \quad (3)$$

where

$$(dT/dt)_c = \text{cooling rate (K s}^{-1}\text{)}$$

Solving Eq. (3) for  $c_p$  one obtains

$$c_p = \frac{\epsilon \sigma A_s (T^4 - T_e^4)}{-n(dT/dt)_c} \quad (4)$$

### c. Relations for Properties

Combination of Eqs. (2) and (4) yields

$$ei = \epsilon \sigma A_s (T^4 - T_e^4) - \epsilon \sigma A_s (T^4 - T_e^4) \left[ \frac{(dT/dt)_h}{(dT/dt)_c} \right] \quad (5)$$

Defining,

$$M = - \frac{(dT/dt)_h}{(dT/dt)_c} \quad (6)$$

and substituting Eq. (6) in Eq. (5) and solving for  $\epsilon$  one obtains

$$\epsilon = \frac{ei}{\sigma A_s (T^4 - T_e^4) (1 + M)} \quad (7)$$

In this study Eq. (7) is used to calculate hemispherical total emittance of the specimen which, in turn, is substituted in Eq. (2) to obtain heat capacity.

Electrical resistivity is calculated with the aid of the equation

$$\rho = \frac{RA_c}{L} \quad (8)$$

where,

$\rho$  = electrical resistivity ( $\Omega$  m)

R = resistance of effective specimen ( $\Omega$ )

$A_c$  = cross-sectional area ( $m^2$ )

L = effective length (m)

### III. Description of the System

The system used in this study consists of a principal electrical circuit and auxiliary measuring circuits. The principal circuit includes the specimen in series with a battery bank, a variable resistance, a shunt, and a switch. The measuring circuits include detectors and other related equipment and circuitry necessary for the dynamic measurement and recording of the pertinent quantities. A functional diagram of the complete system is presented in Fig. (1).

#### a. Specimen and Test Cell

The molybdenum specimen used in the experiments is a tube of the following nominal dimensions: length = 4 in.(101.6 mm), outside diameter = 0.25 in.(6.35 mm), thickness = 0.02 in.(0.51 mm). A small rectangular hole (1.09 mm long, 0.56 mm wide) was fabricated in the wall at the middle of the specimen to approximate blackbody conditions. Calculations indicate that the quality of blackbody, based



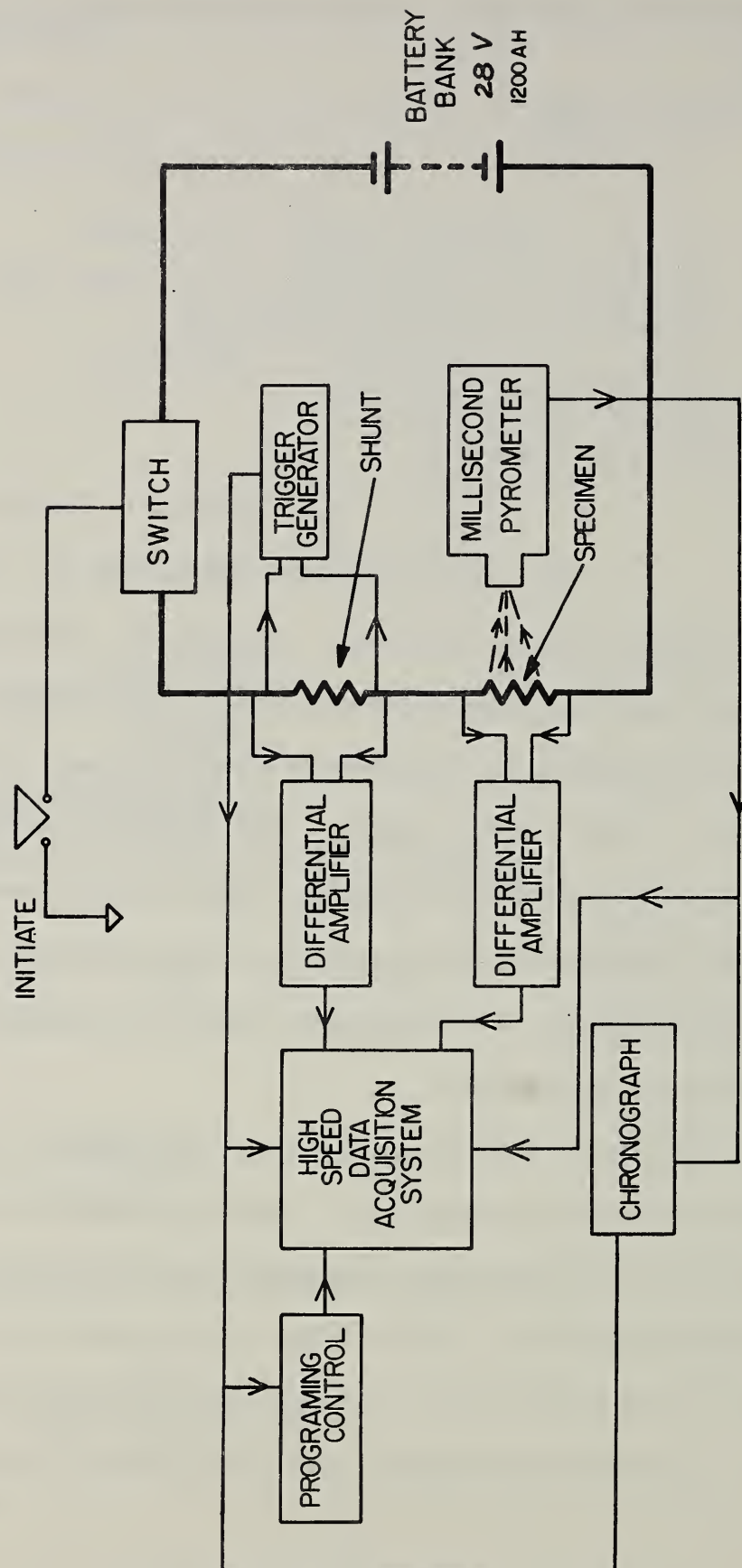


Fig. 1. Functional Diagram of Millisecond Thermodynamic Measurements System.

on geometrical considerations, thus achieved is 99.5 percent. Potential measurements were made using molybdenum knife edges each at a distance of 12.5 mm from the end clamps. This allows the "effective" portion of the specimen to be free from sharp temperature gradients. It is calculated that for the longest pulse (highest temperature) used in the experiments temperature non-uniformity between the midpoint of the specimen and the plane of the voltage probe due to transient axial thermal conduction is less than 0.1 percent. The specimen is free to expand in the downward direction. The specimen clamps and the walls of the test cell are water cooled. Experiments can be conducted either with the specimen in vacuum or in inert gas.

b. Rest of Main Circuit

The power supply for the pulse heating of the specimen is a 28 V heavy-duty battery bank. A series connected, water-cooled, variable resistance enables one to adjust the main current and thus to control the heating rate. The fast-acting switch is operated by a series of time-delay units which control the pulse length in addition to providing timing pulses to other electronic measuring and recording instruments. A standard resistor ( $0.001\ \Omega$ ) placed in the main circuit enables one to measure the heavy pulse current flowing through the specimen.

c. High-Speed Pyrometer

The temperature of the rapidly heating specimen is measured by means of a high-speed photoelectric pyrometer, which permits 1200

evaluations of the specimen temperature per second. The pyrometer passes a precisely timed sample of radiation from the specimen through an interference filter (wavelength 650 nm, bandwidth 10 nm) to an electron multiplier photocell. The anode current of the photocell during the exposure of 208  $\mu$ s is integrated and the resulting integrator voltage is recorded. Then, the integrator is reset to permit it to integrate the anode current due to a similar sample of radiation from a calibrated, gas-filled tungsten filament lamp, suitably attenuated by an optical attenuator. Thus, the pyrometer collects the results of an interlaced sequence of exposures to specimen and reference source. Successive exposures to the reference lamp are taken through a sequence of three different optical attenuators mounted on a rotating disc, resulting in a staircase of reference exposures with approximately 50 percent attenuation for each step. This scheme is used for temperature measurements up to 2500 K, the limit of reliable operation of gas-filled lamps. For the measurement of higher temperatures, calibrated optical attenuators are placed in the path of the radiation from the specimen.

d. High-Speed Digital Data Acquisition System

The signals at the output of detectors corresponding to the voltage, current, and temperature are in analog form. Normally, in dynamic experiments such signals are measured by oscilloscopic techniques. However, the expected recording accuracy of such methods cannot be better than one percent. In order to improve the overall accuracy, a high-speed digital data acquisition system has been

designed and constructed to meet the special requirements of the experiments. The system consists of a multiplexer, analog-to-digital converter, a core memory together with control and interfacing equipment. Oscilloscopes are used to monitor the general pattern of the experimental results, and to detect any anomalies.

All signals are brought to the multiplexer through isolation amplifiers in order to avoid the inaccuracies arising from common ground points. The multiplexed signals (aperture time 50 ns) go to the analog-to-digital converter which has a full-scale reading of  $\pm 10$  V, and a full-scale resolution of one part in 8192. Digital output from the converter consists of 13 binary bits plus a sign bit. This output is stored in a core memory having a capacity of 2048 words of sixteen bits each.

All the above takes place during a dynamic experiment of sub-second duration. After the experiment is over, information stored in the core memory, which is in parallel binary coded form, is converted to serial binary coded decimal form and retrieved in the form of numeric printing and punched paper tape. Since the laboratory has access to a remote-control, time-sharing computer, it is possible to unload the memory directly to the computer. This allows one to process the data immediately after an experiment, bypassing the intermediate stage of punching paper tape. A functional diagram of the high-speed data acquisition system is presented in Fig. (2).



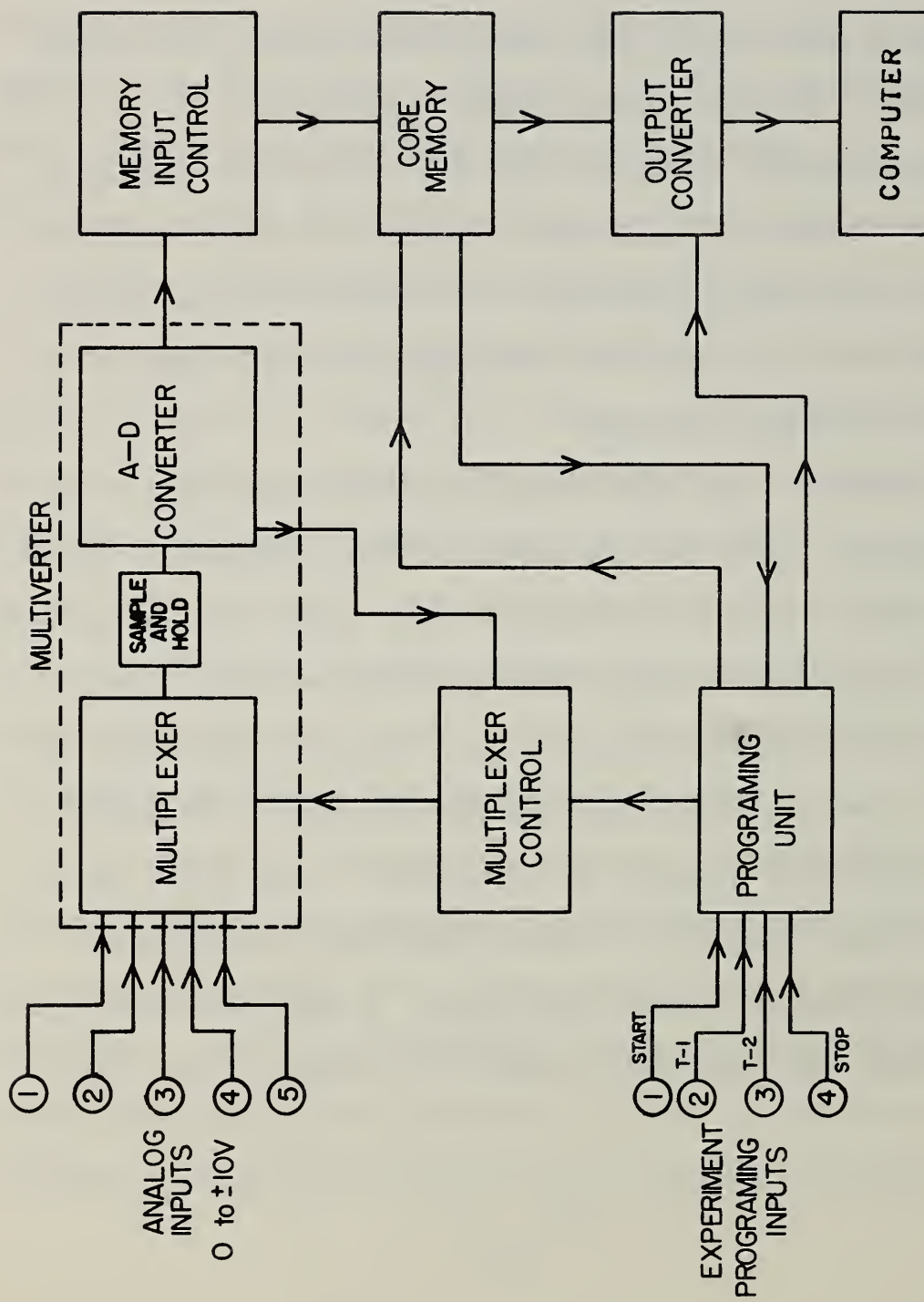


Fig. 2. Functional Diagram of High-Speed Digital Data Acquisition System.

#### IV. Experimental Results

The molybdenum specimen (99.9<sup>+</sup> percent pure, outer surface polished) was pulse heated in vacuum and data were taken during heating, as well as cooling periods. Pulse length varied from 285 ms to 380 ms depending on the temperature level. The entire temperature range (1800 - 2800 K) was covered in three steps. Hemispherical total emittance was calculated from Eq. (7), and a linear function for the entire range was obtained by least mean square approximation of the individual results which yields a standard deviation of 2 percent. Heat capacity was calculated from Eq. (2) after substituting the function for emittance. A quadratic fit over the entire temperature range gave a standard deviation of 0.3 percent. Electrical resistivity was calculated from Eq. (8). A linear fit over the entire range gave a standard deviation of 0.2 percent. Dimensions, in electrical resistivity and hemispherical total emittance calculations, were based on their room temperature values. Preliminary results on heat capacity, electrical resistivity and hemispherical total emittance are presented in graphical form in Figs. (3), (4), and (5), respectively. Pertinent preliminary equations for the above properties in the range 1800 to 2800 K are given below.

$$c_p = 34.58 - 1.096 \times 10^{-2} T + 5.696 \times 10^{-6} T^2 \quad (9)$$

$$\rho = -9.798 + 3.146 \times 10^{-2} T \quad (10)$$

$$\epsilon = 5.209 \times 10^{-2} + 1.139 \times 10^{-4} T \quad (11)$$

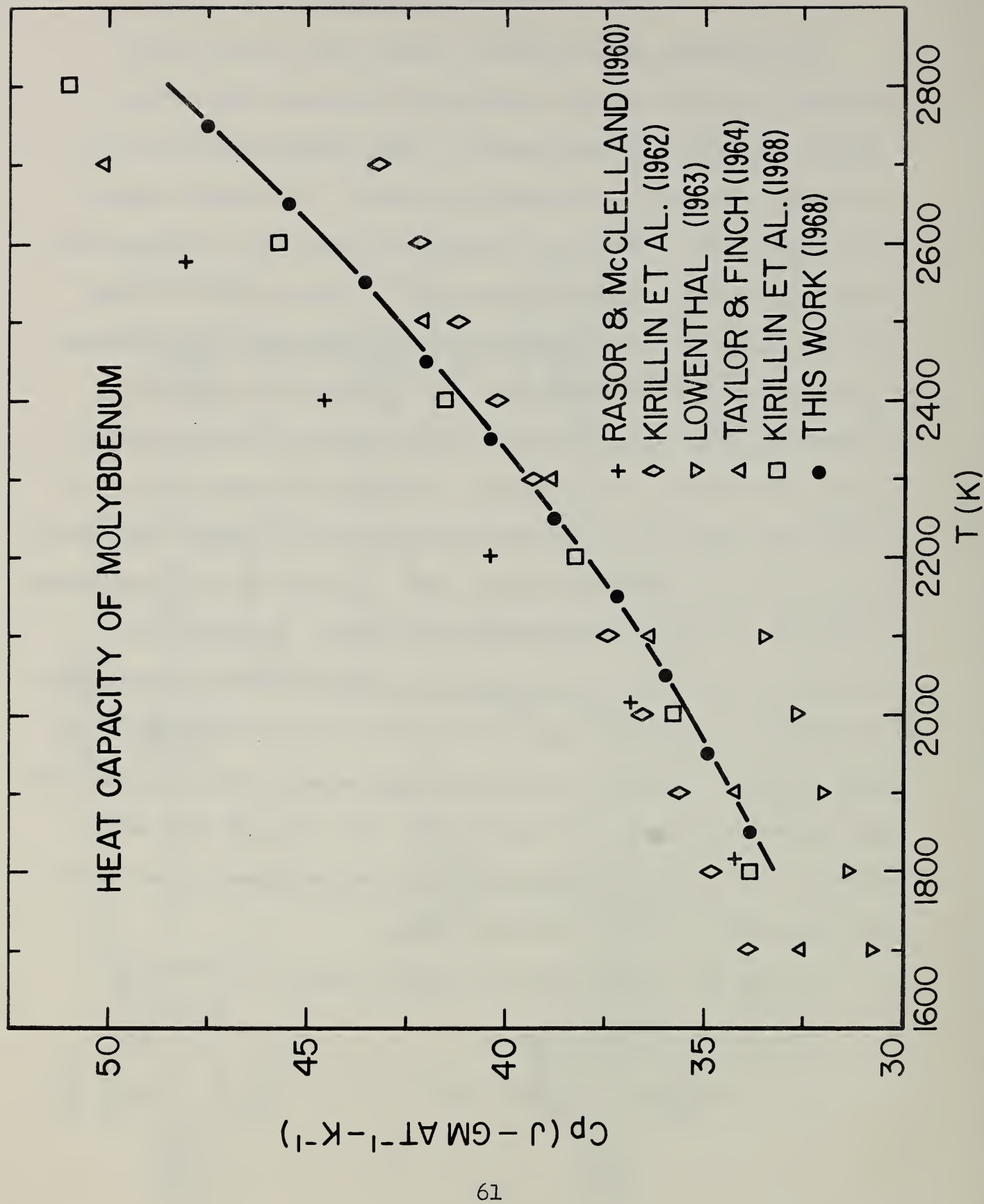


Fig. 3. Heat Capacity of Molybdenum as a Function of Temperature.

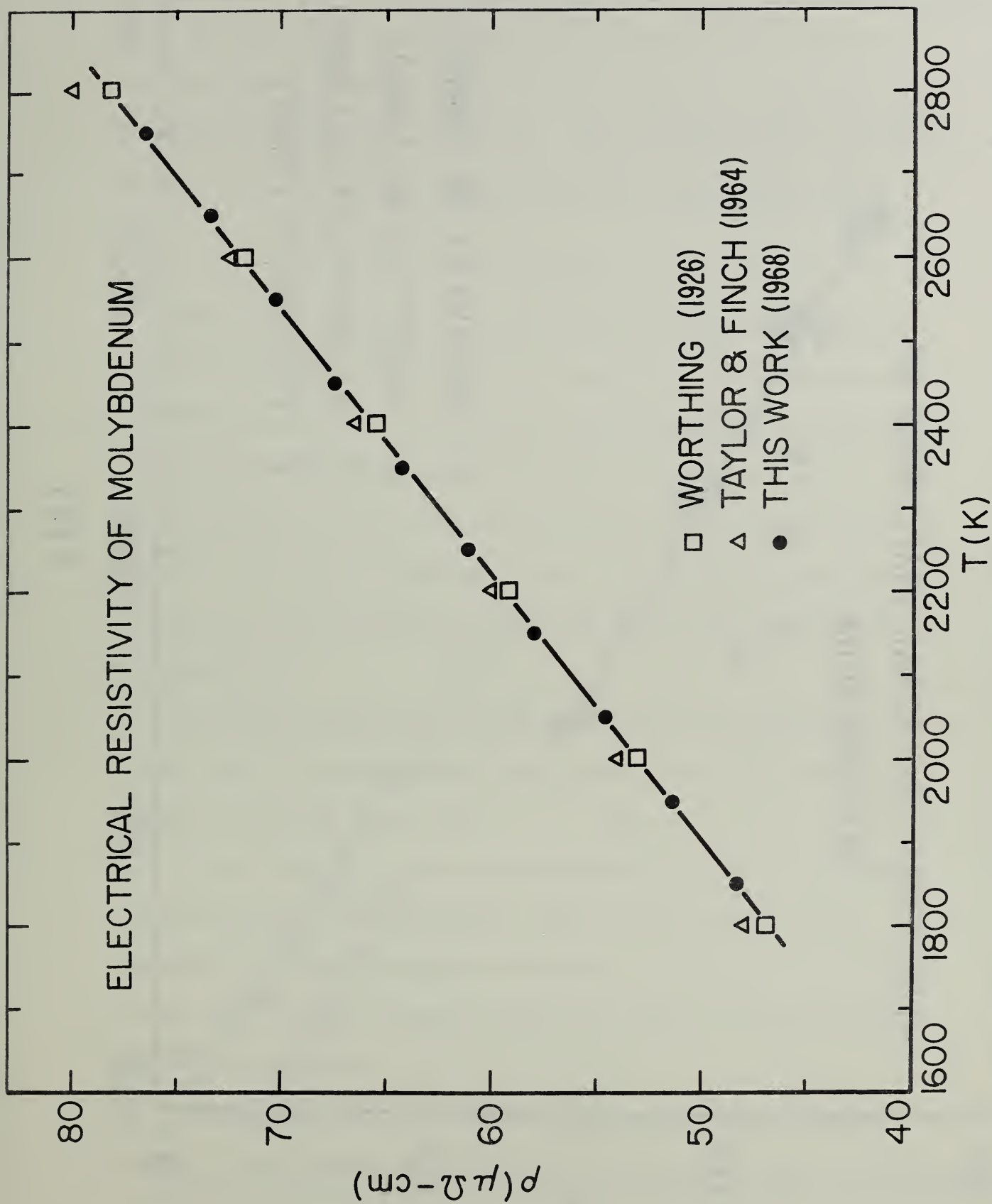


Fig. 4. Electrical Resistivity of Molybdenum as a Function of Temperature.



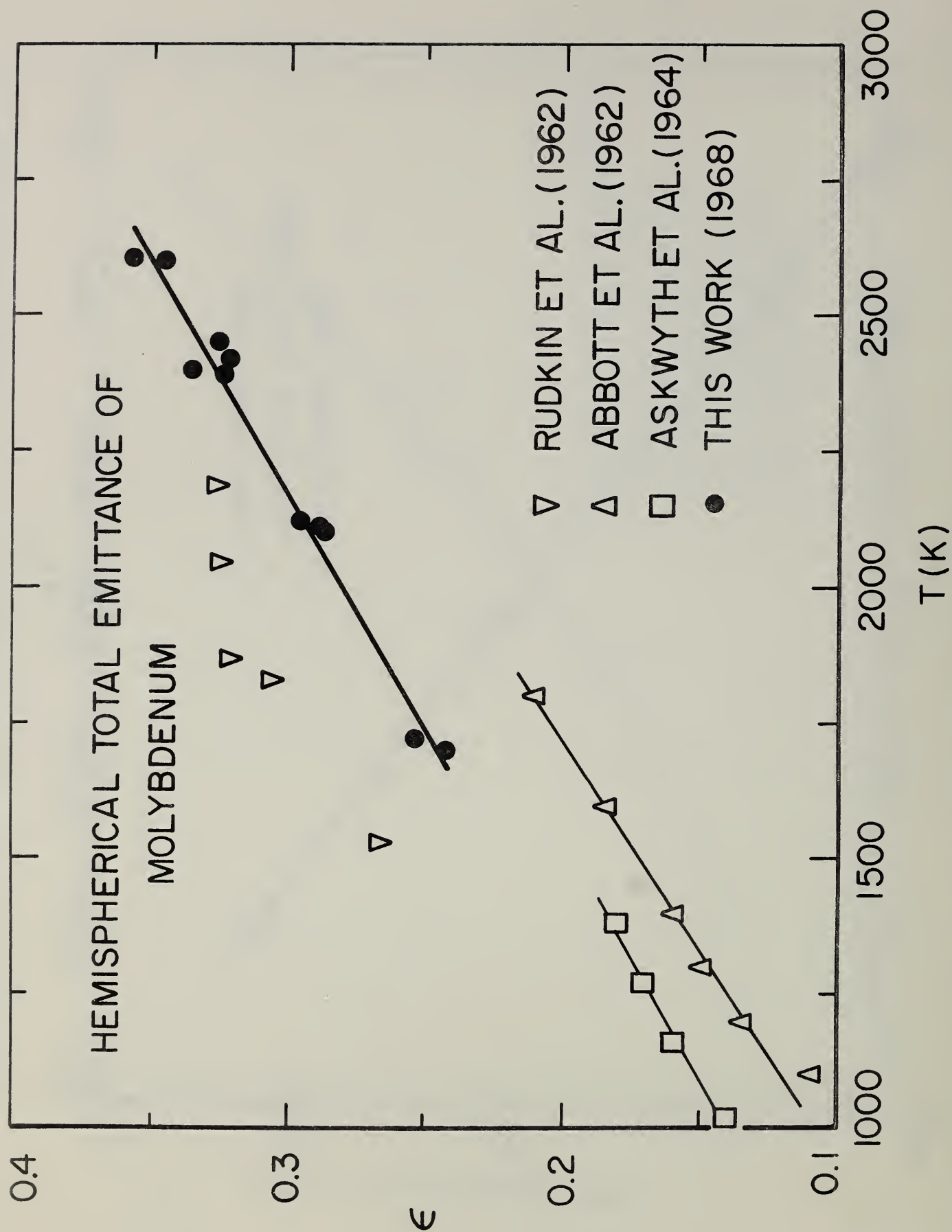


Fig. 5. Hemispherical Total Emittance of Molybdenum as a Function of Temperature.

In temperature calculations, the scattered light effect in the high-speed pyrometer, as well as the departure from blackbody conditions were taken into account. The scattered light correction factor was 0.953 and the computed blackbody quality was 0.995.

## V. Discussion

The results based on a limited number of experiments do not indicate any sharp increase of heat capacity at high temperatures ( $T < 0.96T_m$ , where  $T_m$  is the melting point). Comparison of the results of this work with those in the literature shows that present values are, in general, higher than those obtained by most "drop" methods, with the exception of Kirillin et al. [8], and lower than those of the two "pulse" methods of Taylor and Finch [19] and Rasor and McClelland [17].

Electrical resistivity agrees very closely with Worthing's [23] results and it is approximately two percent lower than the values given by Taylor and Finch [19].

In the literature, there is considerable scatter in the values of hemispherical total emittance. This can be expected since emittance is strongly dependent on surface conditions. The results of this work fall, in general, within the limits of the available data in the literature.

A preliminary list of estimated errors is given in Table 1. Studies so far indicate that temperature measurements have an estimated

Table 1

## Estimated Errors\*

1. <u>In Temperature Measurements</u>	<u>Estimated error in K</u>	
	<u>at 1800 K</u>	<u>at 2500 K</u>
Pyrometer reproducibility	1	2
Scattered light correction	1	2
Light source alignment	1	2
Radiation standard lamp	1	2.5
Blackbody quality (geometrical)	1	2
Specimen temperature non-uniformity	2	3
Magnetic fields	<1	<1
Estimated total error in temperature	3	6
2. <u>In Electrical Measurements</u> (for single determination with ms resolution)	<u>Estimated error in percent</u>	
Skin effect		<0.01
Inductive effects		<0.01
Thermoelectric effects		<0.01
Voltage measurement		<0.05
Current measurement		<0.05
Power measurement		<0.07
Resistance measurement		<0.07
3. <u>In Interpretation of Results</u>	<u>Estimated error in percent</u>	
Effect of specimen evaporation		<0.01 (at 2800 K)
Effect of thermionic		<0.02 (at 2800 K)
Time synchronization		<0.01
Length measurement		0.02
Weight measurement		0.01
Effective specimen weight		0.1
Heating rate		0.3 (at 1800 K)
		0.6 (at 2500 K)
4. <u>Estimated Total Error in Properties</u>	<u>at 1800 K</u> <u>at 2500 K</u>	
	<u>percent</u>	
Heat capacity	1	1.5
Electrical resistivity	0.6	0.6
Hemispherical total emittance	2	3

---

\* Estimates of both random and systematic errors are given as being equivalent to "one standard deviation".

error of 3 K at 1800 K, and 6 K at 2500 K. Errors in the measurement of electrical quantities give an estimated error of 0.07 percent in power and resistance. Combination of various errors gives an approximate value of the total error in each of the properties measured: heat capacity 1 percent at 1800 K, 1.5 percent at 2500 K, electrical resistivity 0.6 percent at both levels, hemispherical total emittance 2 percent at 1800 K and 3 percent at 2500 K.

It should be emphasized that the results reported in the chapter are preliminary. The final results will be presented when the processing of the entire data on molybdenum is completed.

#### Acknowledgment

The authors would like to extend their appreciation to Messrs, J. Queiser, A.N. Graef, and M.E. Wilke for their expert assistance in constructing the test cell, auxiliary mechanical components, and machining of the specimen.



## References

1. Abbott, G.L., N.J. Alvares, and W.J. Parker, WADD-TR-61-94, II (1962).
2. Askwyth, W.H., R.J. Yahes, R.D. House, and G. Mikk, NASA-CR-56496 (1964).
3. Avramescu, A., Z. Tech. Physik, 20, p. 213, (1939).
4. Baxter, H.W., Nature, 153, p. 316, (1944).
5. Beckett, C.W., and A. Cezairliyan, "High-Speed Thermodynamic Measurements and Related Techniques," in J.P. McCullough, Ed., EXPERIMENTAL THERMODYNAMICS, Vol. I, CALORIMETRY OF NON-REACTING SYSTEMS, Butterworths, Washington, to be published.
6. Cezairliyan, A., "A High-Speed (Millisecond) Method for the Simultaneous Measurement of Enthalpy, Specific Heat, and Resistivity of Electrical Conductors at High Temperatures, in ADVANCES IN THERMOPHYSICAL PROPERTIES AT EXTREME TEMPERATURES AND PRESSURES, ASME, New York, 1965.
7. Kirillin, V.A., A.E. Sheindlin, and V.Y. Chekhovskoi, Int. J. Heat Mass Transfer, 5, p. 1, (1962).
8. Kirillin, V.A., A.E. Sheindlin, V.Y. Chekhovskoi, and V.A. Petrov. "Enthalpy and Heat Capacity of Molybdenum at Extremely High Temperatures", in J.R. Moszynski, ed., PROC. OF FOURTH SYMPOSIUM ON THERMOPHYSICAL PROPERTIES, ASME, New York, 1968, p. 54.
9. Kurrelmeyer, B., W.H. Mais, and E.H. Green, Rev. Sci. Instr., 14, p. 349. (1943).
10. Lowenthal, G.C., Aust. J. Phys., 16, p. 47, (1963).
11. Nathan, A.M., J. Appl. Phys., 22, p. 234, (1951).
12. Pallister, P.R., J. Iron Steel Inst., 161, p. 87, (1949).
13. Pasternak, R.A., E.C. Fraser, B.B. Hansen, and H.U.D. Wiesendanger, Rev. Sci. Instr., 33, p. 1320, (1962).
14. Pasternak, R.A., H.U.D. Wiesendanger, and B.B. Hansen, J. Appl. Phys., 34, p. 3416, (1963).
15. Pochapsky, T.E., Acta Met., 1, p. 747, (1953).
16. Pochapsky, T.E., Rev. Sci. Instr., 25, p. 238, (1954).
17. Rasor, N.S., and J.D. McClelland, J. Phys. Chem. Solids, 15, p. 17, (1960).

18. Rudkin, R.L., W.J. Parker, and R.J. Jenkins, "Measurement of Thermal Properties of Metals at Elevated Temperatures", in C.M. Herzfeld, ed., TEMPERATURE, ITS MEASUREMENT AND CONTROL IN SCIENCE AND INDUSTRY, Vol. III, Reinhold, New York, 1962, Part 2, p. 523.
19. Taylor, R.E., and R.A. Finch, J. Less-Common Metals, 6, p. 283, (1964).
20. Wallace, D.C., Phys. Rev., 120, p. 84, (1960).
21. Wallace, D.C., P.H. Sidles, and G.C. Danielson, J. Appl. Phys., 31, p. 168, (1960).
22. Worthing, A.G., Phys. Rev., 12, p. 199, (1918).
23. Worthing, A.G., Phys. Rev., 28, p. 190, (1926).



## Chapter 4

### MASS SPECTROMETRIC STUDY OF THE BERYLLIUM-ALUMINA REACTION

J. Efimenko

#### Introduction

The reduction reaction of alumina with beryllium was performed as an adjunct to the beryllia-alumina system which has been investigated in a metallic environment. Beryllium was selected as the reducer since it has a lower vapor pressure than aluminum. It was of interest to observe the predominant vapor species under such reducing conditions and to obtain data on the vapor reactions occurring in this system.

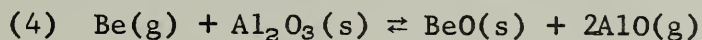
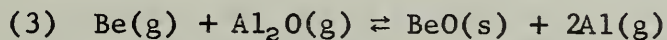
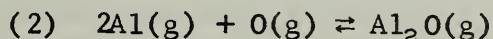
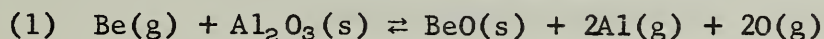
#### Experimental

For this study, beryllium powder, less than 200 mesh, was tried and metal chips were used. Beryllium powder was mixed with carbon-free alumina and placed into a tungsten cup inside a tungsten effusion cell. In the second case, a chip of beryllium metal was placed on the bottom of the cup and covered with alumina. The mass spectrometer and geometry were those used for the alumina-beryllia studies. An effusion cell with one millimeter orifice was employed with the beryllium powder-alumina mixture and a 0.5 mm orifice-effusion cell with beryllium chip-alumina mixture. A silver calibration was carried out with the 0.5 mm orifice effusion cell.

#### Results

It was possible to observe ion intensities of the reactant, beryllium, as well as the products, aluminum, its reduced oxides and oxygen, employing the second cell. Table 1 presents ion intensity-temperature data for the range 1511-1743K.

From the various equations that could describe this reducing system, the following were selected for computation:





From the data, Table 1, and auxiliary data in Table 2, apparent equilibrium constants were computed. Second law plots for these reactions are shown in Figures 1, 2, 3, and 4. Enthalpies of these reactions were computed and are listed in Table 3.

### Discussion

The reduction reaction with beryllium powder produced copious amounts of Al and  $\text{Al}_2\text{O}$  species at a rapid rate. It was difficult to detect gaseous Be and AlO under these conditions. Also, a decrease in intensities of  $\text{Al}^+$  and  $\text{Al}_2\text{O}^+$  occurred and on examining the effusion cell at the end of the experiment, the orifice was found to be filled with a solid.

Only the data from the second experiment, using a chip of beryllium underneath a layer of alumina, were employed. The data with index nos. 1 and 13 appear anomalous and were not considered in the second law treatment. The last points taken at the maximum temperature,  $1420^\circ\text{C}$  (uncorr.), show a loss of ion intensity and this effect is assumed to be coincident with the filling of this orifice. The ion intensities, identified by index no. 1, are larger than others at equivalent temperatures and this is probably due to contamination from the previous energetic experiment.

The causes for the scatter in the ion intensities are unknown and should require further investigation. During the experiments, ion intensities could be duplicated at a fixed temperature, which indicated that the electronic circuits were dependable. Since the ion intensities at  $1200^\circ\text{C}$ , Table 1, index nos. 2 and 10, could not be duplicated, unknown changes may have occurred inside the effusion cell. The data shown in Table 1 were obtained over a period of five days with discontinuous operation. The effusion cell was maintained at a selected temperature on the average for thirty minutes and many times for one hour while the data were recorded.

Reaction enthalpies, Table 3, were obtained by the second law and third law calculations. For the second law least squares fit, data corresponding to index nos. 2, 3, and 7 were given weights of 0.5, the remaining points, weights of 1.0. The tabulated enthalpies are mean values. The second law values in this table are least squares fit with the standard deviations in the slopes.

The reaction enthalpies show a reasonable inter-consistency. The enthalpy difference between reaction 4 and 1 give the formation enthalpy of two AlO molecules. Reaction 2 gives the enthalpy of forming two Al-O bonds in the  $\text{Al}_2\text{O}$  molecule. Although the Al-O bonds in

these two molecules are not the same, they differ by approximately 5 kcal. The difference in enthalpies from reactions 4 and 1 is 147 kcal, and reaction 2 gives 161 kcal. However, this type of calculation does not indicate the reliability of the enthalpy values themselves.

The partial pressures in Table 4 were obtained with the aid of a silver calibration using the 0.5 mm orifice effusion cell. These pressures involve the usual error associated with ionization cross-sections of molecules but are of interest for relative comparison of partial pressure magnitude among the species observed.

TABLE 1

Data - Ion Intensities

Index No.	Obs. Temp. °C	$I_{\text{Be}}^+$	$I_{\text{O}}^+$	$I_{\text{Al}}^+$	$I_{\text{AlO}}^+$	$I_{\text{Al}_2\text{O}}^+$
1	1.3650 × 10 <sup>3</sup>	1.17 × 10 <sup>-2</sup>	1.80 × 10 <sup>-3</sup>	2.37 × 10 <sup>-1</sup>	5.20 × 10 <sup>-2</sup>	7.20 × 10 <sup>-1</sup>
2	1.2000 × 10 <sup>3</sup>	5.00 × 10 <sup>-4</sup>	3.00 × 10 <sup>-4</sup>	7.65 × 10 <sup>-2</sup>	1.30 × 10 <sup>-3</sup>	2.19 × 10 <sup>-2</sup>
3	1.2330 × 10 <sup>3</sup>	6.00 × 10 <sup>-4</sup>	7.00 × 10 <sup>-4</sup>	1.54 × 10 <sup>-1</sup>	2.10 × 10 <sup>-3</sup>	3.80 × 10 <sup>-2</sup>
4	1.2700 × 10 <sup>3</sup>	1.00 × 10 <sup>-3</sup>	3.10 × 10 <sup>-3</sup>	2.58 × 10 <sup>-1</sup>	3.50 × 10 <sup>-3</sup>	6.30 × 10 <sup>-2</sup>
5	1.2750 × 10 <sup>3</sup>	6.00 × 10 <sup>-4</sup>	1.90 × 10 <sup>-3</sup>	1.41 × 10 <sup>-1</sup>	1.60 × 10 <sup>-3</sup>	2.80 × 10 <sup>-2</sup>
6	1.2650 × 10 <sup>3</sup>	5.00 × 10 <sup>-4</sup>	4.50 × 10 <sup>-4</sup>	9.90 × 10 <sup>-2</sup>	1.00 × 10 <sup>-3</sup>	2.00 × 10 <sup>-2</sup>
7	1.3400 × 10 <sup>3</sup>	1.75 × 10 <sup>-3</sup>	1.80 × 10 <sup>-3</sup>	4.15 × 10 <sup>-1</sup>	4.80 × 10 <sup>-3</sup>	8.00 × 10 <sup>-2</sup>
8	1.2860 × 10 <sup>3</sup>	9.50 × 10 <sup>-4</sup>	9.00 × 10 <sup>-4</sup>	1.98 × 10 <sup>-1</sup>	2.90 × 10 <sup>-3</sup>	5.70 × 10 <sup>-2</sup>
9	1.2430 × 10 <sup>3</sup>	5.00 × 10 <sup>-4</sup>	5.00 × 10 <sup>-4</sup>	9.30 × 10 <sup>-2</sup>	7.00 × 10 <sup>-4</sup>	1.65 × 10 <sup>-2</sup>
10	1.2000 × 10 <sup>3</sup>	1.35 × 10 <sup>-4</sup>	2.50 × 10 <sup>-4</sup>	3.60 × 10 <sup>-2</sup>	3.00 × 10 <sup>-4</sup>	7.00 × 10 <sup>-3</sup>
11	1.3000 × 10 <sup>3</sup>	1.50 × 10 <sup>-3</sup>	1.45 × 10 <sup>-3</sup>	5.00 × 10 <sup>-1</sup>	8.70 × 10 <sup>-3</sup>	1.38 × 10 <sup>-1</sup>
12	1.3440 × 10 <sup>3</sup>	1.65 × 10 <sup>-3</sup>	3.15 × 10 <sup>-3</sup>	7.10 × 10 <sup>-1</sup>	1.53 × 10 <sup>-2</sup>	2.85 × 10 <sup>-1</sup>
13	1.4200 × 10 <sup>3</sup>	3.50 × 10 <sup>-3</sup>	5.40 × 10 <sup>-3</sup>	3.50 × 10 <sup>-1</sup>	3.00 × 10 <sup>-3</sup>	1.55 × 10 <sup>-3</sup>

The ion intensities are expressed in volts; the ionization potential was 53.5 ev.

TABLE 2

## Auxiliary Data

Specie	Multiplier Efficiency	Ionization Cross-section
$M^+$	$\gamma, (1)$	$\sigma, (2)$
$Be^+$	280	2.5
$O_{16}^+$	180	1.6
$Al^+$	294	5.0
$AlO^+$	250	6.6
$Al_2O^+$	260	11.6
$Ag_{107}$	153	10.1

(1) Author's values.

(2) R. F. Pottie, J. Chem. Phys. 44, 916 (1966).

Window-prism transmissivity, A =  $1.71 \times 10^{-5} \text{ } ^\circ K^{-1}$   
 Ag sample  $5.950 \times 10^{-3} \text{ gm (99.9\% pure)}$   
 Silver sensitivity  $1.1683 \times 10^{-6} \text{ amp/atm at } 1361^\circ K$

## Enthalpy Functions - Free Energy Functions

(Be, O, Al, AlO, BeO) NBS Report 6928, July 1960  
 ( $Al_2O_3$ ) NBS Report 6484, July 1959



TABLE 3

## Reaction Enthalpies

Reaction	2nd Law		3rd Law
	$\Delta H_{1682}^{\circ}$ kcal/mol	$\Delta H_{\infty}^{\circ}$ kcal/mol	$\Delta H_{\infty}^{\circ}$ kcal/mol
1	265 $\pm$ 0.5	264	286.7
2	- 155 $\pm$ 3	- 150	- 161.2
3	3 $\pm$ 8	- 0.7	- 39
4	134 $\pm$ 3.0	126	140.0

---

NOTE: Cal.  $\times$  4.1840 = joule

TABLE 4

Partial Pressures, atms.

Index No.	Temp. Corr. °K	P <sub>Be</sub>	P <sub>O</sub>	P <sub>Al</sub>	P <sub>AlO</sub>	P <sub>Al<sub>2</sub>O</sub>
1	1685	2.74 × 10 <sup>-6</sup>	1.02 × 10 <sup>-6</sup>	2.64 × 10 <sup>-5</sup>	5.16 × 10 <sup>-6</sup>	3.91 × 10 <sup>-5</sup>
2	1511	1.05 × 10 <sup>-7</sup>	1.53 × 10 <sup>-7</sup>	7.64 × 10 <sup>-6</sup>	1.16 × 10 <sup>-7</sup>	1.07 × 10 <sup>-6</sup>
3	1546	1.29 × 10 <sup>-7</sup>	3.65 × 10 <sup>-7</sup>	1.58 × 10 <sup>-5</sup>	1.91 × 10 <sup>-7</sup>	1.89 × 10 <sup>-6</sup>
4	1585	2.20 × 10 <sup>-7</sup>	1.66 × 10 <sup>-6</sup>	2.70 × 10 <sup>-5</sup>	3.27 × 10 <sup>-7</sup>	3.22 × 10 <sup>-6</sup>
5	1590	1.32 × 10 <sup>-7</sup>	1.02 × 10 <sup>-6</sup>	1.49 × 10 <sup>-5</sup>	1.50 × 10 <sup>-7</sup>	1.44 × 10 <sup>-6</sup>
6	1580	1.10 × 10 <sup>-7</sup>	2.40 × 10 <sup>-7</sup>	1.03 × 10 <sup>-5</sup>	9.31 × 10 <sup>-8</sup>	1.02 × 10 <sup>-6</sup>
7	1659	4.03 × 10 <sup>-7</sup>	1.01 × 10 <sup>-6</sup>	4.55 × 10 <sup>-5</sup>	4.69 × 10 <sup>-7</sup>	4.28 × 10 <sup>-6</sup>
8	1602	2.11 × 10 <sup>-7</sup>	4.87 × 10 <sup>-7</sup>	2.10 × 10 <sup>-5</sup>	2.74 × 10 <sup>-7</sup>	2.94 × 10 <sup>-6</sup>
9	1556	1.08 × 10 <sup>-7</sup>	2.63 × 10 <sup>-7</sup>	9.57 × 10 <sup>-6</sup>	6.42 × 10 <sup>-8</sup>	8.28 × 10 <sup>-7</sup>
10	1511	2.83 × 10 <sup>-8</sup>	1.27 × 10 <sup>-7</sup>	3.60 × 10 <sup>-6</sup>	2.67 × 10 <sup>-8</sup>	3.41 × 10 <sup>-7</sup>
11	1616	3.37 × 10 <sup>-7</sup>	7.91 × 10 <sup>-7</sup>	5.35 × 10 <sup>-5</sup>	8.29 × 10 <sup>-7</sup>	7.19 × 10 <sup>-6</sup>
12	1663	3.81 × 10 <sup>-7</sup>	1.77 × 10 <sup>-6</sup>	7.81 × 10 <sup>-5</sup>	1.50 × 10 <sup>-6</sup>	1.53 × 10 <sup>-5</sup>
13	1743	8.47 × 10 <sup>-7</sup>	3.18 × 10 <sup>-6</sup>	4.04 × 10 <sup>-5</sup>	3.08 × 10 <sup>-7</sup>	8.71 × 10 <sup>-8</sup>

---

 Partial pressures in atmospheres of vapor species observed in the beryllium-alumina system.

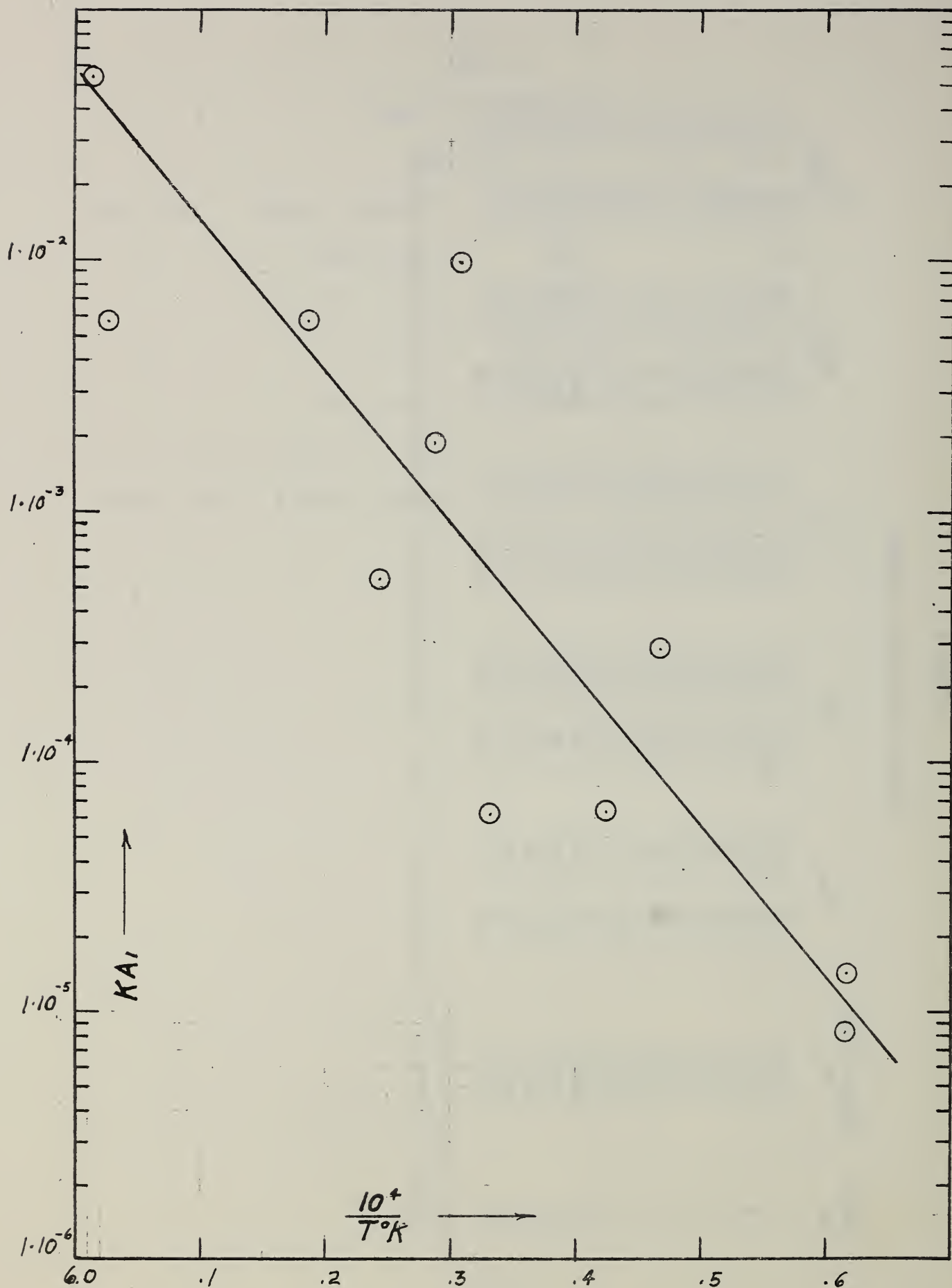


Figure 1. A van't Hoff plot for the reaction:  
 $\text{Be(g)} + \text{Al}_2\text{O}_3(\text{s}) \rightleftharpoons \text{BeO(s)} + 2\text{Al(g)} + 2\text{O(g)}$ ,  $\Delta H_{1582}^\circ = + 265 \text{ kcal/mol}$   
 at the mean reciprocal temperature,  $6.3210 \times 10^{-4} \text{ }^\circ\text{K}^{-1}$ .

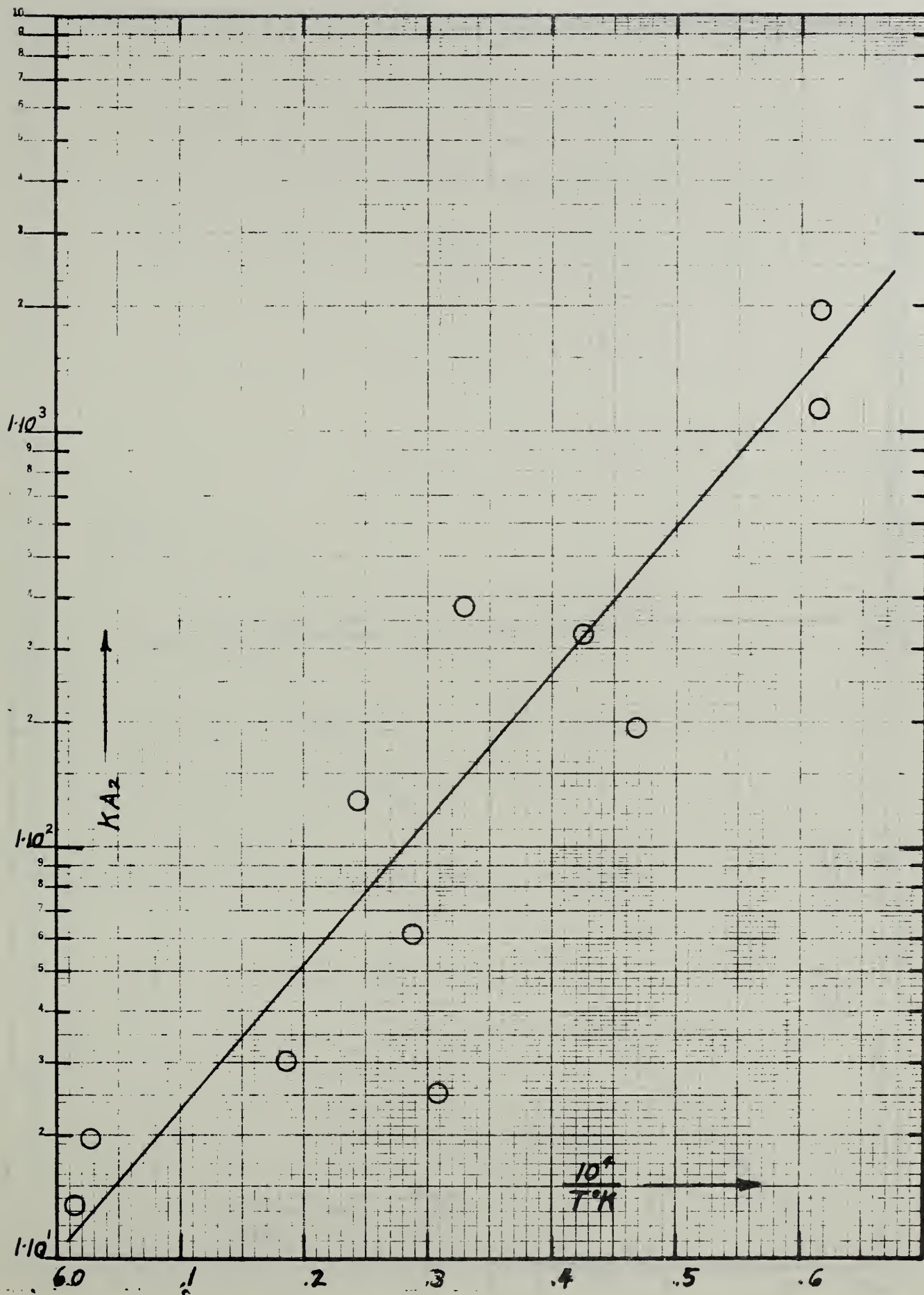


Figure 2. A van't Hoff plot for the reaction:  
 $2Al(g) + O(g) \rightleftharpoons Al_2O(g)$ ,  $\Delta H_{1582}^\circ = -155$  kcal/mol.



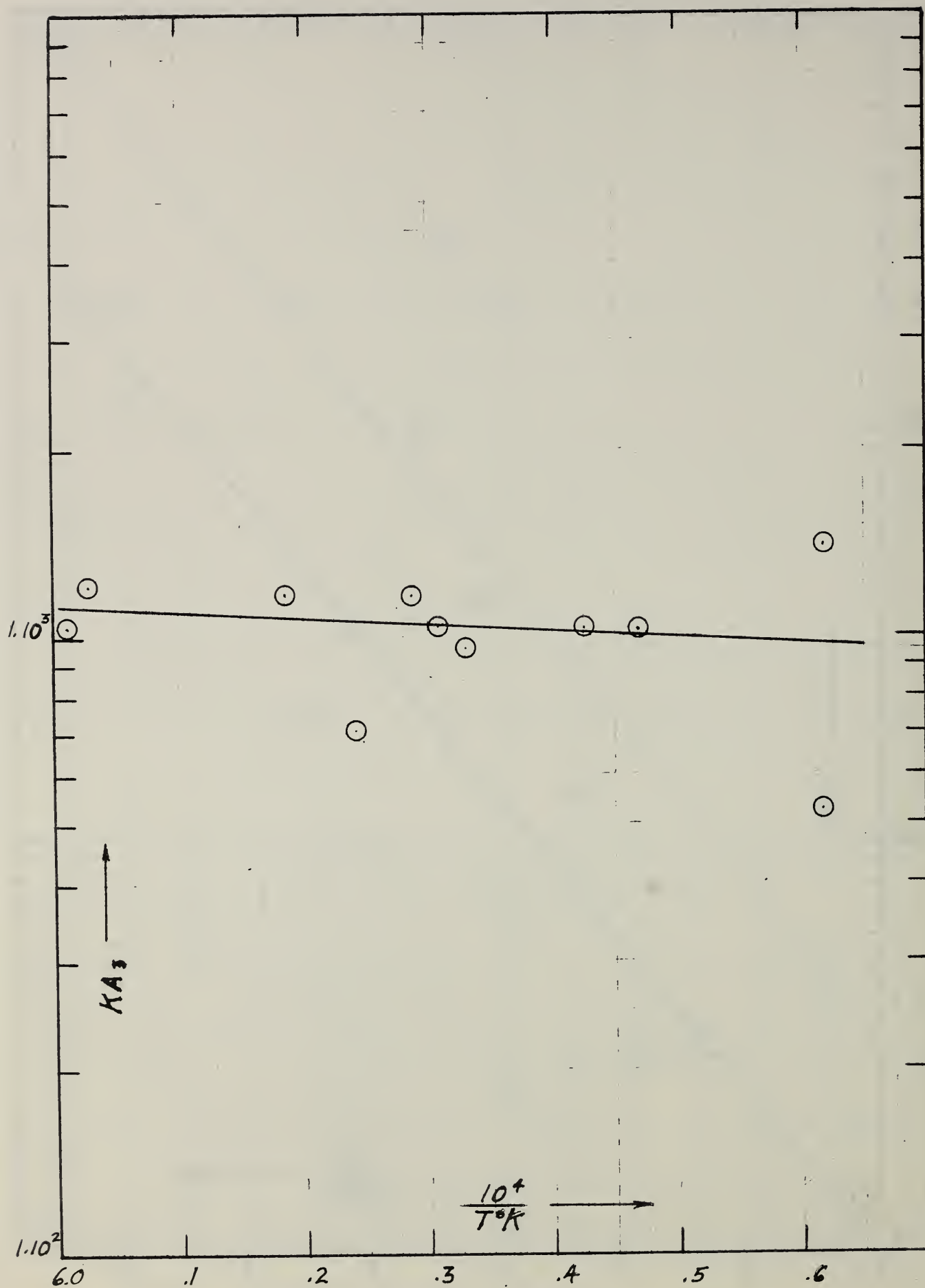


Figure 3. A van't Hoff plot for the reaction:  
 $\text{Be(g)} + \text{Al}_2\text{O(g)} \rightleftharpoons \text{BeO(s)} + 2\text{Al(g)}$ ,  $\Delta H_{1582}^\circ = 3 \text{ kcal/mol}$ .

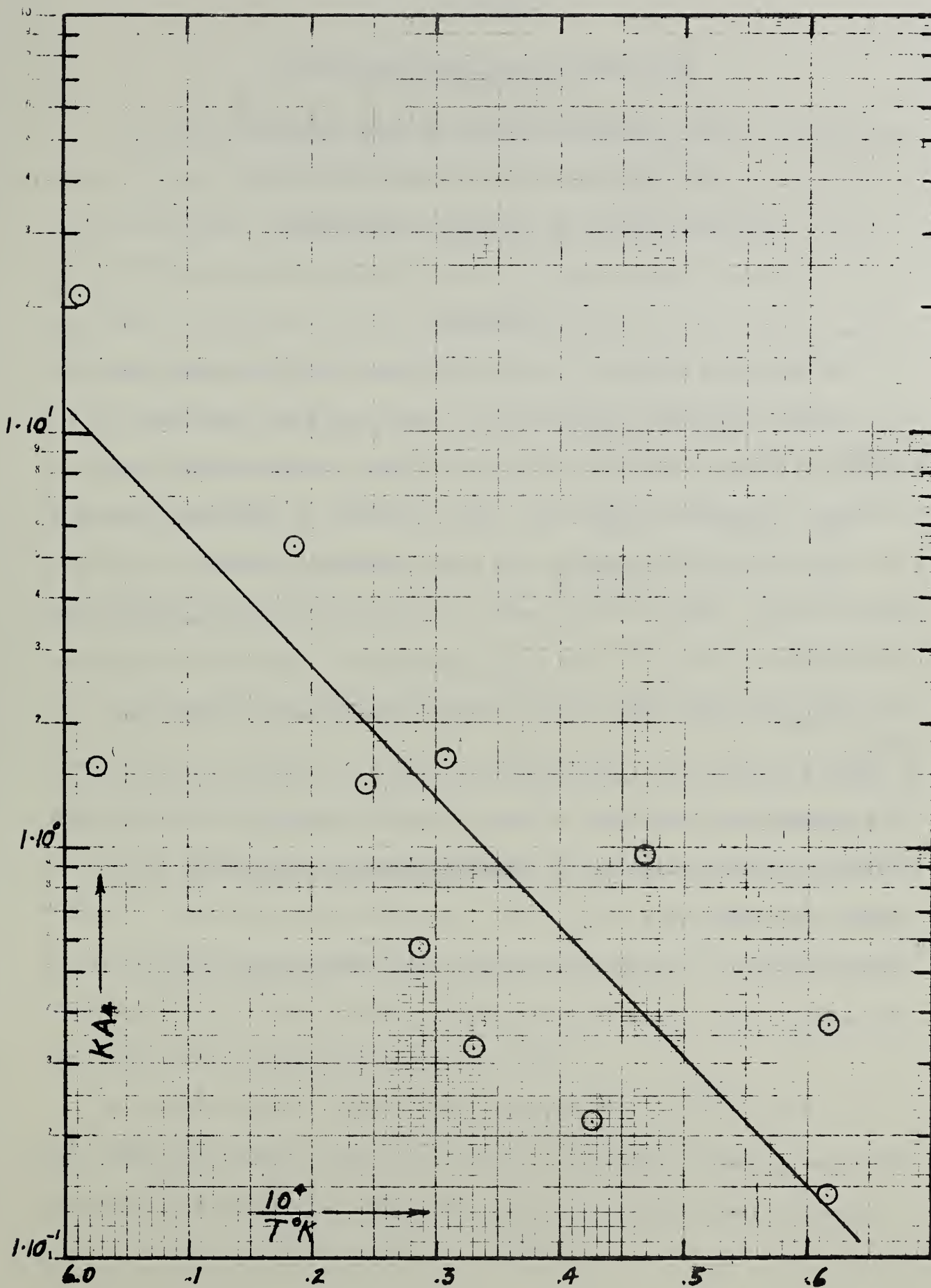


Figure 4. A van't Hoff plot for  
 $\text{Be(g)} + \text{Al}_2\text{O}_3\text{(s)} \rightleftharpoons \text{BeO(s)} + 2\text{AlO(g)}$ ,  $\Delta H_{1582}^\circ = 134 \text{ kcal/mol}$ .

## Chapter 5

### STRUCTURE OF THE ALKALI HYDROXIDES.

#### III. MICROWAVE SPECTRA OF RbOH and RbOD<sup>†</sup>

Chi Matsumura\* and David R. Lide, Jr.

National Bureau of Standards, Washington, D. C.

#### ABSTRACT

The microwave spectra of gaseous RbOH and RbOD have been measured with a high-temperature spectrometer. The spectra are generally similar to those observed in CsOH and indicate an essentially linear structure for rubidium hydroxide. The variation of rotational constant with excitation of the bending mode shows anomalies similar to those found in CsOH. The Rb-O bond length is found to be  $2.30_5 \text{ \AA}$ , while the O-H distance is  $0.96_5 \text{ \AA}$ . Analysis of the nuclear quadrupole hyperfine structure gives eqQ values of  $-67.9 \text{ Mc/s}$  in  $\text{Rb}^{85}\text{OH}$  and  $-35 \text{ Mc/s}$  in  $\text{Rb}^{87}\text{OH}$ .

---

<sup>†</sup>This research was supported by the U.S. Air Force Office of Scientific Research. Contribution of the National Bureau of Standards, not subject to copyright.

\*Present address: Government Chemical Research Institute, Tokyo, Japan.

## INTRODUCTION

As reported in paper I of this series,<sup>1</sup> the microwave spectrum of gaseous cesium hydroxide indicates a linear or near-linear structure for the molecule. However, the dependence of the rotational constant  $B_v$  on the vibrational quantum number  $v_2$  showed several anomalies.  $B_v$  was found to decrease with increasing excitation of the bending mode  $v_2$ , which is opposite from the normal behavior in linear molecules. Furthermore, the dependence on  $v_2$  was strongly non-linear, and the deuterium isotope effect was very large. A study has now been carried out on the spectrum of rubidium hydroxide. Similar anomalies have been found, which suggests that they are a general feature of the alkali hydroxide molecules.

## EXPERIMENTAL

The microwave spectrometer used in this study was the same as described in I, except for a small modification. The pumping system was improved and a larger diameter tube was used for the vacuum jacket in order to allow more efficient removal of the water vapor which was formed by the rapid decomposition of RbOH at the operating temperature. In spite of this improvement, the water vapor still caused appreciable broadening of the lines. The RbOH spectrum was weaker and somewhat more difficult to obtain than that of CsOH.

As the Rb atom has two isotopic species 72% of  $\text{Rb}^{85}$  and 28% of  $\text{Rb}^{87}$ , and both species have large nuclear quadrupole moments, many weak lines had to be measured. Therefore, most measurements were done by



slow sweep recording in order to obtain high sensitivity. However, the thermionic emission which was discussed in the previous paper<sup>1</sup> made the application of a high Stark modulation voltage extremely difficult. The thermionic emission caused not only a wandering base line but also large amplitude random noise, so that the observation of  $\Sigma$  states, which required high modulation, was possible only under optimum conditions. The conditions were not easily controlled in these experiments, but the lining of the waveguide with very pure silver (99.99%) was effective for preventing the thermionic emission, and careful cleaning of the waveguide and quartz tube also reduced the difficulties.

The measurement of temperature was done with a thermocouple which was placed at the side of the waveguide. Since both the waveguide and the thermocouple were heated mainly by radiation from the furnace, and the temperature was not homogeneous, the thermocouple gave only a rough indication of the gas temperature. However, 550-600°C was believed to be the typical operating temperature. Because of the inhomogeneity of the temperature, the effective cell length was probably shorter than the oven length (45 cm). It seemed that the sample at the center portion of the cell was vaporized first and the working region expanded gradually. Although this effect reduced the sensitivity of the spectrometer, the gaseous molecules were produced for an extended period (1-2 hours).

## ANALYSIS OF SPECTRUM

Most observations were made on the  $J = 2 \rightarrow 3$  transition, since the sensitivity of the microwave spectrometer was optimized in this frequency region. Another merit of this transition was the convenient magnitude of the nuclear quadrupole splitting. The  $J = 1 \rightarrow 2$  and the  $J = 3 \rightarrow 4$  transitions of some states were observed for confirmation of assignments and calculation of nuclear quadrupole coupling constants. In some cases, the double-resonance procedure was helpful for finding or confirming  $\Sigma$  states. The observed frequencies of the  $J = 2 \rightarrow 3$  transitions are listed in Tables I and II.

As was the case with cesium hydroxide, the spectrum of rubidium hydroxide indicates an essentially linear molecule with a large number of low-lying vibrational states. The assignment of vibrational satellites was done by Stark identification and from considerations of the reasonable relative positions of lines in the series. The separation between lines of molecules containing  $\text{Rb}^{85}$  and  $\text{Rb}^{87}$  is the same order of magnitude as vibrational satellite shifts, so that the spectra overlapped each other. The hyperfine patterns were helpful in discriminating them.

The  $B_v$  values were calculated from  $J = 2 \rightarrow 3$  transitions by using the equation

$$\nu = [2B_v \pm \frac{q}{2} \ell (v_2 + 1)](J + 1) - 4D(J + 1)[(J + 1)^2 - \ell^2]. \quad (1)$$

A value of  $D = 0.0067$  Mc/s was used for this calculation. It was obtained from the equation  $D = 4B_e^3 \sum (\zeta_{2s}^{(x)})^2 / \omega_s'^2$ . It was not possible

to obtain a good experimental D value from the transitions  $J = 2 \rightarrow 3$  and  $J = 1 \rightarrow 2$  because of hyperfine complications, so that the calculated value seems to be more reliable. The  $B_v$  values are listed in Table III, and the values of  $q_\ell$  are given in Table IV.

The frequencies of the  $(02^0_0)$  and  $(12^0_0)$  states of RbOD could not be measured because of the exact overlapping with the  $(01^1_0)$   $\ell$ - and  $(11^1_0)$   $\ell$ - lines, respectively. On the other hand, the latter two lines were measured by using small Stark modulation. The overlapping was confirmed by comparison with the shape of the same lines in the normal isotopic species.

#### NUCLEAR QUADRUPOLE COUPLING

Since the line width in this molecule is fairly large while the hyperfine splitting in the transition  $J = 2 \rightarrow 3$  is small, it was difficult to determine the eqQ values with high accuracy. The splitting in the transition  $J = 1 \rightarrow 2$  is larger, but the line strength of the weak components is not sufficient for accurate measurement. Assumed values of eqQ were used for analysis of weaker satellite lines from the higher vibrational states and for the RbOD species.

The values of eqQ are included in Table III. They are small in spite of the very large Q values of  $\text{Rb}^{85}$  and  $\text{Rb}^{87}$ . This shows that the Rb-O bonding is almost completely ionic. The values of eqQ are the same order as those in  $\text{Rb}^{85}\text{Cl}$  (eqQ = -52.675 Mc/s) and  $\text{Rb}^{87}\text{Cl}$  (eqQ = -25.485 Mc/s). Though the error in the measurement of eqQ is fairly large, it may be concluded that eqQ decreases markedly with increase of  $v_1$ . The patterns of hyperfine structure for  $\ell = 0, 1$ , and



2 states fit exactly to the model of a linear molecule within the experimental error. This is further support for the linearity of the alkali hydroxide molecules.

#### VIBRATION-ROTATION INTERACTIONS

The gross features of the rubidium hydroxide spectrum are very similar to those found in cesium hydroxide. The variation of  $B_v$  with  $v_1$  (see Table V) is quite regular, yielding  $\alpha_1$  values of 43.7 Mc/s in RbOH and 38.2 Mc/s in RbOD. The dependence of  $\alpha_1$  on the Rb isotope is too small to be measured accurately. On the other hand, the variation of  $B_v$  with  $v_2$  is strongly non-linear, is in the opposite direction from that in normal linear molecules, and shows a large deuterium isotope effect. These anomalies are not so pronounced as in the cesium compound but are still quite noticeable.

It was found in cesium hydroxide that the  $B_v$  values could be fit to a power series containing terms in  $(v_2+1)$ ,  $(v_2+1)^2$  and  $\ell^2$ . The same is true for rubidium hydroxide. A least squares fit resulted in the following coefficients:

$$\text{Rb}^{85}\text{OH: } B_v = 6321.57 - 33.38 (v_2+1) + 1.905 (v_2+1)^2 - 2.05 \ell^2$$

$$\text{Rb}^{85}\text{OD: } B_v = 5730.85 - 11.16 (v_2+1) + 1.08 (v_2+1)^2 - 1.15 \ell^2$$

$$\text{Rb}^{87}\text{OH: } B_v = 6297.05 - 32.31 (v_2+1) + 1.613 (v_2+1)^2 - 2.04 \ell^2$$

$$\text{Rb}^{87}\text{OD: } B_v = 5707.57 - 10.32 (v_2+1) + 0.88 (v_2+1)^2 - 1.13 \ell^2.$$

In  $\text{Rb}^{85}\text{OH}$  and  $\text{Rb}^{85}\text{OD}$ , where the fit was over-determined, the inclusion of a  $(v_2+1)^3$  term leads to no significant improvement. In the other two species the number of  $B_v$  values was just sufficient to determine the coefficients given above. The precision of the fit for  $\text{Rb}^{85}\text{OH}$  and



and  $\text{Rb}^{85}\text{OD}$  is illustrated in Table VI.

The general similarity of the vibration-rotation interactions in  $\text{CsOH}$  and  $\text{RbOH}$  suggests that the anomalous behavior is characteristic of the alkali hydroxide molecules, and is not the result of some accidental resonance. Furthermore, the ability to fit the variation of  $B_v$  with  $v_2$  in both molecules to a truncated power series lends some confidence to the identification of the coefficients of the series with the usual spectroscopic constants  $\alpha_2$ ,  $\gamma_{22}$ , and  $\gamma_{22}$ . Some progress has been made in the explanation of the anomalous values of these constants; the details will be reported in a subsequent paper.

#### STRUCTURE

The interatomic distances have been calculated from the rotational constants of  $\text{RbOH}$  and  $\text{RbOD}$  on the assumption of a linear model. Following the procedure used for  $\text{CsOH}$ , the calculation was done both with the ground state constants and with the extrapolated constants obtained from the power-series fit discussed in the last section. The results are given in Table VII. Essentially the same distances were obtained from the constants of the  $\text{Rb}^{85}$  and  $\text{Rb}^{87}$  species.

As was found for  $\text{CsOH}$ , the O-H distance derived from the extrapolated B values has a more reasonable magnitude. The Rb-O distance of  $2.30_5 \text{ \AA}$  is not far from the  $r_e$  value of  $2.265 \text{ \AA}$  in  $\text{RbF}$ .

#### ACKNOWLEDGMENTS

We wish to acknowledge the preliminary search for the  $\text{RbOH}$  spectrum carried out by R. L. Kuczkowski. We also appreciate helpful discussions with J. T. Hougen.

## REFERENCES

1. D. R. Lide and R. L. Kuczkowski, J. Chem. Phys. 46, 4768 (1967).
2. H. H. Nielsen, Rev. Mod. Phys. 23, 90 (1951).

Table I. Observed frequencies in  $\text{Rb}^{85}\text{OH}$  and  $\text{Rb}^{85}\text{OD}$  in Mc/s

(J = 2 $\rightarrow$ 3 transition).					
State	F	$\rightarrow$	F'	$\text{Rb}^{85}\text{OH}$	$\text{Rb}^{85}\text{OD}$
(00 <sup>0</sup> 0)	5/2		5/2	37744.8	
	7/2		(7/2, 9/2)	37741.2	34324.6
	9/2		11/2		
	5/2		7/2	37738.3	34321.6
	3/2		5/2	37734.9	34317.9
	1/2		3/2		
	9/2		(7/2, 9/2)	37728.6	34311.9
(01 <sup>1</sup> 0) $\ell^+$	5/2		3/2	37600.7	
	3/2		1/2		
	5/2		5/2	37594.3	34301.9
	9/2		11/2		
	7/2		(7/2, 9/2)	37591.3	34299.0
	5/2		7/2	37589.4	34297.3
	3/2		5/2		
	9/2		(7/2, 9/2)	37584.7	34292.3
(01 <sup>1</sup> 0) $\ell^-$	5/2		3/2	37541.0	
	3/2		1/2		
	5/2		5/2	37534.9	34242.9
	9/2		11/2		
	7/2		(7/2, 9/2)	37532.0	34240.1
	5/2		7/2	37530.6	34238.5
	3/2		5/2		
	9/2		(7/2, 9/2)	37525.5	34233.5

Table I. Continued

$(02^0 0)$	7/2	(7/2, 9/2)	37430.5	34242.8
	9/2	11/2		
	5/2	7/2	37417.1	34240.0
	3/2	5/2		
	1/2	3/2		34236.0
$(02^2 0)$	1/2	(1/2, 3/2)	37394.0	34228.8
	3/2	(1/2, 3/2, 5/2)	37385.2	34220.1
	9/2	(7/2, 9/2, 11/2)		
	5/2	(3/2, 5/2, 7/2)	37375.6	34210.4
	7/2	(5/2, 7/2, 9/2)	37372.2	34207.1
$(03^1 0) \ell^+$	5/2	5/2	37362.2	34278.3
	9/2	11/2		
	7/2	(7/2, 9/2)	37358.9	34275.4
	5/2	7/2	37357.2	34273.5
	3/2	5/2		
$(03^1 0) \ell^-$	9/2	(7/2, 9/2)	37352.5	
	5/2	5/2	37238.1	34152.2
	9/2	11/2		
	7/2	(7/2, 9/2)	37235.0	34149.3
	5/2	7/2	37233.0	34147.8
	3/2	5/2		



Table I. Continued

$(04^2_0)$	1/2	(1/2, 3/2)	37179.4	
	3/2	(1/2, 3/2, 5/2)	37170.7	34189.2
	9/2	(7/2, 9/2, 11/2)		
	5/2	(3/2, 5/2, 7/2)	37160.9	34179.2
	7/2	(5/2, 7/2, 9/2)	37157.8	34174.8
$(10^0_0)$	7/2	(7/2, 9/2)	37479.1	34095.4
	9/2	11/2		
	3/2	5/2	37472.7	34089.0
	1/2	3/2		
	9/2	7/2	37466.7	34082.9
	9/2	9/2		
$(11^1_0) \ell^+$	5/2	5/2	37333.6	34071.0
	9/2	11/2		
	7/2	(7/2, 9/2)	37330.8	34068.2
	5/2	7/2	37329.0	34066.4
	3/2	5/2		
	9/2	(7/2, 9/2)	37324.1	
$(11^1_0) \ell^-$	5/2	5/2	37269.2	34010.2
	9/2	11/2		
	7/2	(7/2, 9/2)	37266.4	34007.5
	5/2	7/2	37264.9	34006.1
	3/2	5/2		
	9/2	(7/2, 9/2)	37260.0	

Table I. Continued

$(12^0_0)$	7/2	(7/2, 9/2)	37164.5	34010.5
	9/2	11/2		
	5/2	7/2		34007.6
$(12^2_0)$	1/2	(1/2, 3/2)	37140.7	33995.2
	3/2	(1/2, 3/2, 5/2)	37132.0	33986.8
	9/2	(7/2, 9/2, 11/2)		
	5/2	(3/2, 5/2, 7/2)	37122.3	33977.3
	7/2	(5/2, 7/2, 9/2)	37119.2	33974.1
(200)	7/2	(7/2, 9/2)	37216.9	33866.8
	9/2	11/2		
	5/2	7/2	37213.9	33863.9
	3/2	5/2	37210.8	33860.7
	1/2	3/2		
	9/2	(7/2, 9/2)	37204.8	

Table II. Observed frequencies in  $\text{Rb}^{87}\text{OH}$  and  $\text{Rb}^{87}\text{OD}$  in Mc/s  
( $J = 2 \rightarrow 3$  transition).

State	F	$\rightarrow$	F'	$\text{Rb}^{87}\text{OH}$	$\text{Rb}^{87}\text{OD}$
$(00^0 0)$	7/2		9/2	37597.8	34188.4
	5/2		7/2		
	3/2		5/2	37595.6	34186.6
	1/2		3/2		
$(01^1 0) \ell+$	3/2		3/2	37455.1	
	7/2		9/2	37450.8	34165.1
	1/2		3/2		
	5/2		7/2	37448.7	34163.4
	3/2		5/2		
	7/2		7/2	37444.0	
$(01^1 0) \ell-$	7/2		9/2	37391.7	34106.9
	1/2		3/2		
	5/2		7/2	37389.7	34105.1
	3/2		5/2		
$(02^0 0)$	7/2		9/2	37287.5	34106.9
	5/2		7/2		
	3/2		5/2	37285.6	34105.2
	1/2		3/2		

Table II. Continued

(02 <sup>2</sup> 0)	1/2	3/2	37246.8	
	7/2	(5/2, 7/2, 9/2)	37241.1	34082.5
	3/2	(3/2, 5/2)	37238.3	
	5/2	(3/2, 5/2, 7/2)	37232.8	34074.2
(10 <sup>0</sup> 0)	7/2	9/2	37337.1	33960.8
	5/2	7/2		
	5/2	7/2		33959.0
	3/2	5/2		



Table III. Effective rotational constants and nuclear coupling constants (in Mc/s) for various vibrational states of RbOH and RbOD.

State		$B_v$ (Rb <sup>85</sup> OH)	$B_v$ (Rb <sup>85</sup> OD)	$eqQ^a$
00 <sup>0</sup> 0	$\Sigma$	6290.15	5720.77	-67.9
01 <sup>1</sup> 0	$\pi$	6260.55	5711.69	-67.6
02 <sup>0</sup> 0	$\Sigma$	6238.37	5707.08	(-67.9)
02 <sup>2</sup> 0	$\Delta$	6230.13	5702.57	-67.4
03 <sup>1</sup> 0	$\pi$	6216.43	5702.34	(-67.6)
04 <sup>2</sup> 0	$\Delta$	6194.38	5697.42	-67
10 <sup>0</sup> 0	$\Sigma\Sigma$	6246.45	5682.50	-65.9
11 <sup>1</sup> 0	$\pi$	6216.70	5673.24	-67
12 <sup>0</sup> 0	$\Sigma$	6194.03	5668.37	(-66)
12 <sup>2</sup> 0	$\Delta$	6187.95	5663.75	-66.3
20 <sup>0</sup> 0	$\Sigma$	6202.75	5644.40	-64.2
State		$B_v$ (Rb <sup>87</sup> OH)	$B_v$ (Rb <sup>87</sup> OD)	$eqQ$
00 <sup>0</sup> 0	$\Sigma$	6266.35	5698.13	-35
01 <sup>1</sup> 0	$\pi$	6236.84	5689.32	-33
02 <sup>0</sup> 0	$\Sigma$	6214.63	5684.53	-31
02 <sup>2</sup> 0	$\Delta$	6206.48	5680.02	-32
10 <sup>0</sup> 0	$\Sigma$	6222.90	5660.18	(-33)

<sup>a</sup>The numbers in parentheses are assumed values.

Table IV.  $\ell$ -doubling constants (Mc/s).

State	$q$ (Rb <sup>85</sup> OH)	$q$ (Rb <sup>85</sup> OD)	$q$ (Rb <sup>87</sup> OH)	$q$ (Rb <sup>87</sup> OD)
(01 <sup>1</sup> 0)	9.87	9.82	9.85	9.70
(03 <sup>1</sup> 0)	10.33	10.51		
(11 <sup>1</sup> 0)	10.73	10.12		

Table V. Variation of rotational constants with  $v_1$  in Mc/s.

$v_2^l$	$B_{0v_2^l 0} - B_{1v_2^l 0}$	$B_{1v_2^l 0} - B_{2v_2^l 0}$
<hr/>		
$\text{Rb}^{85}\text{OH}$		
$0^0$	43.70	43.70
$1^1$	43.85	
$2^0$	44.34	
$2^2$	42.18	
$\text{Rb}^{85}\text{OD}$		
$0^0$	38.27	38.10
$1^1$	38.45	
$2^0$	38.71	
$2^2$	38.82	
$\text{Rb}^{87}\text{OH}$		
$0^0$	43.45	
$\text{Rb}^{87}\text{OD}$		
$0^0$	37.95	
<hr/>		

Table VI. Fit of  $B_{0v_3^2}^{20}$  to power series in Mc/s.

State	$\text{Rb}^{85}\text{OH}$		Obs-Calc	$\text{Rb}^{85}\text{OD}$		Obs-Calc
	Calc	$B_{0v_2^2}^{20}$		Calc	$B_{0v_2^2}^{20}$	
$00^0_0$	6290.10		0.05	5720.77		0.00
$01^1_0$	6260.38		0.17	5711.70		-0.01
$02^0_0$	6238.57		-0.20	5707.09		-0.01
$02^2_0$	6230.38		-0.25	5702.49		-0.08
$03^1_0$	6216.48		-0.05	5702.34		0.00
$04^2_0$	6194.10		0.28	5697.45		-0.03



Table VII. Structural parameters of rubidium hydroxide in Å.

	From $B_{OOO}^0$	From " $B_e$ " <sup>a</sup>
r (RbO)	2.316	2.305
r (OH)	0.913	0.965

<sup>a</sup>The first term in Eq. (1) was used as " $B_e$ ." This set of values is felt to be the more reliable one.

## Chapter 6

### STRUCTURE OF THE ALKALI HYDROXIDES

#### IV. THE INFRARED SPECTRA OF MATRIX ISOLATED RbOH, RbOD and NaOH, NaOD

N. Acquista and Stanley Abramowitz

#### ABSTRACT

The infrared spectra of matrix isolated RbOH, RbOD, NaOH and NaOD have been observed. Both the alkali metal oxygen stretch,  $\nu_1$ , and the bending mode,  $\nu_2$ , has been assigned for each species. The metal oxygen stretching mode is found at 354.4, 345, 431, and 422  $\text{cm}^{-1}$  for RbOH, RbOD, NaOH, and NaOD, respectively; the bending mode,  $\nu_2$ , is observed at 309.0, 229, 337, and 250  $\text{cm}^{-1}$ , respectively. Combination of the results of this study with the microwave measurements for RbOH and RbOD indicates an essentially linear structure for this species. The isotope shift for  $\nu_2$  observed in NaOH coupled with reasonable bond lengths indicates an equilibrium configuration of NaOH which probably does not deviate significantly from linearity. The assumption of a linear model with a harmonic bending potential yields a force constant of .046 and .053  $\text{md}^{-2}\text{\AA}$  for RbOH and NaOH, respectively. These results are consistent with our previously reported results for CsOH.

## INTRODUCTION

The second paper of this series described the infrared spectra of matrix isolated CsOH and CsOD.<sup>1</sup> With the exception of the work by Spinar and Margrave,<sup>2</sup> this is the only report on the infrared spectrum of an isolated alkali metal hydroxide. Other work on these systems<sup>3</sup> was confined to solutions or single crystals which give little information on the structure of the monomeric species. Encouraged by the success encountered with CsOH a similar experiment was attempted for RbOH and NaOH. The present paper presents the infrared spectra of matrix isolated RbOH, RbOD, NaOH, and NaOD.

## EXPERIMENTAL

The experimental techniques used have been described previously by Mann et al.<sup>4</sup> The infrared spectra were obtained with a Perkin-Elmer 301 grating spectrophotometer with a wavenumber range of 4000-50  $\text{cm}^{-1}$ .<sup>5</sup> Refrigeration was provided by an Air Products Cryotip operated in the range of 20-33°K.<sup>5</sup> An electron bombardment furnace mounted in a vertical housing was utilized to vaporize the samples from double boiler silver Knudsen cells. In the course of this work it was found that the species studied react with tungsten, molybdenum, stainless steel, nickel, nickel oxide, iron, copper, gold, and platinum at the high temperatures needed to obtain the spectra.

The RbOH and NaOH which were obtained from commercial sources were heated gradually to temperatures of about 600°C in order to remove water and other volatile impurities. Extended periods of outgassing were required in order to remove impurities which masked the spectrum of the

various monomeric species. The deuterioxides were prepared from their respective hydroxides as previously described.<sup>6</sup> However, it was difficult to prepare pure deuterioxides in this manner. Impurities thought to be oxides, peroxides, and/or superoxides tended to broaden the spectrum in the alkali metal oxygen stretching regions making it difficult to locate the vibrational frequencies of these modes with the usual accuracy. The difficulties in estimating temperatures of the effusing gas and the ratio of the matrix diluent to the sample (M/S) were similar to those in the case of CsOH.<sup>1</sup> M/S ratios of 300:1 to 1000:1 and temperatures of 700°C and 900°C for RbOH and NaOH, respectively are probably representative of the conditions utilized in these experiments.

Diffusion studies in which the deposited sample was allowed to warm up to 33°K were performed in an effort to differentiate between monomeric and polymeric species. This method was partially successful for NaOH, however as was the case for CsOH, RbOH does not diffuse readily, even at 33°K, probably because of its high molecular weight. The use of double boiler techniques in order to differentiate between monomeric and polymeric absorptions was more useful. It would be desirable, particularly for NaOH to go above 950°C for this purpose, however only silver crucibles were found to be relatively inert to NaOH at these high temperatures. One run was obtained with a platinum crucible at about 1100°C, in which the corrosion of the crucible took place near the pinhole of the cell (as opposed to the bottom or side) allowing some NaOH effusing at this temperature to be trapped in an argon matrix.



The frequencies were determined by using atmospheric water lines as calibration standards. Spectral slit widths of about  $1\text{ cm}^{-1}$  were used for frequency measurements which therefore are accurate to about  $0.5\text{ cm}^{-1}$  except where noted.

#### EXPERIMENTAL RESULTS

These molecules have three normal modes; two of these  $\nu_1$  and  $\nu_3$  are the M-O and O-H stretching mode, while  $\nu_2$  is the bending mode. Several strong bands appear in the region of  $600\text{-}200\text{ cm}^{-1}$  in both RbOH and NaOH. Figure 1 shows the pertinent portion of the spectra of RbOH in this region observed from two samples labeled a and b. Spectrum b was obtained from a sample effusing at a higher temperature than a. The band observed at  $354.4\text{ cm}^{-1}$  is assigned to the Rb-O stretching mode,  $\nu_1$ , while the band at  $309\text{ cm}^{-1}$  is assigned to the bending mode,  $\nu_2$ . A frequency of  $371.3$  has been observed for the  $\nu_o$  vibration of RbF in the gas phase.<sup>7</sup> All other bands in the spectrum decrease in intensity relative to these two as the temperature of the double boiler Knudsen cell (from which RbOH is effusing) is raised. These features also maintain their intensity relative to each other over a wide temperature range also indicating they belong to the same species. The bands whose relative intensity decrease are due to polymeric species of RbOH, however it has not been possible to make definite assignments. Upon deuteration the Rb-O frequency shifts to  $345\pm 3\text{ cm}^{-1}$ . The rather broad band observed for  $\nu_1$  in RbOD is thought to be due to oxide, peroxide, and/or superoxide impurities introduced during

deuteration. All these species could be expected to have bands in this region. A band also appears at  $229 \pm 3 \text{ cm}^{-1}$  which is assigned to  $\nu_2$ , the RbOD bending mode. This isotope shift observed for  $\nu_2$  is in excellent agreement with that calculated for a linear model to the harmonic oscillator approximation using the bond distances derived by Matsumura and Lide<sup>8</sup> from an analysis of the microwave spectrum of RbOH and RbOD.

Infrared spectra of matrix isolated NaOH in the region of the  $\nu_1$  and  $\nu_2$  fundamentals are shown in Figure 2. Spectrum b was obtained from a higher temperature than a and spectrum c results from allowing diffusion to take place in sample b. It can be seen that the  $431 \text{ cm}^{-1}$  is more intense relative to the others in spectrum b than in a, while diffusion results in a diminution of the relative intensity of this feature as can be seen in c. This indicates that the  $431 \text{ cm}^{-1}$  band is due to a low molecular weight species, and it is assigned to  $\nu_1$ , the Na-O stretching mode of monomeric NaOH. Confirmation of this hypothesis as well as an assignment for  $\nu_2$  can be found in Figure 3. This spectrum was obtained at a higher temperature in excess of  $1000^\circ\text{C}$  using a platinum Knudsen cell in which the corrosion took place at the top of the cell. Three features appear in this spectrum at 431, 400, and  $337 \text{ cm}^{-1}$ . The relative intensity of the  $431 \text{ cm}^{-1}$  to the  $400 \text{ cm}^{-1}$  feature confirms its assignment as the  $\nu_1$  vibration. The  $337 \text{ cm}^{-1}$  is then assigned to  $\nu_2$ , the NaOH bending mode. This assignment is in agreement with Spinar and Margrave's observation of  $437 \pm 10 \text{ cm}^{-1}$  in the gas phase for the Na-O stretching mode. Unlike CsOH and RbOH, however the NaOH

$\nu_1$  fundamental is rather far from the  $522\text{ cm}^{-1}$  observed for the  $\nu_0$  vibration of NaF in the gas phase.<sup>7</sup> The assignment of the other features observed in the spectrum between  $450$  and  $250\text{ cm}^{-1}$  to particular polymers of NaOH is not possible.

The spectrum of NaOD observed in this region is shown in Figure 4. A comparable spectrum of NaOH is also given for comparison. By analogy with NaOH the  $\nu_1$  fundamental is found at  $422\pm 3\text{ cm}^{-1}$ . The breadth of this feature is probably due to oxide, peroxide, and/or superoxide impurities introduced during the synthesis of NaOD from NaOH. Confirmation of this assignment is found by observing  $\nu_2$  shifted to  $250\text{ cm}^{-1}$  as shown in Figure 5. This shift is consistent with a linear model for NaOH having bond lengths of  $1.93$  and  $0.97\text{ \AA}$  for the Na-O and O-H bonds, respectively. It is consistent with the explanation of the breadth of  $\nu_1$  to note that two to three times longer deposition times are required to develop  $\nu_2$  in NaOD than is required for NaOH. A compilation of the data obtained together with previous results for CsOH can be found in Table.1.

The O-H stretching modes,  $\nu_3$ , should appear in the neighborhood of  $3600\text{ cm}^{-1}$  for RbOH and NaOH and  $2560\text{ cm}^{-1}$  for RbOD and NaOD. The spectra were studied in these regions, but no meaningful assignments could be made because of water absorption.

TABLE 1

## OBSERVED BANDS FOR MONOMERIC ALKALI METAL HYDROXIDES

Molecule	$\nu_1$	$\nu_2$	$\nu_3$	Microwave	
				$r_{MO}$	$r_{OH}$
CsOH	335.6	309.8		2.40	0.96
CsOD	330.5	226			
RbOH	354.4	309.0		2.31	0.97
RbOD	345 $\pm$ 3	229 $\pm$ 3			
NaOH	431	337			
NaOD	422 $\pm$ 3	250			



## REFERENCES

1. N. Acquista, S. Abramowitz, D. R. Lide, J. Chem. Phys. 49, (July 15) 1968.
2. L. H. Spinar, J. L. Margrave, Spectrochim. Acta 12, 244 (1958).
3. K. Nakamoto, Infrared Spectra of Inorganic and Coordination Compounds (John Wiley & Sons, Inc., New York, 1963) p. 73.
4. D. E. Mann, G. V. Calder, D. White, K. S. Seshadri, M. J. Linevsky, J. Chem. Phys. 46, 1138 (1967).
5. Certain commercial instruments are identified in order to specify the complete experimental procedure. In no case does such identification imply a recommendation or endorsement by the National Bureau of Standards.
6. D. R. Lide, R. L. Kuczkowski, J. Chem. Phys. 46, 4768 (1967).
7. S. E. Veazey, W. Gordy, Phys. Rev. 138, A1303 (1965).
8. C. Matsumura, D. R. Lide, to be published.

RbOH/Ar

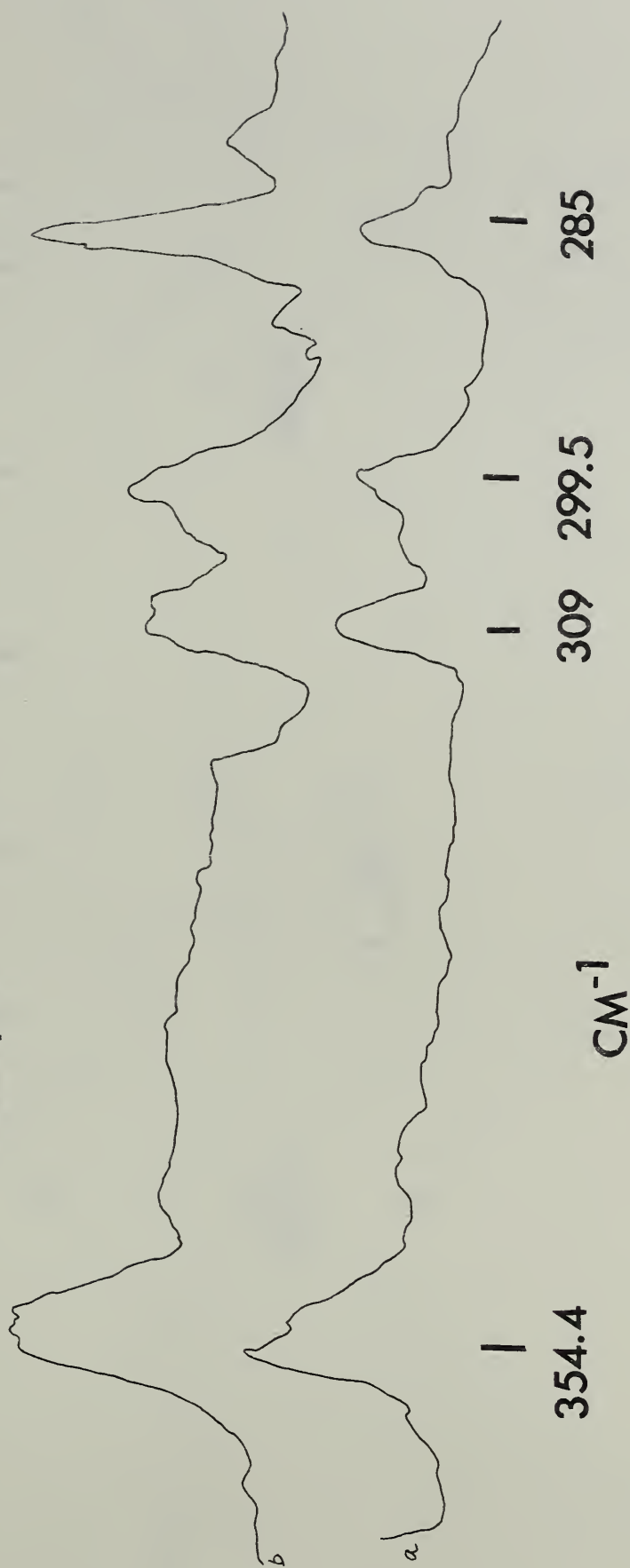


Figure 1 - The spectra of matrix isolated RbOH in argon. Curve a refers to a sample which effused from the crucible at a higher temperature than the sample represented in curve b.

# NaOH/Ar

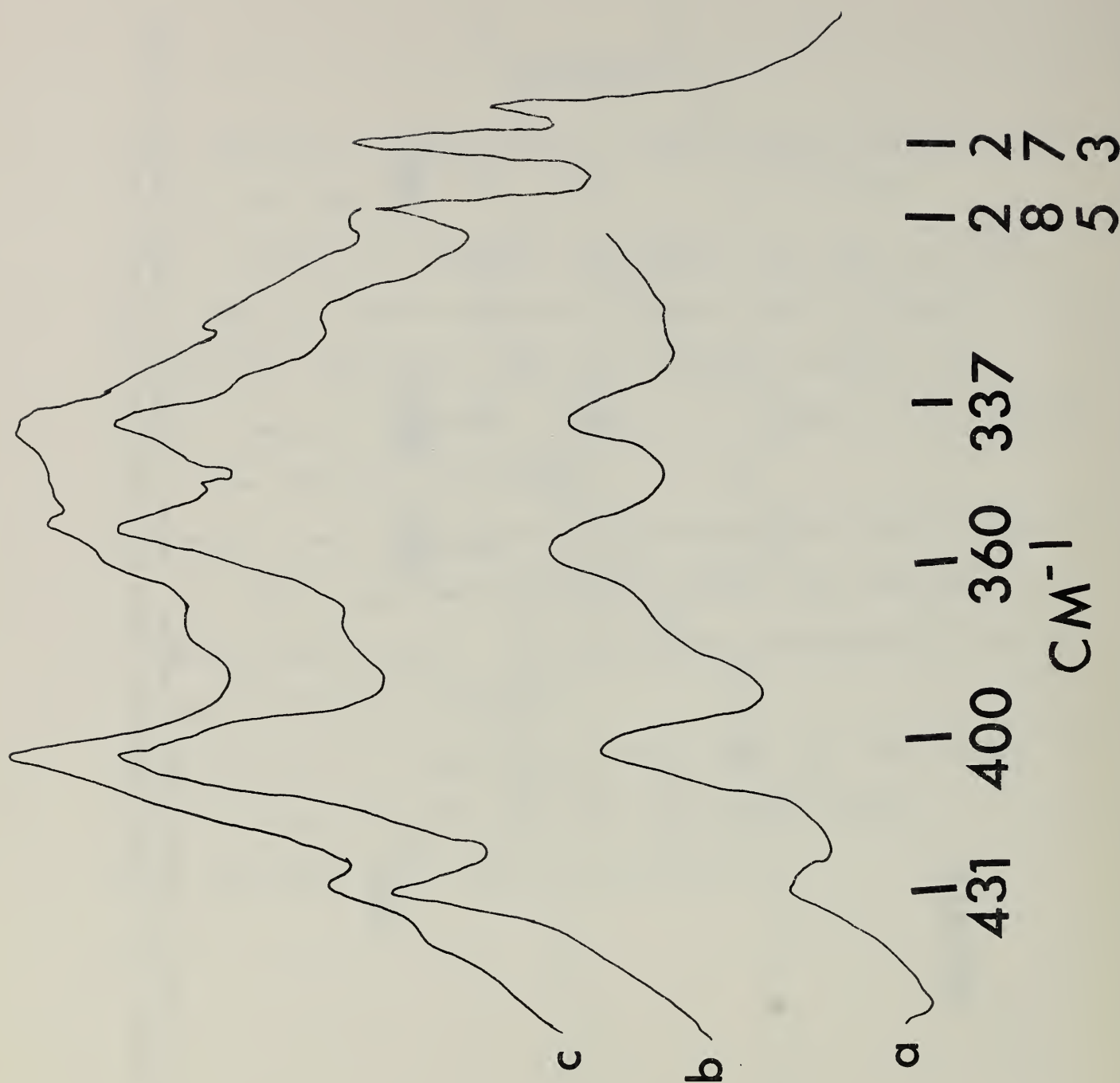


Figure 2 - The spectra of matrix isolated NaOH in argon. Curve a refers to a sample which effused from the crucible at a lower temperature than the sample represented in curve b. Curve c was obtained from the sample represented in curve b by allowing diffusion to

NaOH/Ar

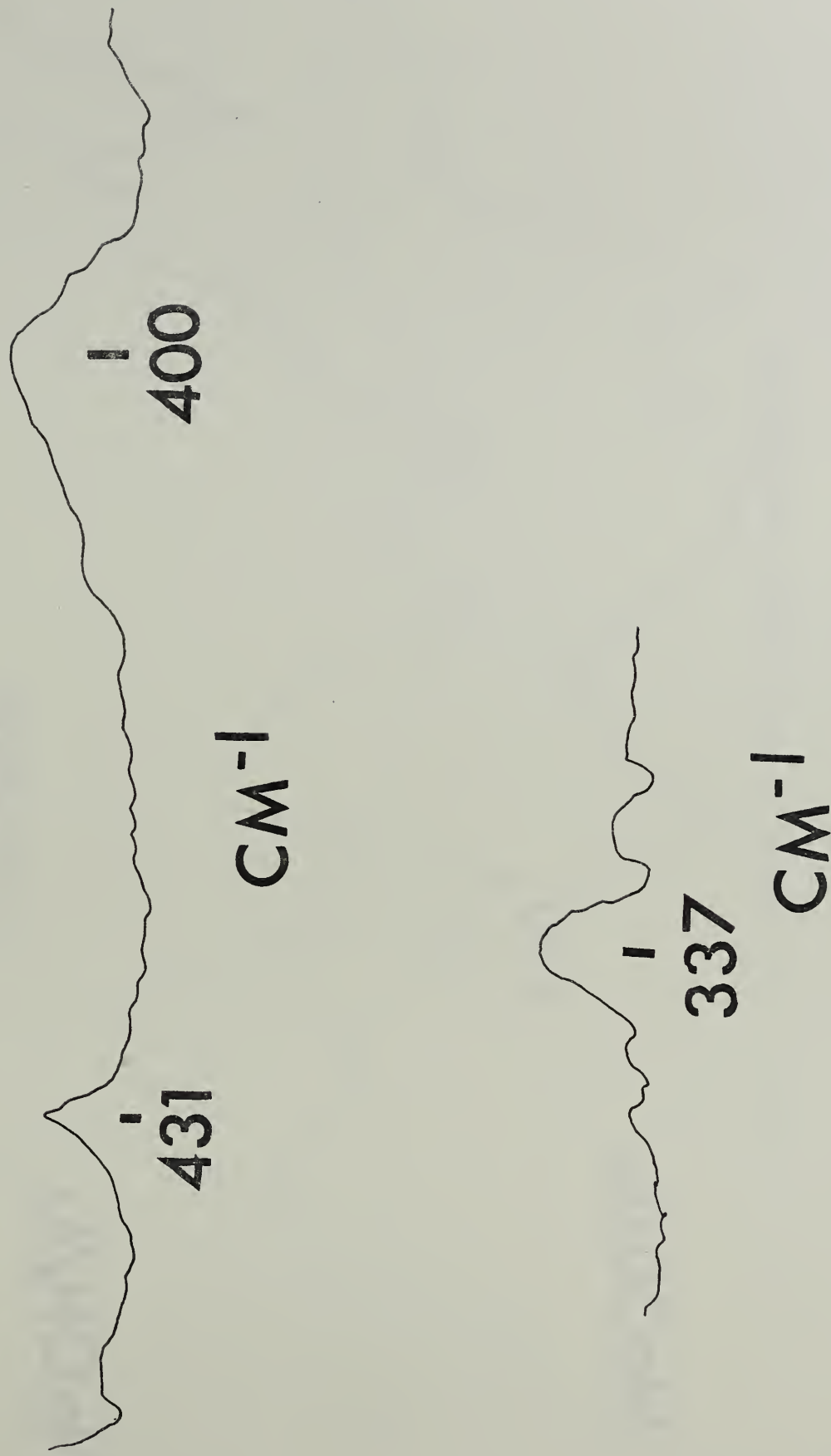


Figure 3 - The spectrum of matrix isolated NaOH in argon.



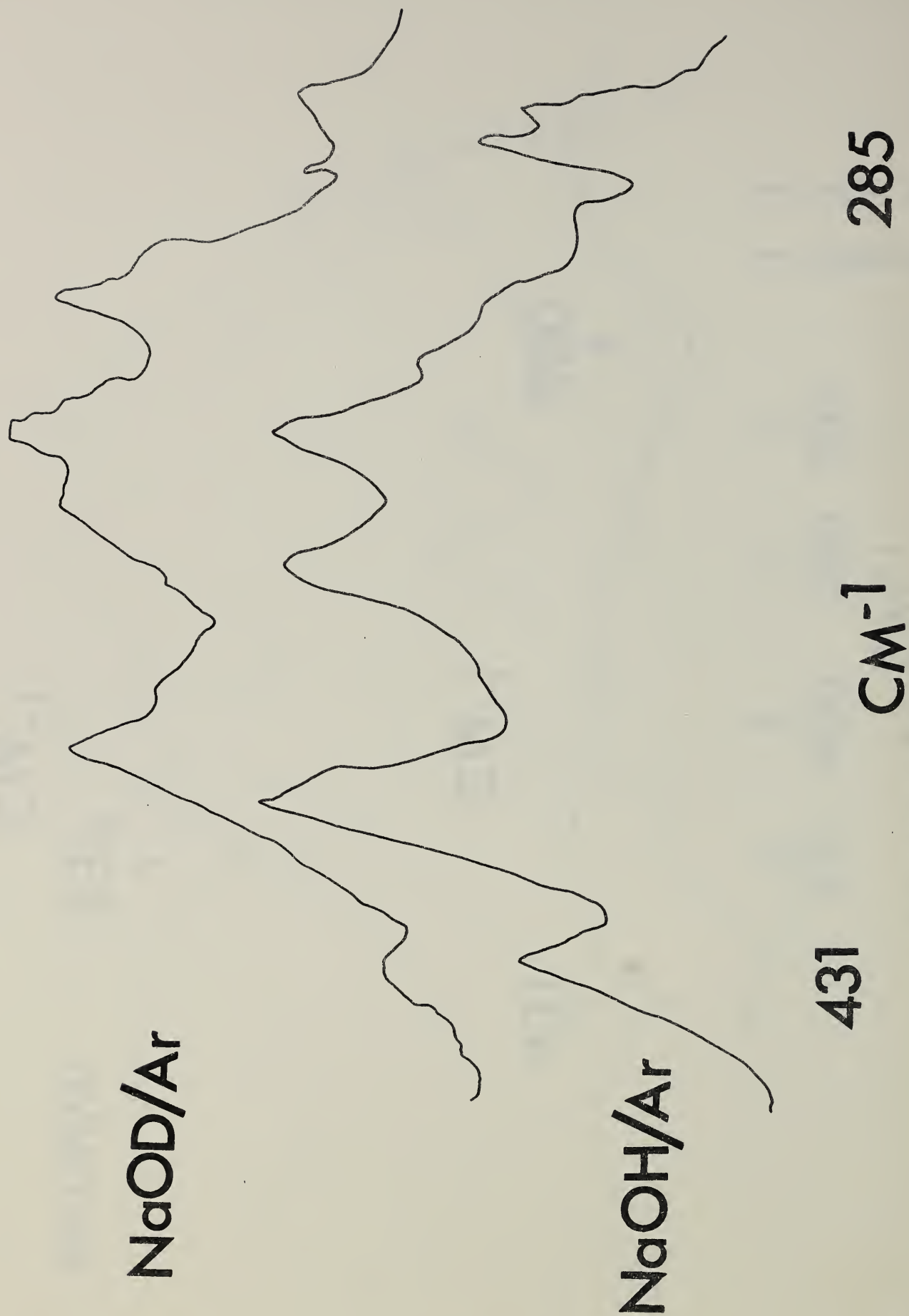


Figure 4 - The spectrum of matrix isolated NaOH in argon. The spectrum of matrix isolated NaOD in argon.

NaOD/Ar

111



Figure 5 - The spectrum of matrix isolated NaOD in argon.







